University College London

Doctoral Thesis

Quantum Entanglement and Networking with Spin-Optomechanics

Author:
Victor Montenegro-Tobar

Supervisor:
Prof. Sougato Bose

A thesis submitted in fulfilment of the requirements for the degree of Doctor of Philosophy

in the

Atomic, Molecular, Optical and Positron Physics Group
Department of Physics and Astronomy

September 2015

Declaration of Authorship

I, Victor Montenegro-Tobar, declare that this thesis titled, 'Quantum Entanglement and Networking with Spin-Optomechanics' and the work presented in it are my own. I confirm that:

- This work was done wholly or mainly while in candidature for a research degree at this University.
- Where any part of this thesis has previously been submitted for a degree or any other qualification at this University or any other institution, this has been clearly stated.
- Where I have consulted the published work of others, this is always clearly attributed.
- Where I have quoted from the work of others, the source is always given. With the exception of such quotations, this thesis is entirely my own work.
- I have acknowledged all main sources of help.
- Where the thesis is based on work done by myself jointly with others, I have made clear exactly what was done by others and what I have contributed myself.

Signed: _____

Date: _____

List of Publications

- Victor Montenegro, Alessandro Ferraro, and Sougato Bose, "Nonlinearity-induced entanglement stability in a qubit-oscillator system", Physical Review A **90**, 013829 (2014).

- Victor Montenegro, Alessandro Ferraro, and Sougato Bose, "Entanglement distillation in optomechanics via unsharp measurements", arXiv:1503.04462 (2015).

- Victor Montenegro and Sougato Bose, "Mechanical Qubit-Light Entanglers in Nonlinear Optomechanics", in preparation.

- Victor Montenegro and Vitalie Eremeev, "Monitoring the correlations in a quantum network of two remotely-located atomic-mechanical systems", in preparation.

- Vitalie Eremeev,Victor Montenegro, and Miguel Orszag, "Thermally generated long-lived quantum correlations for two atoms trapped in fiber-coupled cavities", Physical Review A **85**, 032315 (2012).

UNIVERSITY COLLEGE LONDON

Abstract

Department of Physics and Astronomy

Doctor of Philosophy

Quantum Entanglement and Networking with Spin-Optomechanics

by Victor Montenegro-Tobar

Non-relativistic quantum mechanics have proven to be a significant framework to understand the non-classical behaviour of light and the microcosmos. Perhaps, one of the first technological revolutions within quantum theory came with the invention of the transistor, whereby a purely quantum mechanical description was required. Currently, another outstanding revolution is taking place in a crossroad where information science meets quantum mechanics (this being the quantum information field). Such an area of work contemplates both the fascinating theoretical aspect of quantum correlations, as well as implementations towards quantum tasks performed by a universal quantum computer; tasks that cannot be realised (or they are hard to implement) within the classical domain.

This Thesis is devoted to study the dynamics of quantum entanglement in spin-optomechanics systems. In particular, we explore the quantum stabilization of quantum entanglement, a quantum concentration scheme in opto-mechanics and an interfacing of matter and light towards quantum networking applications. Additionally, we also investigate theoretical aspects of quantum correlations within thermal environments, as well as the topical area of quantum sudden transitions.

In Chapter 1, we provide a brief summary of quantum information and of the quantum optics framework to cover elementary concepts and techniques used subsequently in this work.

Subsequently, in Chapter 2 we present the stabilization of quantum entanglement in a non-linear qubit-oscillator system. The inclusion of a modest nonlinearity gives three results, i) the loss of periodicity of the system, ii) the occurrence of quadrature

squeezing appearing for a short time, and iii) the quantum entanglement reaches higher values in contrast to the case without non-linearity.

In Chapter 3, a technique to concentrate/distill a two-mode vacuum state in optomechanics via unsharp measurements is presented. Here, one of the optical modes is injected into a cavity at first, and thereafter, it is nonlinearly coupled to a mechanical oscillator. Afterwards, the position of the oscillator is measured using pulsed optomechanics and homodyne detection. The results show that this measurement can conditionally increase the initial entanglement.

Next, in Chapter 4, stimulated by optomechanical transducers and quantum networking, a light-matter system is constructed where a qubit is coupled to a cavity mode mediated through a mechanical oscillator. The qubit-oscillator conditionally displaced Hamiltonian and the oscillator-cavity radiation-pressure interaction generate a maximal qubit-cavity entanglement. Additionally, we consider the case in which the cavity mode is coupled to a waveguide, numerical calculations show a promising qubit-fibre entanglement under a weak matter-light coupling. For the quantum network case, we coupled a generic qubit in the first node to a second qubit-cavity distant Jaynes-Cummings system coupled through an optical fibre, where qubit-qubit correlations can be achieved in the quantum open systems scenario.

In Chapter 5, we study the evolution of an open quantum system within the Born-Markov microscopic master equation (MME). Essentially, two distant two-level atoms are trapped in fibre-coupled cavities. Under the approximation of one-excitation allowed in the atom-cavity-fibre basis, we can obtain quantum correlations induced by thermal fluctuations from the environments.

Lastly, in Chapter 6, we bring together previously elements explored in this Thesis. The system is a hybrid atomic-mechanical system formed from two remote qubits interacting with individual harmonic oscillators. This system, as in Chapter 4, explores interesting applications in quantum networking schemes. The two qubits are initially prepared in a Bell-diagonal state, and consequently the two-qubit correlations exhibit few interesting effects such as freezing, sudden changes and revivals in the evolution of the quantum entropic discord.

To conclude, I summarize my findings in Chapter 7.

Acknowledgements

I would never have been able to finish my Doctoral degree without the guidance and support of my supervisor, committee members, and friends, and family.

I would like to express my deepest gratitude to my supervisor Prof. Sougato Bose. His outstanding physics knowledge gave me the in-depth insight to appreciate and approach physical problems from different perspectives. Furthermore, his patience, caring manner, and dedication to myself and my work, from day one, established the perfect environment for me to undertake my academic journey. I am very grateful for having the chance to be one of his students, as well as being part of the Atomic, Molecular, Optical and Positron Physics (AMOPP) group. I am also very happy to see that my research is a contribution to the quantum information field work. Without Professor Bose's help and excellent guidance this result would not have been possible.

Also, I would like to thank my direct collaborator Dr. Alessandro Ferraro who helped me throughout important parts of this work.

Part of this Thesis (Chapter 5) was made in collaboration with colleagues from Santiago de Chile (Pontificia Universidad Católica de Chile). Therefore, I would like to extend my gratitude to Prof. Miguel Orszag and Dr. Vitalie Eremeev for openly discussing my work in many conversations each time I traveled to join and participate in the research group in Chile. This has been an important part of my formation as a physicist.

I would also like to thank my parents, Juan Montenegro and Marisol Tobar, my brother, Daniel, and my little sister, Marisol. They have always supported me and encouraged me with their best wishes.

Lastly, I would like to thank all my friends who have supported me and helped me in this journey, making London an unforgettable city. Special thanks to Lesslie Guerra Jorquera, and : Rebeca Martínez, Simón Pena, Rina Fujita, Umer Zubairy, Felipe Zambrano, Abolfazl (Abol) Bayat, Gentil Neto, Gabriel Saavedra, Catalina Maturana, Sebastián Bahamonde, Ximena Valdebenito, Alejandra (Alecita) Mora, Francisca Massone, Manuela Irarrázabal, Carolina Díaz, Javiera Erazo, Loreto (Lore) Parada, Patricio Velasco, Manuel Matta, Victoria (Vicky), JP Gildea, Marc, Elson Sutanto (who helped me by proofreading my Thesis, cheers mate!), Humera (Hums), Nelson Céspedes, Chiara Pelloja, Mark Taktak, Néstor Marín, Hernán Bobadilla,

Andrés Espejo, Felipe Lanuza, Juan Pablo Astorga, Dom Guevara, Shirwan Abdullah, Bobby Antonio, Andrés Tocornal, Jeremy Cáceres, Inga Feischen, Ning Jia, Ayşegül Için, Sarah and John Donnelly for their kindness during these last years, and to my friend Fidel Cordero.

Last but not least, I would like to acknowledge financial support from the Chilean government for supporting me through my doctoral scholarship Becas Chile (Conicyt).

Contents

List of Figures

To my parents:

Juan Montenegro & Marisol Tobar,

and my friend
Fidel Cordero[†] *(1961 - 2013)*

Chapter 1

Introduction

In this introductory Chapter, we will briefly provide some relevant concepts of quantum mechanics as well as a fundamental framework on quantum information and quantum optics. As this mathematical background can be found in several quantum textbooks, it will not be our aim to give a detailed analysis of them. The Chapter is organized as follows : In Section 1.1, we present the dynamics of pure and mixed quantum states both for unitary dynamics, as well as in the presence of losses (open quantum system). Next, in Section 1.2, we give an introduction to the quantum bit, the quantum harmonic oscillator, some states of the quantized electromagnetic field, and phase space representation. Finally, in Section 1.3, we give a short overview on how to quantify the quantum entanglement of bipartite systems.

1.1 A Few Words On Quantum Mechanics

Quantum Mechanics (QM) together with General Relativity (GR) are undeniably the two most greatest theories ever achieved. On the one hand, GR comes to light as a local classical theory providing a unified description of gravity as a geometric property of spacetime; a generalization being made as a result of merging special relativity and Newton's law of universal gravitation. On the other hand, the situation for QM could not be more different. Firstly, in contrast to GR and its unifying character (summarized in the Einstein field equations), QM was constructed as a set of rules and principles throughout the years. Secondly, unlike GR where the main groundbreaking result was solely made by Albert Einstein, QM emerged as

the result of the work of several physicists in a close experiment-theory collaboration. Lastly, QM stands by definition as a non-classical theory, and also as a non-local theory as beautifully proven later by John Bell [Bell1964].

QM has developed through several distinctive phases. In the early 1900s in order to explain the Black-body radiation, the concept of *quanta* was introduced by Max Planck as a discrete (quantized) energy packet. Later, in 1925, another QM phase took place with contributions from Louis de Broglie, Erwin Schrödinger, Max Born, Werner Heisenberg, Paul Dirac, among others. Here, the QM matrix machinery was built. In the subsequent years, the equivalence between the matrix mechanics and wave mechanics of QM was established, and last but not least, the Uncertainty principle.

For completeness, in the following we will present a few useful definitions and concepts of QM. First, let us commence considering a system at a given time depicted by the vector $|\psi\rangle$. The vector ket $= |\ \rangle$ or *pure state* belongs to a Hilbert space $\mathcal{H}$, and it can be expanded as a linear combination of vectors $|i\rangle \in \mathcal{H}$ ($c_i \in \mathbb{C}$, and $\sum_i |c_i|^2 = 1$) as following:

$$|\psi\rangle = \sum_i c_i \, |i\rangle \, . \tag{1.1}$$

A powerful consequence of the above is that, quantum states satisfy the superposition principle (wave-like nature of QM). Another interesting result due to the Hilbert space structure is the construction of a quantum system composed of different quantum subsystems. In other words, for simplicity let us consider two different quantum states belonging to different Hilbert spaces $|\psi\rangle_A \in \mathcal{H}_A$ and $|\psi\rangle_B \in \mathcal{H}_B$. The whole composite quantum system corresponds to the joint space, a valid state which belongs to a higher dimensional Hilbert space : $|\psi\rangle_{AB} \equiv |\psi\rangle_A \otimes |\psi\rangle_B \in \mathcal{H}_{AB} = \mathcal{H}_A \otimes \mathcal{H}_B$. As the superposition principle has to remain valid in this joint tensor space as well, then some valid states of the joint Hilbert space are for example : $|a_1\rangle \otimes |b_1\rangle$ or $1/\sqrt{2}(|a_1\rangle \otimes |b_1\rangle + |a_2\rangle \otimes |b_2\rangle$, where $|a_i\rangle$ ($|b_i\rangle$) belongs to $\mathcal{H}_A(\mathcal{H}_B)$. The last state (entangled) reveals a quintessential feature of quantum mechanics corresponding to the main issue of this thesis. Of course, we will study this type of states in more detail in subsequent sections (see Section 1.3).

As said, a quantum pure state is represented by a vector in $\mathcal{H}$, whereas every measurable physical quantity A is described by an operator (observable) $\hat{A}$ acting on $\mathcal{H}$. An operator is a functional build as $\hat{A} = \sum_{i,j} a_{i,j} \, |i\rangle \langle j|$, where the mathematical entity bra $= \langle\ |$ belongs to the dual space $\mathcal{H}^*$. Furthermore, the only possible

outcome of the measurement of a physical quantity A is one of the eigenvalues of the corresponding observable $\hat{A}$.

In the case of a non-relativistic closed system, i.e., in absence of energy losses, the time evolution of the state vector $|\psi(t)\rangle$ is governed by the Schrödinger equation:

$$i\hbar\frac{d}{dt}|\psi(t)\rangle = \hat{H}(t)\,|\psi(t)\rangle\,, \tag{1.2}$$

where $\hat{H}(t)$ is the observable associated with the total energy of the system. As the Schrödinger equation is of first order in time any subsequent time is determined by an initial quantum state. It is also important to notice that the Schrödinger equation does not exhibit any indeterminacy in the time evolution of a quantum system in itself. The intrinsic random indeterminacy of QM only appears when the physical quantity is measured. Lastly, if the Hamiltonian of the system is time-independent, the wave-function can be found solving the eigenvalues problem (E being the energy/eigenvalue):

$$\hat{H}\,|\psi(t)\rangle = E\,|\psi(t)\rangle\,. \tag{1.3}$$

A more general evolution in physics is to consider the coupling between the system of interest with the environment, i.e., an open system. As we know, losses play a crucial role in physics and they cannot be avoided.

To present the equation subject to the detrimental effects —*or decoherence*— due to the environment, first we have to introduce the mixed states $\hat{\rho}$. In contrast to pure or vector states where we have a perfect knowledge of our system, when mixed states are considered, we can only know our quantum state probabilistically. Mixed states are linear, semi-positive (eigenvalues greater than or equal to zero), and self-adjoint ($\hat{\rho} = \hat{\rho}^{\dagger}$) operators represented by matrices.

A density matrix $\hat{\rho}$ ($\mathrm{Tr}\{\hat{\rho}\} = 1$) describes a probability distribution of quantum states $|\psi_i\rangle$ as following:

$$\hat{\rho} = \sum_i p_i\,|\psi_i\rangle\,\langle\psi_i| \tag{1.4}$$

where, p_i is the associated probability of finding the quantum system in the quantum state $|\psi_i\rangle$.

To derive the open dynamics, we consider the Hamiltonian of the original quantum system ($\hat{H}_{\rm sys}$), the environment ($\hat{H}_{\rm env}$), and their interaction ($\hat{H}_{\rm int}$) as a whole closed quantum system $\hat{H}_{\rm tot} = \hat{H}_{\rm sys} + \hat{H}_{\rm env} + \hat{H}_{\rm int}$. The equivalent Schrödinger dynamics for density matrices is the so-called Liouville-von Neumann equation:

$$\frac{d}{dt}\hat{\rho}(t)_{\rm tot} = -\frac{i}{\hbar}[\hat{H}_{\rm tot}, \hat{\rho}(t)_{\rm tot}], \tag{1.5}$$

Since we are only interested in the dynamics of the system, we can at this point perform a partial trace over the environmental degrees of freedom $\hat{\rho}(t) = {\rm Tr}_{env}[\hat{\rho}(t)_{\rm tot}]$. The most general trace-preserving and completely positive form of this evolution is the Lindblad master equation for the reduced density matrix.

$$\frac{d}{dt}\hat{\rho}(t) = -\frac{i}{\hbar}[\hat{H}, \hat{\rho}(t)] + \sum_{i,j} a_{i,j}\left(\hat{F}_i\hat{\rho}(t)\hat{F}_j^\dagger - \frac{1}{2}\{\hat{F}_j^\dagger\hat{F}_i, \hat{\rho}(t)\}\right), \tag{1.6}$$

where, $\{\cdots,\cdots\}$ stands for the anticommutator. Operators $\hat{F}$ constitutes a basis in the space of operators for the reduced system of $\hat{\rho}(t)$. Lastly, $a_{i,j}$ is a positive definite hermitian matrix. However, throughout all of this thesis (except in Chapter 5) we will consider the usual standard quantum optical master equation, which for the decoherence of the quantized field $\hat{a}$ reads as:

$$\begin{aligned}\frac{d}{dt}\hat{\rho}(t) &= -\frac{i}{\hbar}[\hat{H}, \hat{\rho}(t)] \\ &+ \frac{\kappa}{2}(\langle n\rangle + 1)\left(\hat{a}\hat{\rho}(t)\hat{a}^\dagger - \frac{1}{2}\{\hat{a}^\dagger\hat{a}, \hat{\rho}(t)\}\right) \\ &+ \frac{\kappa}{2}\langle n\rangle\left(\hat{a}^\dagger\hat{\rho}(t)\hat{a} - \frac{1}{2}\{\hat{a}\hat{a}^\dagger, \hat{\rho}(t)\}\right).\end{aligned} \tag{1.7}$$

In the right hand side of Eq. 1.7, the first line represents the unitary Liouville-von Neumann evolution, meanwhile the second line is the dissipative Lindbladian part. As $\langle n\rangle = (e^{\hbar\omega/k_BT} - 1)^{-1}$ is the average photon number, where k_B is the Boltzmann constant, and T is the temperature. It is straightforward to obtain the master equation at zero temperature:

$$\frac{d}{dt}\hat{\rho}(t) = -\frac{i}{\hbar}[\hat{H}, \hat{\rho}(t)] + \frac{\kappa}{2}\left(\hat{a}\hat{\rho}(t)\hat{a}^\dagger - \frac{1}{2}\{\hat{a}^\dagger\hat{a}, \hat{\rho}(t)\}\right). \tag{1.8}$$

In the derivation of the above master equation the following approximations were made:

- *Separability* : We assume that at the initial time of the evolution there are no correlation between the system of interest and the environment. Therefore, we can write the density operator as a tensor product between them.

- *Born approximation* : i) we require a quasi-static evolution of the environment, i.e., the reservoir does not change as a result of the interaction with the system, ii) the system-environment remain (approximately) separable throughout the dynamics, in other words, we require weak system-environment coupling.

- *Markov approximation* : Sometimes called "short-memory environment. It means that, the environmental correlation functions decay much faster than those of the system.

- *Secular approximation* : All fast rotating terms in the interaction picture are neglected.

In contrast to the Schrödinger equation, the Lindblad Born-Markov master equation represents a more realistic evolution of a quantum system describing the dissipation in the quantum system due to its interaction with the environment.

1.2 Quantum Optics & Information Framework

1.2.1 The quantum bit

On the one hand, a *bit* is the basic unit of information in modern computation. Essentially, a bit constitutes a way to encode two distinguishable states being valued in one and only one of two possible outcomes or logical values, such as : up or down, on or off, 0 or 1, true or false, etc. These states can be stored/processed in real physical systems such as two different voltages (or currents) in a circuit, for instance, a voltage below a certain value $V_{\text{threshold}}$ represents 0, and 1 otherwise. Other implementations might be two distinct levels of light intensity, two directions of magnetization or polarization, etc.

On the other hand, in the rapid growing quantum computing field, a *quantum bit* (or *qubit*) is the quantum analogue of the classical bit. However, the qubit exhibits crucial differences with its classical counterpart. For example, as mentioned above, a bit is single valued, i.e., it can be in one and only one states 0 or 1, meanwhile

a qubit due to the superposition principle of QM it could be in a superposition of both states at the same time, becoming a key feature for quantum processing.

To define the qubit mathematically we shall denote a two-dimensional orthonormal vector basis $\{|0\rangle, |1\rangle\}$ (computational basis) in the Hilbert space $\mathcal{H}$ over the field of complex numbers $\mathbb{C}$, thus in the Dirac's ket notation a qubit reads as:

$$a\,|0\rangle + b\,|1\rangle \tag{1.9}$$

where, $\{a, b\}$ are two complex coefficients satisfying the following normalization constraint : $|a|^2 + |b|^2 = 1$. Eq. 1.9 represents the most general qubit state. Here, the quantities $|a|^2$ and $|b|^2$ represent the probabilities associated to the outcome $|0\rangle$ or $|1\rangle$ after a measurement is performed in their corresponding computational basis.

A natural realization for a qubit is a spin$-\frac{1}{2}$ particle, e.g., an electron. The computational basis is interpreted then as $|0\rangle = |\uparrow\rangle$ (spin up), and $|1\rangle = |\downarrow\rangle$ (spin down).

To give the representation of a spin qubit in the Bloch sphere, we consider the Pauli vector in spherical coordinates as follows:

$$\mathbf{n}\cdot\hat{\boldsymbol{\sigma}} = \begin{pmatrix} \cos\theta & e^{-i\phi}\sin\theta \\ e^{i\phi}\sin\theta & -\cos\theta \end{pmatrix}, \tag{1.10}$$

where, the polar angle $0 \leq \theta \leq \pi$ and the azimuthal angle $0 \leq \phi \leq 2\pi$. The unitary vector $\mathbf{n} = (\cos\phi\sin\theta, \sin\phi\sin\theta, \cos\theta)$, and $\hat{\boldsymbol{\sigma}} = (\hat{\sigma}_x, \hat{\sigma}_y, \hat{\sigma}_z)$ is the Pauli vector, being its components the Pauli matrices (computational basis):

$$\hat{\sigma}_x = \begin{pmatrix} 0 & 1 \\ 1 & 0 \end{pmatrix} \qquad \hat{\sigma}_y = \begin{pmatrix} 0 & -i \\ i & 0 \end{pmatrix} \qquad \hat{\sigma}_z = \begin{pmatrix} 1 & 0 \\ 0 & -1 \end{pmatrix}. \tag{1.11}$$

The eigenvector of Eq. 1.10 is:

$$|\psi(\theta,\phi)\rangle = \begin{pmatrix} e^{-i\phi/2}\cos\frac{\theta}{2} \\ e^{i\phi/2}\sin\frac{\theta}{2} \end{pmatrix} = \cos\frac{\theta}{2}|\uparrow\rangle + e^{i\phi}\sin\frac{\theta}{2}|\downarrow\rangle \tag{1.12}$$

the above pure state describes the orientation of the qubit in the surface of the Bloch sphere illustrated in Fig. 1.1-a. Additionally, the 2×2 mixed states can be described by the interior of the sphere, see Fig. 1.1-b.

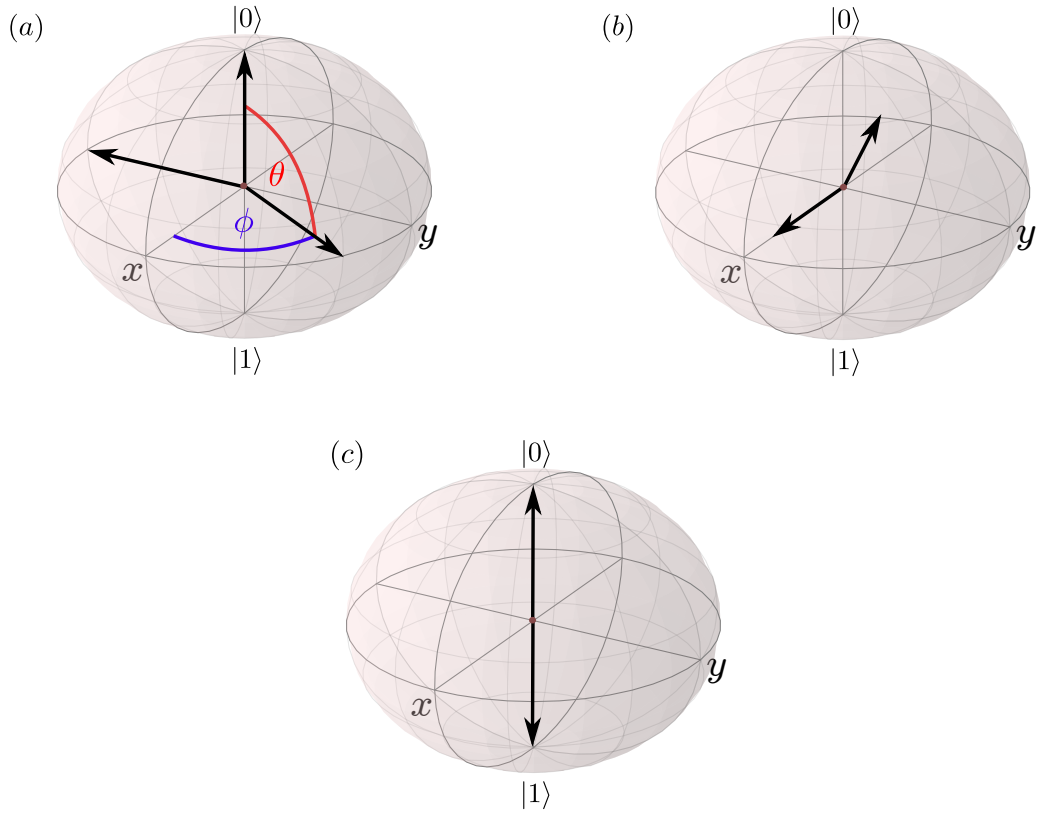

FIGURE 1.1: Qubit representation in the Bloch sphere. In a) a pure or vector state corresponds at any point in the surface of the sphere, b) a mixed state is represented inside the sphere, and c) the computational basis $\{|0\rangle, |1\rangle\}$.

Of course, a straightforward generalization might be made for a d-dimensional orthonormal vector basis (*qudit*). However, throughout all of this work only qubits will be considered.

1.2.2 Quantum harmonic oscillator

Let us start from a collection of N classical harmonic oscillators, the Hamiltonian reads as:

$$H = \sum_{j=1}^{N} \frac{1}{2m_j} p_j^2 + \frac{1}{2} m_j \omega_j^2 x_j^2 \tag{1.13}$$

where, m_j is the mass for the *jth*-particle oscillating with an angular frequency ω_j. The variables x_j and p_j are the position and momentum for the *jth*-particle, respectively. The above Eq. 1.13 can be quantized using the canonical commutation relation $[\hat{x}_n, \hat{p}_m] = i\hbar\delta_{nm}$, where $\hat{x}_n$ and $\hat{p}_m = -i\hbar\nabla_m$ are the position and momentum operator for a wave function $|\psi\rangle$, respectively. Hence, the quantized

Hamiltonian is:

$$\hat{H} = \sum_{j=1}^{N} \frac{1}{2m_j}\hat{p}_j^2 + \frac{1}{2}m_j\omega_j^2\hat{x}_j^2. \tag{1.14}$$

Considering the one-dimensional time-independent Schrödinger equation $\hat{H}\,|\psi\rangle = E\,|\psi\rangle$ for a single particle, we can solve the eigenvalue problem in the coordinate representation $\langle x|\psi\rangle = \psi(x)$ and obtain the $nth-$spatial wave-function mode as $(n = 0, 1, 2, 3, \ldots)$:

$$\psi_n(x) = \frac{1}{\sqrt{2^n n!}} \left(\frac{m\omega}{\pi\hbar}\right)^{1/4} e^{-m\omega x^2/2\hbar} \mathrm{H}_n\left(\sqrt{\frac{m\omega}{\hbar}}x\right), \tag{1.15}$$

where $\mathrm{H}_n(x) = (-1)^n e^{x^2}\frac{d^n}{dx^n}\left(e^{-x^2}\right)$ are the Hermite polynomials, and the corresponding energy levels are:

$$E_n = \hbar\omega\left(n + \frac{1}{2}\right). \tag{1.16}$$

The above Eq. 1.16 shows that the energy spectrum is discrete and equally spaced. In addition, in contrast to the classical case, the minimum energy state ($n = 0$, the ground state of the system) corresponds to a non-zero value $\hbar\omega/2$, being this in accordance with the Uncertainty principle.

To give another useful representation of Eq. 1.14, we introduce the non-hermitian bosonic annihilation operator for a single particle ($[\hat{a}, \hat{a}^\dagger] = 1$):

$$\hat{a} = \frac{1}{\sqrt{2\hbar\omega}}(\omega\hat{x} + i\hat{p}) \tag{1.17}$$

and therefore we can get:

$$\hat{x} = \sqrt{\frac{\hbar}{2m\omega}}(\hat{a}^\dagger + \hat{a}), \tag{1.18}$$

$$\hat{p} = i\sqrt{\frac{m\hbar\omega}{2}}(\hat{a}^\dagger - \hat{a}), \tag{1.19}$$

The Hamiltonian for a single quantum harmonic oscillator then reads as:

$$\hat{H} = \frac{1}{2m}\hat{p}^2 + \frac{1}{2}m\omega^2\hat{x}^2 = \left(\hat{a}^\dagger\hat{a} + \frac{1}{2}\right)\hbar\omega. \tag{1.20}$$

a useful basis closely related to the annihilation operator is the Fock basis $\{|n\rangle\}$, where n stands for the number of photons in the quantum state. If $\hat{a}$ ($\hat{a}^\dagger$) acts on

$|n\rangle$ this can annihilate (create) one photon. Therefore;

$$\hat{a}\,|n\rangle = \sqrt{n}\,|n-1\rangle\,, \tag{1.21}$$

$$\hat{a}^\dagger\,|n\rangle = \sqrt{n+1}\,|n+1\rangle\,, \tag{1.22}$$

$$\hat{N} \equiv \hat{a}^\dagger\hat{a}\,|n\rangle = n\,|n\rangle\,, \tag{1.23}$$

using the above, the Eq. 1.20 can be rewrite as following: $\hat{H} = (\hat{N} + 1/2)\hbar\omega$. The eigenvalue problem then in the Fock basis is easily solved as $\hat{H}\,|n\rangle = E_n\,|n\rangle$, where $E_n = (n + 1/2)\hbar\omega$.

1.2.3 Coherent and thermal states

Perhaps, the most common states of the electromagnetic field both in the quantum optics and quantum information field are the coherent and thermal states. The first type of states were introduced by Glauber [Glauber1963] and Sudarshan [Sudarshan1963]. Coherent states are defined as the eigenstate of the annihilation operator. For a single mode it reads as ($\alpha \in \mathbb{C}$):

$$\hat{a}\,|\alpha\rangle = \alpha\,|\alpha\rangle\,. \tag{1.24}$$

Furthermore, they are commonly represented in the Fock basis as following:

$$|\alpha\rangle = e^{-|\alpha|^2/2}\sum_{n=0}^{\infty}\frac{\alpha^n}{\sqrt{n!}}\,|n\rangle\,. \tag{1.25}$$

In addition, it is straightforward to show that this state exhibits equal uncertainty in the position and momentum quadratures, i.e., $(\Delta x)^2_\alpha = \hbar/2\omega$ and $(\Delta p)^2_\alpha = \hbar\omega/2$, and therefore minimizing the Uncertainty principle (coherent states are minimum uncertainty states)

$$(\Delta x)^2_\alpha(\Delta p)^2_\alpha = \frac{\hbar^2}{4}. \tag{1.26}$$

Furthermore, they form a set of overcomplete non-orthogonal ($\langle\alpha|\beta\rangle \neq 0, \forall\,|\alpha\rangle \neq |\beta\rangle$) basis:

$$\langle\alpha|\beta\rangle = e^{-\frac{1}{2}(|\alpha|^2+|\beta|^2)}e^{\alpha\beta^*} \tag{1.27}$$

$$\int d^2\alpha\,|\alpha\rangle\,\langle\alpha| = \pi. \tag{1.28}$$

Another way to define coherent states is using the Displacement operator, defined as:

$$\hat{D}(\alpha) = e^{(\alpha\hat{a}^\dagger - \alpha^*\hat{a})} \tag{1.29}$$

with the above definition, a coherent state is just the vacuum state $|vac\rangle = |0\rangle$, $\alpha = 0$ displaced by a complex amplitude α:

$$\hat{D}(\alpha)\,|0\rangle = |\alpha\rangle\,. \tag{1.30}$$

Coherent states obeys a Poisson statistics, the probability of having n photons in a coherent state is (see Fig. 1.2):

$$P_n = e^{-|\alpha|^2}\frac{|\alpha|^{2n}}{n!}, \tag{1.31}$$

with average photon number and variance giving by $\langle n\rangle = |\alpha|^2$, $\langle n^2\rangle = |\alpha|^2 + |\alpha|^4$.

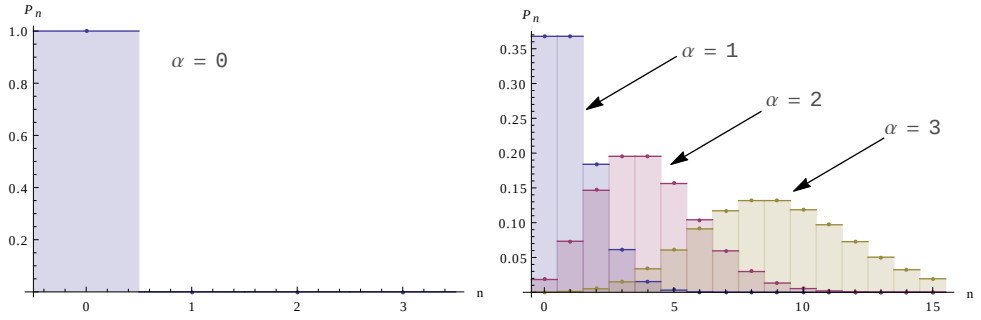

FIGURE 1.2: The figure shows the probability of having n photons in a coherent state P_n as a function of n. In the left panel, the probability of having zero photons in a coherent state (vacuum state $\alpha = 0$) is the unity. In the right panel, we plot $\alpha = 1, 2, 3$.

Finally, the normalized $q-$representation ($q = x\sqrt{m\omega/\hbar}$) for a general coherent state α is given by ($\psi_\alpha(q) \equiv \langle q|\,\alpha\rangle$)

$$\psi_\alpha(q) = \frac{1}{\pi^{1/4}}\exp\left(\frac{\alpha^{*2} - \alpha^2}{4}\right)\exp\left(-\frac{1}{2}(q - \sqrt{2}\mathbb{R}e[\alpha])^2\right)\exp\left(iq\sqrt{2}\mathbb{I}m[\alpha]\right).$$

The second state to consider is the thermal state. It is known that any quantum system $\in \mathcal{H}$ at thermal equilibrium is in a thermal state given by:

$$\hat{\rho}^{th} = \frac{e^{-\hat{H}/k_BT}}{\mathrm{Tr}[e^{-\hat{H}/k_BT}]}, \tag{1.32}$$

where, k_B is the Boltzmann constant, and T is the temperature of the state. Another useful representation is:

$$\hat{\rho}^{th} = \frac{1}{\pi\bar{n}} \int |\alpha\rangle \langle\alpha| \exp\left(-\frac{|\alpha|^2}{\bar{n}}\right) d^2\alpha \tag{1.33}$$

$$\bar{n} = \frac{1}{\exp\left(\hbar\omega_c/k_B T\right) - 1} \tag{1.34}$$

above, the normalized thermal state corresponds to a collection of coherent states at temperature T ($\bar{n}$ is the average photon number). Lastly, in the Fock basis the thermal state is:

$$\hat{\rho}^{th} = \sum_n P_n^{th} |n\rangle \langle n| , \tag{1.35}$$

here, the thermal photon statistics P_n^{th} is given by (see Fig. 1.3):

$$P_n^{th} = \frac{\bar{n}^n}{(\bar{n}+1)^{n+1}}. \tag{1.36}$$

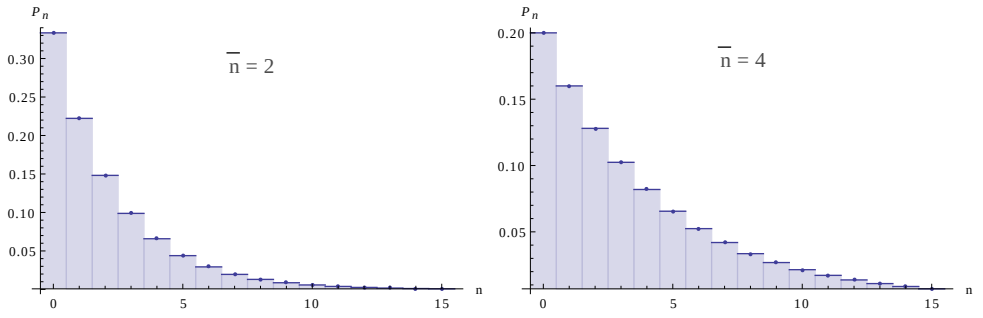

FIGURE 1.3: We illustrate the thermal photon statistics P_n^{th} as a function of the photon number n. In the left (right) panel, we consider $\bar{n} = 2(\bar{n} = 4)$. Of course, for the vacuum state $\bar{n} \to 0$ the thermal state coincides with the left panel of Fig. 1.2.

1.2.4 Squeezed states

As coherent states in the previous section, squeezed states are also minimum uncertainty states, i.e., $(\Delta x)^2_{sq}(\Delta p)^2_{sq} = \hbar^2/4$. However, one of its quadratures can be *squeezed* to a value less than the coherent case, at the expense of the other quadrature to increase. In the coherent scenario, as both quadratures are equal, it is natural to represent this state in the complex plane $\{\langle x\rangle_\alpha = \mathrm{Re}[\alpha], \langle y\rangle_\alpha = \mathrm{Im}[\alpha]\}$

as a circle displaced by α. In contrast to that case, the squeezed state is the vacuum state, which is first squeezed into an ellipse, tilted by an angle ϕ, and then displaced by α (see Fig. 1.4), where the angle ϕ corresponds to rotation angle for the new pair of orthogonal axis $\{\langle \hat{x}_r \rangle, \langle \hat{y}_r \rangle\}$

$$\hat{x}_r = \sqrt{\frac{\hbar}{2m\omega}}(\hat{a}^\dagger e^{i\phi} + \hat{a}e^{-i\phi}), \tag{1.37}$$

$$\hat{y}_r = i\sqrt{\frac{m\hbar\omega}{2}}(\hat{a}^\dagger e^{i\phi} - \hat{a}e^{-i\phi}), \tag{1.38}$$

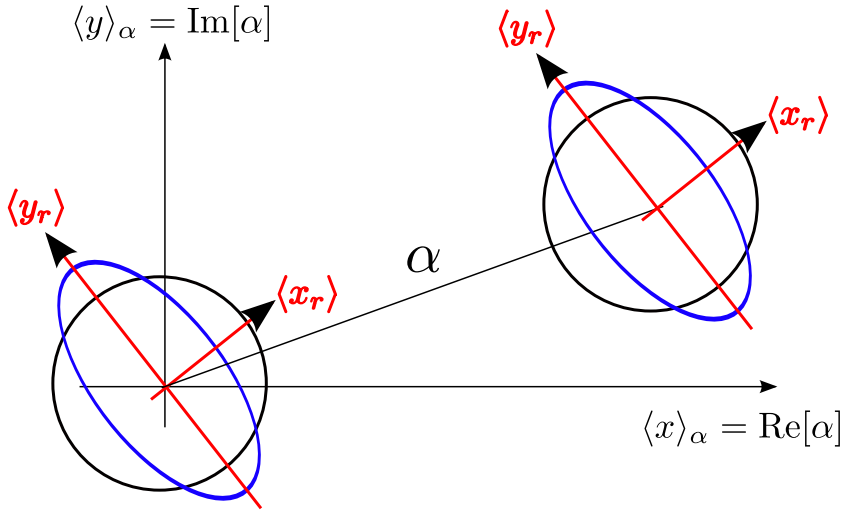

FIGURE 1.4: The figure shows the coherent state (black circle) of complex amplitude α, and the squeezed state (blue ellipse) in a rotated orthogonal axis $\{\langle \hat{x}_r \rangle, \langle \hat{y}_r \rangle\}$.

Let us define the squeeze operator as following:

$$\hat{S}(\xi) = \exp\left[\frac{1}{2}(\xi^* \hat{a}^2 - \xi \hat{a}^{\dagger 2})\right], \tag{1.39}$$

where $\xi = re^{i\theta}$ is an arbitrary complex number called the squeezed parameter. The unitary operator ($\hat{S}^\dagger(\xi) = \hat{S}^{-1}(\xi) = \hat{S}(-\xi)$) give us the following transformation:

$$\hat{S}^\dagger(\xi)\hat{a}\hat{S}(\xi) = \hat{a}\cosh r - \hat{a}^\dagger e^{i\theta}\sinh r, \tag{1.40}$$

therefore, it is straightforward to obtain the squeezed coherent state $|\alpha, \xi\rangle$ as:

$$|\alpha, \xi\rangle = \hat{D}(\alpha)\hat{S}(\xi)\,|0\rangle\,, \tag{1.41}$$

and,

$$|\xi\rangle = \hat{S}(\xi)\,|0\rangle\,, \tag{1.42}$$

corresponding to the squeezed vacuum state. The representation of squeezed vacuum states in the basis of number states is (only even number states are expanded):

$$|\xi\rangle = \frac{1}{\sqrt{\cosh r}} \sum_{m=0}^{\infty} (-1)^m \frac{\sqrt{(2m)!}}{2^m m!} e^{im\theta} \tanh^m r\,|2m\rangle\,. \tag{1.43}$$

Hence, the probability of detecting odd states is zero. On the other hand, the probability distribution for even photons in the field is given by (see Fig. 1.5):

$$P_{even=2m} = \frac{(2m)!}{2^{2m}(m!)^2} \frac{\tanh^{2m} r}{\cosh r}, \tag{1.44}$$

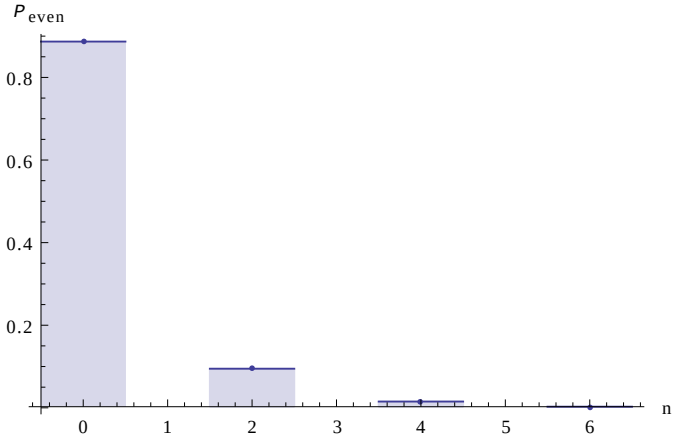

FIGURE 1.5: Probability of detecting even photons in the field $P_{even=2m}$ for a squeezed vacuum state, $r = 0.5$.

and the photon distribution for a squeezed coherent state is (see Fig. 1.6):

$$P_n = |\,\langle n|\,\alpha, \xi\rangle|^2, \tag{1.45}$$

where

$$\langle n|\,\alpha, \xi\rangle = \frac{\tanh r^{n/2} r}{\sqrt{2^n n!\cosh r}} H_n\left(\frac{\alpha}{\sqrt{2\sinh r \cosh r}}\right) e^{-\frac{1}{2}|\alpha|^2 + \frac{1}{2}\alpha^2 \tanh r} \tag{1.46}$$

H_n being the nth order Hermite polynomial.

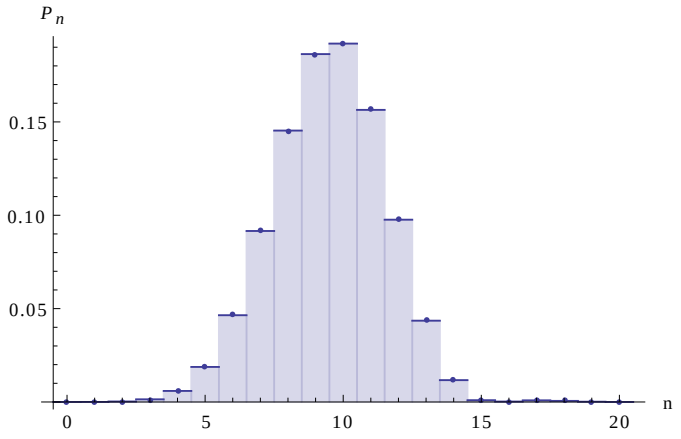

FIGURE 1.6: Photon distribution for a squeezed coherent state, $r = 0.5, \alpha = 5$.

1.2.5 Representation in phase space

In classical physics, the state of a particle (or electromagnetic field) with position (q) and momentum (p) is characterized by a phase space distribution $\mathrm{w}(q,p)$, which quantify the probability of finding simultaneously a set of values $\{q,p\}$ at some time t. On the other hand, in quantum mechanics (due to the Uncertainty principle) it is not allowed to find simultaneously canonical conjugate variables. Additionally, the phase space distribution can be negative for some regions. Therefore, we shall refer to the quantum analogue $\mathcal{W}(q,p)$ as a quasiprobability distribution. A derivation of $\mathcal{W}(q,p)$ is given in Ref. [Leonhardt-Book] as following. Let us first consider, the reduced distributions $\int_{-\infty}^{+\infty}\mathcal{W}(q,p)dp$ and $\int_{-\infty}^{+\infty}\mathcal{W}(q,p)dq$. These must yield the position or the momentum distribution, respectively —where, we have not made any assumption regarding simultaneous set of measurements on $\{q,p\}$. Furthermore, after performing an arbitrary rotation θ in q-p space, the probability of measuring the q-position is:

$$\Pr(q,\theta) \equiv \langle q|\,\hat{U}(\theta)\hat{\rho}(t)\hat{U}^{\dagger}(\theta)\,|q\rangle\,, \tag{1.47}$$

$$= \int_{-\infty}^{+\infty}\mathcal{W}(q\cos\theta - p\sin\theta, q\sin\theta + p\cos\theta)dp. \tag{1.48}$$

Thereafter, we introduce the Fourier-transformed distribution or *characteristic function* $\tilde{\mathcal{W}}(u,v)$, and the Fourier-transformed position probability distribution $\tilde{\Pr}(\xi,\theta)$:

$$\tilde{\mathcal{W}}(u,v) \equiv \int_{-\infty}^{+\infty}\int_{-\infty}^{+\infty}\mathcal{W}(q,p)e^{-iuq-ivp}dqdp, \tag{1.49}$$

$$\tilde{\Pr}(\xi,\theta) = \int_{-\infty}^{+\infty}\Pr(q,\theta)e^{-i\xi q}dq. \tag{1.50}$$

It is straightforward to show that the Fourier-transformed position probability distribution is the characteristic function in polar coordinates:

$$\tilde{\Pr}(\xi,\theta) = \tilde{\mathcal{W}}(\xi\cos\theta,\xi\sin\theta). \tag{1.51}$$

Moreover, the quantum contribution is taking into account when we substitute the probability as a projection measurement of Eq. 1.47 into Eq. 1.50, where we obtain:

$$\tilde{\Pr}(\xi,\theta) = \mathrm{Tr}[\hat{\rho}\hat{U}^{\dagger}(\theta)e^{-i\xi\hat{q}}\hat{U}(\theta)] \tag{1.52}$$

the above expression is the so-called Weyl operator, and it reads as : $\hat{U}^{\dagger}(\theta)e^{-i\xi\hat{q}}\hat{U}(\theta) = e^{-i\hat{q}\xi\cos\theta - i\hat{p}\xi\sin\theta}$

$$\tilde{\mathcal{W}}(u,v) = \mathrm{Tr}[\hat{\rho}e^{-i\hat{q}\xi\cos\theta - i\hat{p}\xi\sin\theta}]. \tag{1.53}$$

Lastly, computing the trace in coordinate representation, i.e., $\int_{-\infty}^{+\infty}\langle q|\cdots|q\rangle\,dq$, and the Baker-Hausdorff formula we finally get ($q = x - v/2$):

$$\tilde{\mathcal{W}}(u,v) = \int_{-\infty}^{+\infty}e^{-iux}\langle x-\frac{v}{2}\,|\hat{\rho}|\,x+\frac{v}{2}\rangle dx, \tag{1.54}$$

$$\mathcal{W}(q,p) = \frac{1}{2\pi}\int_{-\infty}^{+\infty}e^{ipx}\langle q-\frac{x}{2}\,|\hat{\rho}|\,q+\frac{x}{2}\rangle dx. \tag{1.55}$$

Where, $\mathcal{W}(q,p)$ is the Wigner function a quantum mechanical quasiprobability distribution which is real for hermitian operators.

Others commonly used phase space description in quantum optics are the $Q-$ and $P-$representation. The first, is a description of the density matrix through its diagonal elements in a coherent basis, meanwhile the P distribution represents the density operator as an ensemble of coherent states.

The definition of the normalized ($\int d^2\alpha Q(\alpha,\alpha^*)=1$) Q distribution function is:

$$Q(\alpha,\alpha^*)\equiv\frac{1}{\pi}\left\langle\alpha\right|\hat{\rho}\left|\alpha\right\rangle. \tag{1.56}$$

From the above Eq. 1.56 we can construct the density matrix, once the Q function is known. Let us commence by

$$Q(\alpha,\alpha^*)=\frac{e^{-|\alpha|^2}}{\pi}\sum_{n,m}\frac{\left\langle n\right|\hat{\rho}\left|m\right\rangle\alpha^m\alpha^{*n}}{\sqrt{n!m!}}\equiv\sum_{n,m}Q_{n,m}\alpha^m\alpha^{*n}. \tag{1.57}$$

expanding the exponential and comparing equal powers in α and α^*, we get:

$$\sum_r\frac{Q_{n-r,m-r}}{r!}\pi\sqrt{n!m!}=\left\langle n\right|\hat{\rho}\left|m\right\rangle. \tag{1.58}$$

In general, throughout this thesis we will compute only the Wigner function. In Fig. 1.7 we illustrate a gallery of the Q- and $Wigner$ phase space representation for the vacuum, Fock, coherent, thermal, squeezed, and Schrödinger cat states.

1.3 Quantum Entanglement

Non-relativistic quantum theory was firmly set in the 1920's establishing —among other things— the fundamental limits on the amount of information that one can extract from a system with a single set of measurements. Within this mathematical framework, QM has been proven to be extremely successful experimentally speaking. In other words, it describes accurately the microscopic non-classical world. However, even nowadays the interpretation of QM seems to be an open question among the physics community [Schlosshauer2013]. Certainly, a pivotal point in the interpretation of quantum mechanics goes back to 1935, where in their seminal paper Einstein, Podolsky, and Rosen (EPR) [EPR1935] and E. Schrödinger [Schroedinger1935] claimed that there must exist some elements of reality that, within the mathematical background of quantum mechanics together with the "reality criterion" cannot be described by quantum theory.

At the heart of those papers lies the quantum entity called *verschränkung* or *entanglement*, both names given by Schrödinger. Entanglement is understood as correlations purely of quantum nature between quantum states of the system, *e.g.*,

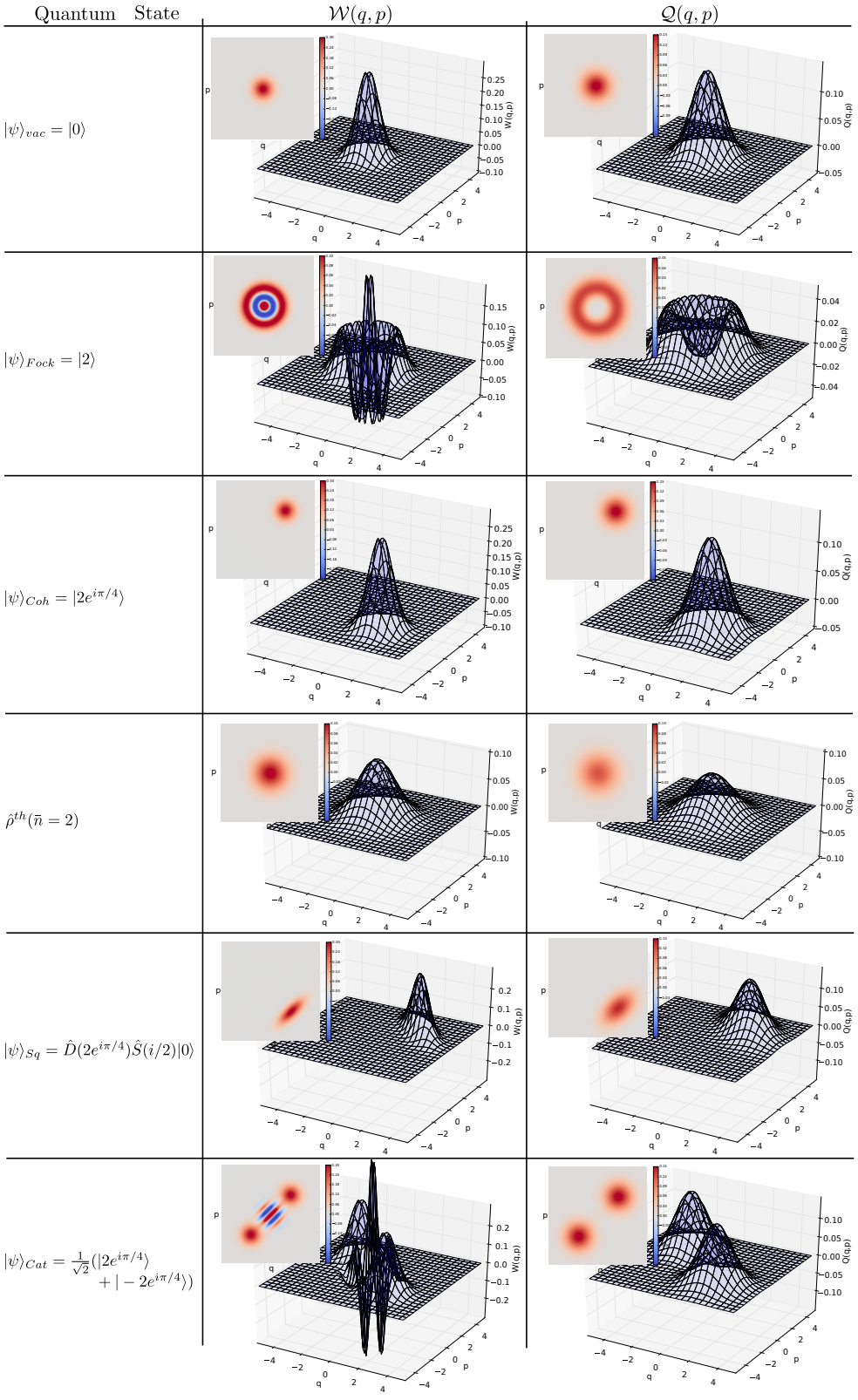

FIGURE 1.7: From top to bottom, we show the *Wigner* and Q phase space distribution for the vacuum, Fock, coherent, thermal, squeezed, and Schrödinger cat states.

position, momentum, polarization, atomic energy levels, etc. Basically, quantum entanglement emerges from the intrinsic non-locality of quantum theory, a feature that can be summarize in the mathematical Hilbert space structure of QM together with the Copenhagen interpretation (an exhaustive review of quantum entanglement can be found in Ref. [Horodecki2009]).

Surprisingly, in quantum information science the quantum entanglement far from being a theoretical curiosity plays a crucial role experimentally, for instance, in quantum algorithms and processing, as well as in quantum teleportation, quantum cryptography, etc. In fact, the bare implementation of quantum entangled states might lead towards quantum tasks that would seem impossible or at least difficult to perform in the classical domain.

1.3.1 Quantum entanglement for pure states

Let us consider two different quantum systems labeled A and B, we say that : $|\psi\rangle_{AB} \in \mathcal{H}_A \otimes \mathcal{H}_B$ is a product state, if there is $|\phi_a\rangle \in \mathcal{H}_A$, and $|\phi_b\rangle \in \mathcal{H}_B$, such that $|\psi\rangle_{AB} = |\phi_a\phi_b\rangle = |\phi_a\rangle \otimes |\phi_b\rangle$. Otherwise, we say that $|\psi\rangle_{AB}$ is an entangled state.

A bipartite vector or pure state can be represented in a joint tensor Hilbert space $\mathcal{H}_{AB} = \mathcal{H}_A \otimes \mathcal{H}_B$ as following:

$$|\psi\rangle_{AB} = \sum_{i,j} c_{i,j} |i\rangle \otimes |j\rangle = \sum_{i,j} c_{i,j} |i,j\rangle \tag{1.59}$$

where, the coefficients c_{ij} corresponds to a specific representation in the chosen basis $\{|i\rangle \in \mathcal{H}_A, |j\rangle \in \mathcal{H}_B\}$. As an example, it is obvious (in the computational basis) that the states $|01\rangle$ and $|10\rangle$ are product states. However, the so-called Bell states defined by:

$$\begin{aligned} \left|\phi^{\pm}\right\rangle &\equiv \frac{1}{\sqrt{2}}(|00\rangle \pm |11\rangle), \\ \left|\psi^{\pm}\right\rangle &\equiv \frac{1}{\sqrt{2}}(|01\rangle \pm |10\rangle) \end{aligned} \tag{1.60}$$

are entangled states, i.e., they cannot be written as in Eq. 1.59.

As said, the most remarkable feature of the entangled states is that they carry quantum correlations (of course, correlations also occur in classical physics). For

instance, a measuring of an observable of an entangled state in the subsystem A will instantaneously affect the state in the subsystem B regardless the distance between parties. A result no longer valid for product states, in other words, the temporal operator evolution for product states acts independently on each subsystem as $\hat{U}(t) = \hat{U}_A(t) \otimes \hat{U}_B(t)$, where the operator $\hat{U}(t)$ is called local operator (LO).

1.3.1.1 Schmidt decomposition

The Schmidt decomposition allows us to know if a pure quantum system is entangled or not. In addition, this decomposition establishes a close relationship between the mixedness of a quantum system and its separability.

Let us commence considering the general bipartite quantum state as in Eq. 1.59:

$$|\psi\rangle_{AB} = \sum_{i,j} c_{i,j} |i,j\rangle , \tag{1.61}$$

where, the coefficients $c_{i,j}$ are elements of $C = \sum_{i=1}^{d_A} \sum_{j=1}^{d_B} c_{i,j} |i\rangle \langle j|$, a $d_A \times d_B$ dimensional matrix.

Using the Singular Value Decomposition theorem, i.e., taking unitary matrices U and V with dimensions $d_A \times d_A$ and $d_B \times d_B$, respectively, we can always write the matrix C in a diagonal form as $C = UDV$, with D being a diagonal matrix of $d_A \times d_B$ dimension with real and positives elements in its diagonal. Hence, the matrix elements of C can be written as:

$$c_{i,j} = \sum_{k=1}^{\min[d_A,d_B]} u_{i,k} d_{k,k} v_{k,j}, \tag{1.62}$$

replacing Eq. 1.62 into Eq. 1.61, we easily get

$$|\psi\rangle_{AB} = \sum_{k=1}^{\min[d_A,d_B]} d_{k,k} |a_k, b_k\rangle , \tag{1.63}$$

where $|a_k\rangle = \sum_{i=1}^{d_A} u_{i,k} |i\rangle$, and $|b_k\rangle = \sum_{j=1}^{d_B} v_{k,j} |j\rangle$. The corresponding density matrix is $\hat{\rho}_{AB} = \sum_{i,k} d_{k,k} d_{i,i} |a_i, b_i\rangle \langle a_k, b_k|$. It is straightforward to calculate the

reduced density matrices,

$$\begin{aligned} \hat{\rho}_A &= \sum_k d_{kk}^2 \left|a_k\right\rangle \left\langle a_k\right|, \\ \hat{\rho}_B &= \sum_k d_{kk}^2 \left|b_k\right\rangle \left\langle b_k\right| \end{aligned} \tag{1.64}$$

where, $0 \leq d_{k,k}^2 \leq 1$ and $\sum_k d_{k,k}^2 = 1$. As a pure state can be defined as $\hat{\rho} = \hat{\rho}^2$, we can notice that in the case of a product state, there is only one Schmidt term different from zero, and equal to one. Conversely, if we have a state with only one Schmidt coefficient, it must be a product state.

Finally, the bipartite quantum state $|\psi\rangle_{AB}$ is a product state if and only if the corresponding reduced density matrices correspond to pure states. This implies that if we have an entangled state, the corresponding reduced density operators must correspond to a mixed state (more than one Schmidt coefficient different from zero). In other words, the quantum entanglement is directly related to the mixedness of the reduced state.

1.3.1.2 Entropy of entanglement

Given a state $|\psi\rangle$, we define the entropy of entanglement $E(\psi)$ as the von Neumann entropy of the reduced density operator:

$$E(\psi) = S(\hat{\rho}_B) = S(\hat{\rho}_A) = -\sum_{k=1}^{d} d_k^2 \log_2 d_k^2. \tag{1.65}$$

In the above equation, we have used that $S(\hat{\rho}) = -\mathrm{Tr}[\hat{\rho}\log_2\hat{\rho}]$, together with Eq.1.64. As seen, the more mixed the reduced density operator is, the more entangled the original state is.

Moreover, the entropy of entanglement cannot increase on the average by local operations. If p_k is the probability of finding $|\psi_k\rangle$ after performing independent measurements in A and B the von Neumann entropy for each subsystem $|\psi_k\rangle$ is related with the von Neumann entropy of the whole system as:

$$E(\psi) \geq \sum_k p_k E(\psi_k). \tag{1.66}$$

The above inequality does not imply that none of the $E(\psi_k)$ can be larger than $E(\psi)$. In fact, this is the key ingredient for the *distillation of quantum entangled states.*

1.3.2 Quantum entanglement for mixed states

We shall denote the set of operators self-adjoint by $A(\mathcal{H})$, and the set of positive operators as $P(\mathcal{H})$, with $P(\mathcal{H}) \subset A(\mathcal{H})$. Additionally, we will denote a linear map $M(\mathcal{H}, \mathcal{H}')$ as $\epsilon : A(\mathcal{H}) \to A(\mathcal{H}')$.

As for pure states, we say that a density matrix $\hat{\rho}$ is a separable state if and only if there are Real numbers $p_k \geq 0$, and vector states $\{|a_k\rangle\}(\{|b_k\rangle\}) \in \mathcal{H}_A(\mathcal{H}_B)$, such that:

$$\hat{\rho} = \sum_k p_k \left|a_k, b_k\right\rangle \left\langle a_k, b_k\right| = \sum_k p_k \hat{\rho}_k^A \otimes \hat{\rho}_k^B. \tag{1.67}$$

As density operators might be written in infinite ways, an attempt to achieve Eq. 1.67 seems to be impossible. To overcome this bottleneck, we can introduce an Entanglement Witnesses (EW). This corresponds to an observable that detects the presence of an entangled state. It is defined as a functional $\hat{W} \in A(\mathcal{H}_A \otimes \mathcal{H}_B)$, such as: If $\hat{\rho}$ is separable, then $\mathrm{Tr}\{\hat{W}\hat{\rho}\} \geq 0, \forall EW$. On the other hand, if $\hat{\rho}_0$ is entangled, then there is an entanglement witnesses W, such that

$$\mathrm{Tr}\{W\hat{\rho}_0\} < 0 \tag{1.68}$$

Although this is a powerful tool, in principle, we do not know how to construct all the possibles entanglement witnesses. Thus, the efforts to construct all W are comparable to checking all the decompositions of $\hat{\rho}$.

1.3.2.1 Positive maps

All physical actions corresponds to positive maps, because they transform density operators into density operators, being always positive.

A linear map $\epsilon \in M(\mathcal{H}, \mathcal{H}')$ is a positive map (PM) if for all $\hat{\rho} \geq 0 \in A(\mathcal{H}), \epsilon(\hat{\rho}) \geq 0$. For instance, the transposition is a PM.

A more general extension reads as follows. Consider a linear map $\epsilon \in M(\mathcal{H}, \mathcal{H}')$ and another Hilbert space $\mathcal{H}''$, we define the extension of ϵ as the linear map $\epsilon \otimes I \in$

$M(\mathcal{H}\otimes\mathcal{H}^{''},\mathcal{H}^{'}\otimes\mathcal{H}^{''})$:

$$(\epsilon\otimes I)\left(\sum_k A_k\otimes B_k\right)=\sum_k \epsilon(A_k)\otimes B_k \tag{1.69}$$

where $A_k\in A(\mathcal{H})$ and $B_k\in A(\mathcal{H}^{''})$. In addition, we say that, a linear map is a completely positive map (CPM) (all CPM corresponds to a physical action), if all the extensions are PM. For entangled states this is crucial, because we must ensure that changes made on the system will preserve the positive character of each subsystem.

Not all PM are CPM, for example the partial transpose. Such maps are particularly useful for detecting entanglement as we will exemplify below. Let us consider the Bell state $\hat{\rho}=|\Phi^+\rangle\langle\Phi^+|$ (an entangled state)

$$\hat{\rho}=\frac{1}{2}(|00\rangle\langle 00|+|00\rangle\langle 11|+|11\rangle\langle 00|+|11\rangle\langle 11|) \tag{1.70}$$

the transposition only of the system A give us:

$$\hat{\rho}^{T_A}=\frac{1}{2}(|00\rangle\langle 00|+|10\rangle\langle 01|+|01\rangle\langle 10|+|11\rangle\langle 11|) \tag{1.71}$$

where, the state $\hat{\rho}^{T_A}$ has negative eigenvalues. The Peres-Horodecki partial transposition criterion is based on the above idea. It reads as following : a density matrix $\hat{\rho}\in A(C^2\otimes C^N)$ with $N\leq 3$ is separable. If and only if $\hat{\rho}^{T_{1,2}}\geq 0$ ($T_{1,2}$ stands for the partial transpose for the first or second subsystem).

In this thesis, we will consider the negativity as the main entanglement measures, as we will eventually also compute the same entanglement for an open system, and negativity is a measure also valid for that case. This quantity is based on the Peres-Horodecki criterion, as $\hat{\rho}^{T_{1,2}}$ will have negative eigenvalues for entangled states, we compute the degree of negativity as follows [Horodecki2009, Vidal2002]:

$$N(t)=\sum_i(|\lambda_i|-\lambda_i), \tag{1.72}$$

where the λ_i are the eigenvalues of the partially transposed bipartite system at fixed time t.

Chapter 2

Entanglement Stabilization in a Non-Linear Qubit-Oscillator System

In this chapter we will study a quartic (undriven) non-linear quantum mechanical oscillator coupled to a spin qubit. To elaborate upon our results, we will present a summary on the conditioned displacement Hamiltonian, i.e., when the position of the oscillator is monitored/conditioned by each spin qubit component.

Firstly, in order to produce an experimentally operational regime of the qubit-oscillator coupling, we will introduce several feasible architectures on hybrid qubit-oscillator (linear) systems under this type of interaction. Thereafter, we will briefly present some typical features on quartic non-linear classical oscillators otherwise known as the Duffing equation. We will also highlight both important features of its quantum counterpart and possible feasible implementations. Subsequently, we will investigate the main results of this study, which is the entanglement dynamics between a qubit coupled to a quartic non-linear mechanical oscillator. Lastly, we explore the entanglement witnessing of the non-linear system, and how the Bell's inequality might be violated under certain restrictions, resulting in a full benchmark of the hybrid quantum entanglement achieved.

The next section regarding two-level systems coupled to mechanics in solid-state physics is based on the academic paper "Hybrid mechanical systems" [Treutlein2015] *where the reader can find a more detailed analysis.*

2.1 Hybrid Linear Quantum-Oscillator Systems

Over the last few decades, the interaction between micro and nano-mechanical resonators in the quantum regime and quantum two-level systems have shown remarkable milestones. For example, a macroscopic mechanical oscillator can be driven into a superposition of spatially separated states, which is a result interesting in itself. Furthermore, qubit-oscillator systems have been proven to be of paramount importance in other applications, such as fast, ultrasensitive force and displacement detectors [Blencowe2000], electrometers [Cleland1998, Erbe2001], and radio frequency signal processors [Wang2000]. In addition, the bare motion of the mechanical oscillator can be used as a sensitive probe to extract information regarding static and dynamical properties of the microscopic quantum system. As we will study in Chapter 4, quantum mechanical oscillators can be used as suitable candidates for light-matter transducers.

In general, qubit-oscillator systems are quite topical in the quantum information field, and have been studied in different operational regimes under several types of interactions. For the purpose of this study we will just focus on a particular type of interaction, namely conditioned displacement Hamiltonian. Here, the interaction is given by $\hat{\sigma}_z \otimes \hat{x}$, where $\hat{\sigma}_z$ is the Pauli-z operator, and $\hat{x}$ is the deviation of the oscillator from its equilibrium position. Hence, the relevant Hamiltonian in the Schrödinger picture reads as:

$$\hat{H} = \hat{H}_q + \frac{1}{2m}\hat{p}^2 + \frac{1}{2}m\omega_m^2\hat{x}^2 - \hbar\lambda\hat{\sigma}_z\hat{x} \tag{2.1}$$

in the above equation ($\hbar$ is the Planck constant), $\hat{H}_q$ is the qubit Hamiltonian. The single-mode mechanical oscillator is characterized by its position $\hat{x}$, momentum $\hat{p}$, mass m, and angular frequency ω_m; λ is the qubit-mechanics coupling strength. Using the expressions in 1.19, we can easily rewrite the Hamiltonian as:

$$\hat{H} = \hat{H}_q + \hbar\omega_m\hat{b}^\dagger\hat{b} - \hbar\lambda\hat{\sigma}_z\hat{x}. \tag{2.2}$$

Eq. 2.2 can be implemented under several schemes (see Fig. 2.1 for a list of solid-state qubits coupled to mechanical resonators). In particular, the linear qubit-oscillator interaction in solid-state systems can be justified due to the strong dependence on the local electrostatic and magnetic field with the qubit. Hence, the gap energy (E_{eg}) between the excited (e) and the ground (g) state of the qubit can be expanded

in Taylor series as : $E_{eg}(\hat{x}) = E^0_{eg} + \partial_x E_{eg}\hat{x} + 1/2 \times \partial^2_x E_{eg}\hat{x}^2 + \ldots$, being $\hat{x} = x_{\text{zpf}} \times (\hat{b}^\dagger + \hat{b})$, as the zero-point fluctuation $x_{\text{zpf}} \approx 10^{-13}m$ is much smaller than other relevant dimensions in the system, the linear approximation is enough to validate the Hamiltonian in Eq. 2.2.

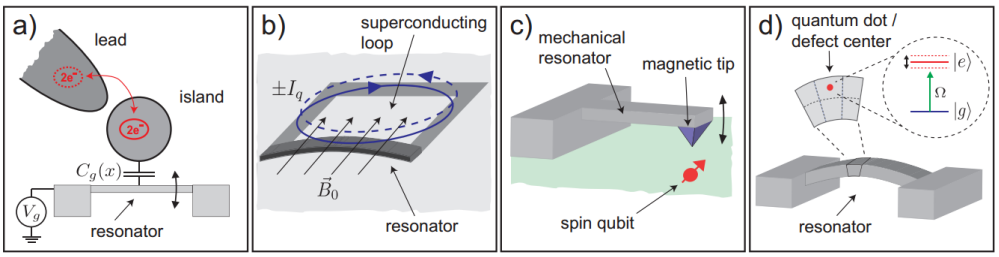

FIGURE 2.1: Four architectures to couple a hybrid qubit-oscillator system via conditioned displacement Hamiltonian. a) A micromechanical resonator capacitively coupled to a quantized charge, b) a qubit encoded in circulating currents in a superconducting loop interacts with an arm of the loop, c) an electronic spin coupled to a quantized motion of a magnetized resonator tip, and d) a deformation potential coupled to quantum dots (a qubit embedded in the material resonator bar). As demonstrated later, the last two schemes have been found to be appropriate candidates to include non-linearities. **This figure was taken from the paper review in Ref. [Treutlein2015].**

Now, let us briefly explore the physical schemes shown in Fig. 2.1 to give an order of magnitude of the qubit-oscillator coupling parameter λ.

Starting with the micromechanical resonator capacitively coupled to a quantized charge shown in Fig. 2.1-a, for instance, it could be a Cooper-pair box or an electron on a quantum dot. In particular, Cooper boxes have attracted much attention since they can mimic a controllable two-level system [Makhlin2001, Echternach2001], being a perfect qubit candidate. Essentially, Cooper boxes are composed of a small superconducting island weakly coupled to a superconducting reservoir [Bouchiat1998, Makhlin2001], characterized by Coulomb charging energy, and the strength of the Cooper-pair tunneling between the island and the reservoir.

When the Cooper box interacts with a cantilever (mechanical oscillator) it causes displacement in the cantilever, whose sign depends on which of the two charge states the Cooper box is in. As it is possible to prepare the Cooper box in a superposition of charge states, it leads to an entangled state between the Cooper box and the oscillator, being in a superposition of spatially separated states. The macroscopicity of this superposition depends on how strong the coupling strength

is. The Hamiltonian corresponds to:

$$\hat{H} = 4E_C\delta n\hat{\sigma}_z - \frac{1}{2}E_J\hat{\sigma}_x + \hbar\omega_m\hat{b}^\dagger\hat{b} + \lambda_{cb}\hat{\sigma}_z(\hat{b}+\hat{b}^\dagger), \tag{2.3}$$

where $\delta n = n_g - (n+1/2)$ with $n_g = -(C_g^c V_g^c + C_g^m V_g^m)/2e$ the dimensionless, total gate charge. The control gate voltage V_g^c and cantilever gate electrode voltage V_g^m ranges are restricted such that $-1/2 \leq \delta n \leq 1/2$ for some chosen n, so that only Cooper charge states $|n\rangle \equiv |-\rangle \equiv \binom{1}{0}$ and $|n+1\rangle \equiv |+\rangle \equiv \binom{0}{1}$ play a role. Thus it is natural to use spin notation where $\hat{\sigma}_x$ and $\hat{\sigma}_z$ are the usual Pauli matrices. The coupling constant between the box and cantilever electrode is $\lambda_{cb} = -4E_C n_g^m \frac{\Delta x_{zpf}}{d}$, where $n_g^m = -C_g^m V_g^m/2e$, Δx_{zpf} is the zero-point fluctuation displacement uncertainty of the cantilever, and $d \gg \Delta x_{zpf}$ is the cantilever electrode-island gap. Only the in-plane fundamental flexural mode of the cantilever, with frequency ω_m and operators $\hat{b}$ and $\hat{b}^\dagger$, is taken into account. All other modes have a much weaker coupling to the box and will be neglected. We assume that the Josephson junction capacitance $C_J \gg C_g^c$ and C_g^m, so that the charging energy of the box $E_C \approx e^2/2C_J$.

Some of the values used in Ref. [Armour2002] are $E_C = 150\mu$eV, $n_g^m \approx -63V_g^m$, $\Delta x_{zpf} \approx 1.4\times10^{-13}$m, $d = 0.1\mu$m. $\lambda_{cb}/\omega_m \approx 0.14 - 0.41$, where $\omega_m = 50$ MHz.

In addition, a qubit system can alternatively be encoded in clockwise and anti-clockwise circulating currents in a superconducting loop as shown in Fig. 2.1-b. The coupling for this scheme is $\hbar\lambda_c \approx B_0 I_q l x_{\mathrm{ZPF}}$. Some typical values are $B_0 \leq$ 10mT for the perpendicular magnetic field to the bending motion, $I_q \approx 100$ nA for the circulating current, and $l \approx 5\mu$m for the length of the resonator. Hence, $\lambda_c/2\pi \approx 0.1 - 1$MHz.

Qubit-oscillator schemes can also be prepared in systems where an electronic spin qubit is coupled to a quantized motion of a magnetized resonator tip as shown in Fig. 2.1-c. The spin qubit can be associated with a nitrogen-vacancy (NV) impurity in diamond and the nano-mechanical resonator to a cantilever of fundamental frequency bending mode ω_r and dimensions (l, w, t) being its length, width, and thickness, respectively. NV centers in diamond are essentially a lattice defect consisting of a nitrogen atom adjacent to a missing carbon, resulting in a defect that might occur naturally or with ion implantation. The long spin coherence time ($\approx$ 20ms), scalability, and precision control (initialized - control - readout) make a perfect candidate for several quantum applications. As a result of the high sensitivity of the spin qubit to the magnetic tip motion, the coherent spin-motion

exchange excitations can lead both to ground state cooling, as well as macroscopic quantum superposition states of the oscillator [Rabl2009], and also to quantum spin transducer [Rabl2010]

As the magnetic tip produces a field $\approx G_m\hat{z} = G_m z_0(\hat{b}+\hat{b}^\dagger)$ ($\hat{b}$ is the boson annihilation operator for the oscillator), the Hamiltonian reads as:

$$\hat{H} = \hat{H}_{NV} + \hbar\omega_r\hat{b}^\dagger\hat{b} + \hbar\lambda_m\hat{\sigma}_z(\hat{b}+\hat{b}^\dagger), \tag{2.4}$$

where $\hat{H}_{NV} = \sum_{i=\pm1} -\hbar\Delta_i \left|i\right\rangle\left\langle i\right| + \hbar\Omega_i/2(\left|0\right\rangle\left\langle i\right| + \left|i\right\rangle\left\langle 0\right|)$ is the spin qubit Hamiltonian, being $\Delta_\pm$ and $\Omega_\pm$ the detunings and the Rabi frequencies of the two microwave transitions [Rabl2009].

The coupling strength $\lambda_m = g_s\mu_B G_m z_0$, where $g_s \approx 2$, μ_B is the Bohr magneton, G_m the magnetic field gradient and z_0 is the zero-point fluctuation. As an example, we will refer to Ref. [Rabl2009], where the authors consider a Si-cantilever of dimensions $(l, w, t) = (3,\ 0.05,\ 0.05)\mu$m with a fundamental frequency of $\omega_r \approx 7$ MHz and a $z_0 \approx 5\times10^{-13}$m. A magnetic tip of size ≈ 100 nm and a magnetic gradient of $G_m \approx 7.8\times10^6$ T/m at a distance $h \approx 25$ nm away from the tip and results in a coupling strength $\lambda_m/2\pi \approx 115$ kHz.

In Ref. [Kolkowitz2012] the NV centers are implanted ~ 5 nm below the surface of a bulk diamond sample. The spin sublevels $|m_s = 0\rangle$ and $|m_s = \pm1\rangle$ of the electronic ground state exhibit a zero-field splitting of ~ 2.87GHz. In the presence of a static magnetic field, the degeneracy between $|+1\rangle$ and $|-1\rangle$ is lifted, allowing us to selectively address the $|0\rangle \rightarrow |1\rangle$ transition with microwave radiation.

Finally, in Fig. 2.1-d the qubit (for instance, quantum dots or defect centers) can be coupled by changing the local lattice configuration of the host material. This deformation is illustrated in where flexural vibrations of the resonator induce a local stress $\sigma \sim z_0 x_{zpf}/l^2$, where l is the resonator length and z_0 is the the distance of the defect from the middle of the beam. The associated level shift is then:

$$\hbar\lambda_l \approx (D_e - D_g) z_0 x_{zpf}/l^2 \tag{2.5}$$

where D_e and D_g are deformation for the ground and excited electronic states. For quantum dots a coupling strength of $\lambda_l \approx 1-10$MHz can be achieved.

2.2 Non-linear Quartic Classical Oscillator

Let us commence introducing some basic notions of classical non-linear oscillators. For our purpose, it will be enough to consider the so-called Duffing oscillator [Duffing1918]. In general, the Duffing equation describes an oscillator with a lossy non-linear oscillator under an external periodical driving force. The equation of motion reads as follows (where we have scaled the below expression by its mass m):

$$\frac{d^2}{d^2t}x(t) + c_1\frac{d}{dt}x(t) + c_2x(t) + c_3x(t)^3 = F_0\cos\omega t \tag{2.6}$$

where, the given constants c_1, c_2, c_3 are the strength of the damping, size of stiffness, and amount of non-linearity in the restoring force, respectively. Predominantly, $c_2 = \omega_0^2$ stands for the natural angular frequency of the oscillator, and F_0 controls the amplitude of the periodic driving force; ω is the angular frequency of the driving force. In the top panel of Fig. 2.2 we have plotted the force exerted on the mass particle in Eq. 2.6 (in absence of damping, the losses has been included by hand being proportional to the velocity of the particle) when $c_3 = \pm 1/1000$ (for plotting purposes we consider $c_2 = 1$). In the bottom panel of Fig. 2.6 we have illustrated its corresponding potential energy.

When all $\{c_i\} \neq 0$ the Eq. 2.6 does not exhibit an analytical solution. However, a damped driven harmonical oscillator can be found quite often in physical systems. For instance, it represents a simple LCR circuit driven with an external voltage. The explicit solution for this case ($c_3 = 0$) reads as:

$$\begin{aligned} x(t) &= \frac{e^{-\frac{1}{2}t\left(\sqrt{c_1^2-4c_2}+c_1\right)}}{2\sqrt{c_1^2-4c_2}\left(c_1^2\omega^2+(c_2-\omega^2)^2\right)}\Big(\sqrt{c_1^2-4c_2}\left(e^{t\sqrt{c_1^2-4c_2}}+1\right)\left(F_0(\omega^2-c_2)\right. \\ &+ \left. x_0(c_1^2\omega^2+(c_2-\omega^2)^2)\right) + c_1\left(e^{t\sqrt{c_1^2-4c_2}}-1\right)\left(x_0\left(c_1^2\omega^2+\left(c_2-\omega^2\right)^2\right)\right. \\ &- \left. F_0\left(c_2+\omega^2\right)\right) \\ &+ 2F_0\sqrt{c_1^2-4c_2}e^{\frac{1}{2}t\left(\sqrt{c_1^2-4c_2}+c_1\right)}\left(c_1\omega\sin(\omega t)+\left(c_2-\omega^2\right)\cos(\omega t)\right)\Big). \end{aligned} \tag{2.7}$$

where we have considered $x(t)|_{t=0} = x_0$ and $dx(t)/dt|_{t=0} = 0$. Another interesting case corresponds to an undamped and unforced particle in an anharmonic potential, in other words, $F_0 = c_1 = 0$. Here, we can easily get a Hamiltonian system from

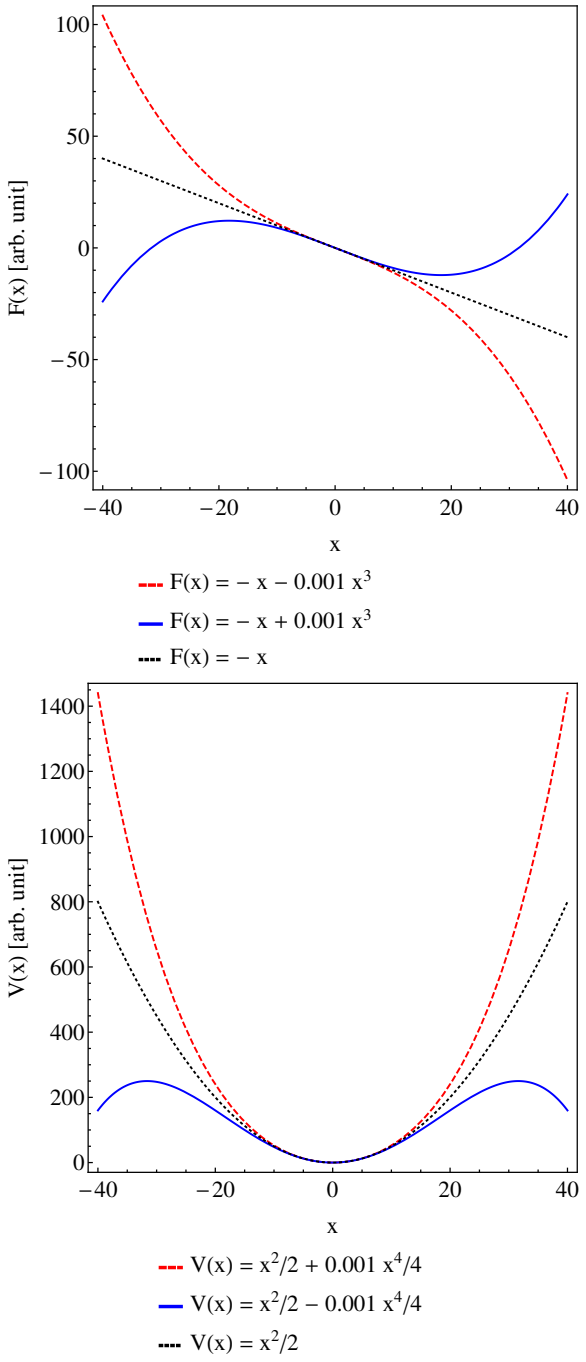

FIGURE 2.2: We illustrate the deviation both from the Hooke's law (top), as well as the potential energy stored in a harmonic oscillator (bottom). For plotting purposes we set $c_2 = 1$, and $c_3 = 1/1000$.

Eq. 2.6 as following:

$$\frac{1}{2}\left(\frac{d}{dt}x(t)\right)^2 + \frac{1}{2}c_2x(t)^2 + \frac{1}{4}c_3x(t)^4 = H = constant. \tag{2.8}$$

To link this with the quantized case, we will only consider the scenario when $c_{2,3} > 0$. In this case, the solution is bounded as:

$$|x(t)| \leq \sqrt{2H/c_2}, \qquad |\dot{x}(t)| \leq \sqrt{2H} \tag{2.9}$$

a full numerical solution it is shown in Fig. 2.3 for a centre shifted potential, i.e., $\frac{d^2}{dt^2}x(t) + c_1\frac{d}{dt}x(t) + c_2x(t) + c_3x(t)^3 + x_0 = F_0\cos(\omega t)$.

2.3 Non-linear Qubit-Oscillator System

As shown in previous sections, two-level quantum systems and quantum harmonic oscillators are the two most basic building blocks due to the remarkable experimental progresses in the accurate control of the interaction in qubit-oscillator systems, including: trapped ions [Blatt2008], cavity-QED [Raimond2006], ultracold atomic Bose-Einstein condensate [Treutlein2007, Hunger2010], quantum dots or Cooper-pair boxes [Hennessy2007, Steele2009, Armour2002, Bose2006], optomechanical systems [Scala2013, Yin2013], superconducting qubits coupled to superconducting resonators [Chiorescu2004, Wallraff2004, Clarke2008], etc. Furthermore, they have been investigated in different qubit-oscillator coupling regimes, including the recently so-called ultrastrong regime, where the qubit-oscillator coupling strength is comparable to the qubit and oscillator energy scales [Grimsmo2013, Ashhab2010, Hausinger2010, Bourassa2009].

In general, the quantum oscillator is modeled harmonically, however this is typically an approximation of more complicated scenarios. In fact, quantum non-linear oscillators (NLO) have been implemented in several settings, including optomechanical systems (where tunable non-linearities have been realized [Sankey2009]), trapped ions (where the trapping potential can be modified to include non-linearities [Home2011]), and atoms in optical lattices [Lewenstein2013]. Interestingly, it has been shown that the inclusion of strong enough non-linearities in the oscillator potential allows new possibilities to generate non-classical states [DiVincenzo2012, Ong2011, Peano2006, Kolkiran2006, Joshi2011, Rips2013]. However, despite the

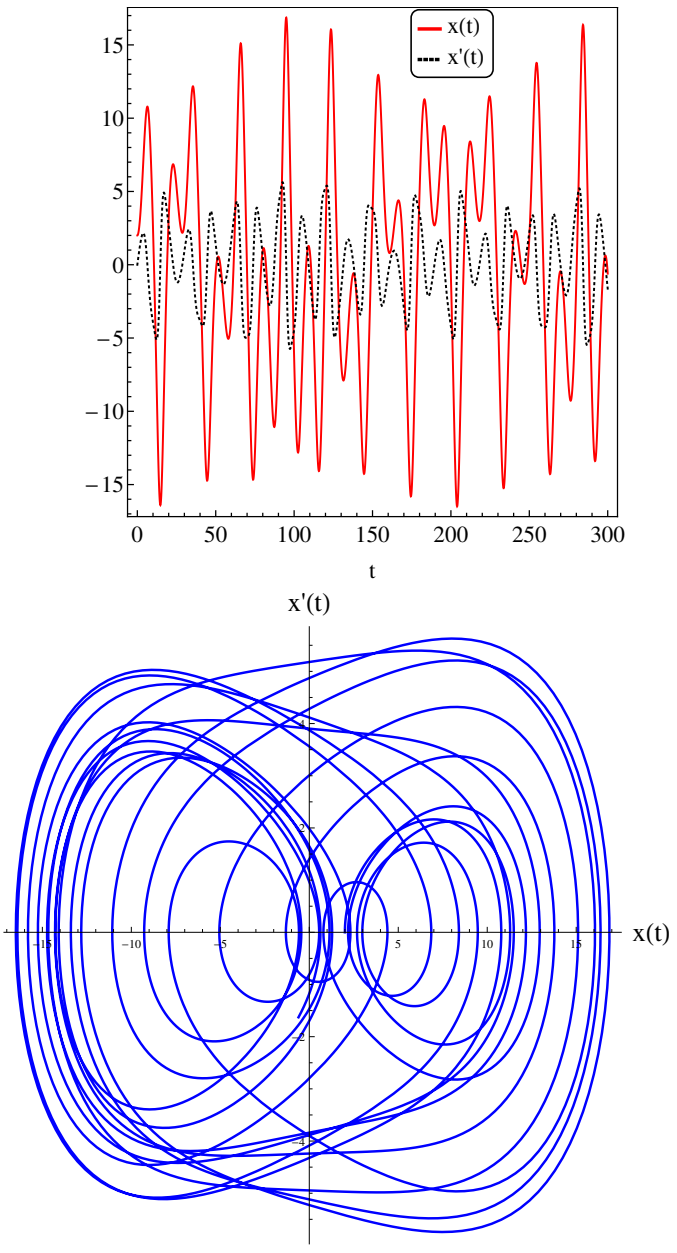

FIGURE 2.3: In the top panel we plot the position (solid red line) and velocity (dashed orange line) of the mass particle subject to a quartic potential. In the bottom panel we illustrate the phase-space of the same situation. The equation considered was : $\frac{d^2}{dt^2}x(t) + 0.001\frac{d}{dt}x(t) + 0.04x(t) + 0.001x(t)^3 + 0.1 = \cos(0.2t)$.

promising experimental progresses in the control and fabrication of NLO, it is still a challenge to achieve significant non-linearities (for a more detailed discussion about the non-linear regimes and their possible experimental implementations see Sec. 2.6). Remarkably, we will show here that also weak non-linearities suffice to provide non-trivial and potentially useful features in the context of a qubit-NLO setting.

In the following, we consider a quantum system composed of a qubit interacting with a quartic (undriven) NLO through a conditional displacement Hamiltonian. In order to contrast our results when the non-linearity is included in the potential, we first solve the simplest case, i.e., a qubit interacting with a quantum harmonic oscillator. In this case, the entanglement is generated periodically as a consequence of the superposition principle. First, by including a weak non-linear perturbation in the oscillator potential, we have obtained analytically the wave function in the rotating-wave approximation — in a regime where both the qubit-NLO coupling as well as the non-linearity strength are small compared to the oscillator frequency. In this case, an explicit Kerr-like term in the evolution appears, generating quadrature squeezing for short times. In particular, we will show that the entanglement generated in this non-linear scenario is larger with respect to the linear case and, in addition, it dynamically reaches a stabilization region. For very large times the oscillator shows an intricate behavior exhibiting negative values in the Wigner distribution.

The second main result of this Chapter is obtained by taking into account a strong qubit-NLO coupling, while still considering a weak non-linear regime. The novelty with respect to previous works is the inclusion of the two- and four-phonon processes, i.e. the full numerical dynamics of the system without any approximation. In this case *i)* the entanglement stabilization region is achieved faster than in the weak qubit-NLO coupling case, and *ii)* the entanglement reaches its maximum value. Finally, we have solved the Markovian master equation, taking into account only the damping of the oscillator, and even in this case the system dynamics remains robust showing the main features just described for a considerable number of cycles.

In section 2.4 we present the system under consideration for the non-dissipative case. In section 2.5 we solve the system in the linear case for the sake of comparison with the results presented in section 2.6 where we consider the full non-linear dynamics. We focus on two regimes: in subsection 2.6.1 we consider the weak qubit-NLO coupling regime, in which an analytical approximation can be obtained for the dynamics of the system wave-function; in subsection 2.6.2 we show the full numerical solution for the strong coupling regime. Furthermore, we present the case when

losses are present in the system and suggest possible experimental implementations. Finally, we give some concluding remarks in section 2.8.

2.4 The Model

We consider a two-level system (qubit) coupled to a quartic non-linear oscillator, as described by the Hamiltonian

$$\hat{H} = \hat{H}_q + \hat{H}_o + \hat{H}_{q-o} \,, \tag{2.10}$$

where $\hat{H}_q$ ($\hat{H}_o$) is the free qubit (NLO) Hamiltonian and $\hat{H}_{q-o}$ is their mutual interaction. Each term above is defined as follows

$$\hat{H}_q = \hbar\omega_q \hat{\sigma}_z, \tag{2.11}$$

$$\hat{H}_o = \frac{1}{2m}\hat{p}^2 + \frac{1}{2}m\omega_o^2\hat{x}^2 + \tilde{\delta}\hat{x}^4, \tag{2.12}$$

$$\hat{H}_{q-o} = -\hbar\tilde{g}\hat{\sigma}_z\hat{x}, \tag{2.13}$$

where $\hbar\omega_q$ corresponds to the qubit separation energy between its ground ($|\downarrow\rangle$) and excited ($|\uparrow\rangle$) states, $\hat{\sigma}_z$ is the usual Pauli z—(pseudo)spin matrix ($\hat{\sigma}_z|\uparrow\rangle = |\uparrow\rangle, \hat{\sigma}_z|\downarrow\rangle = -|\downarrow\rangle$), ω_o is the frequency of the oscillator in absence of non-linearities, $\tilde{\delta}$ is the quartic non-linear strength, whereas $\hat{x}$ and $\hat{p}$ are the usual position and momentum operators, respectively. In Eq. (2.13) the interaction strength is parametrized by $\tilde{g}$ (assumed to be positive throughout) and it is linear in the position operator $\hat{x}$. This type of interaction has been realized/proposed in various experimental settings — including ion traps [Mintert2001], cavity-QED [Solano2003], and nanomechanical resonators [Rabl2009] — and its action can be understood as a displacement of the oscillator conditioned on the state of the qubit. As such, it has been exploited for example as a tool for reconstructing the state of quantum oscillators in various physical systems [Tufarelli2011, Tufarelli2012], or as a mediator to induce qubit-qubit interactions [Mintert2001].

Let us notice that in order for the Hamiltonian (2.12) to be valid, in the following we will consider a modest non-linear quartic perturbation. In particular, we require that $\tilde{\delta}\langle\hat{N}\rangle \ll \omega_o$ during the evolution (where $\langle\hat{N}\rangle$ is the average phonon number for the oscillator), thus ensuring that the single-frequency assumption for the oscillator (ω_o) remains valid.

Using the expressions in Eq. 1.19, rescaling Eq. (2.10) by $\hbar\omega_o$ and switching to the interaction picture with respect to the qubit, the relevant Hamiltonian reads

$$\hat{H}_{int} = \hat{a}^\dagger\hat{a} + \delta(\hat{a}^\dagger + \hat{a})^4 - k\hat{\sigma}_z(\hat{a}^\dagger + \hat{a}), \tag{2.14}$$

where,

$$g = \tilde{g}\sqrt{\frac{\hbar}{2m\omega_o}}, \tag{2.15}$$

$$\delta = \frac{\tilde{\delta}}{\hbar\omega_o}\left(\frac{\hbar}{2m\omega_o}\right)^2, \tag{2.16}$$

$$k = \frac{g}{\omega_o}. \tag{2.17}$$

In general, throughout this work we will consider the following initial state:

$$|\psi(0)\rangle = \frac{1}{\sqrt{2}}(|\uparrow\rangle + |\downarrow\rangle) \otimes |\alpha\rangle\,, \tag{2.18}$$

where the oscillator coherent state is defined as $|\alpha\rangle = \exp\left[\alpha\hat{a}^\dagger - \alpha^*\hat{a}\right]|0\rangle = \hat{D}(\alpha)|0\rangle$ ($\hat{D}(\alpha)$ is the usual displacement operator).

2.5 Dynamics in Absence of Non-linearity

For the sake of comparison with the genuine features of an anharmonic oscillator, we briefly summarize here the results for the case of a simple quantum harmonic oscillator [$\delta = 0$ in Eq. (2.14)]. In order to obtain the time evolution operator for this case, we use a direct consequence of the similarity transformation which holds the following

$$\hat{T} f\left(\{\hat{X}_i\}\right)\hat{T}^\dagger = f\left(\{\hat{T}\hat{X}_i\hat{T}^\dagger\}\right), \tag{2.19}$$

the above equation is satisfied for any function f, unitary operator $\hat{T}$, and arbitrary set of operators $\{\hat{X}_i\}$. Hence we take in particular

$$\hat{T} = e^{-k\hat{\sigma}_z(\hat{a}^\dagger - \hat{a})}, \tag{2.20}$$

$$f\left(\{\hat{X}_i\}\right) = \hat{U}(t) = e^{-it\hat{H}_{int}} \tag{2.21}$$

here $\{\hat{X}_i\} = \{\hat{a}, \hat{\sigma}_z\}$. Using the Baker-Campbell-Hausdorff (BCH) relation, it is straightforward to show the following transformations

$$\hat{T}\hat{a}\hat{T}^\dagger = \hat{a} + k\hat{\sigma}_z, \tag{2.22}$$

$$\hat{T}\hat{\sigma}_z\hat{T}^\dagger = \hat{\sigma}_z. \tag{2.23}$$

Using both the Similarity Transformation as well as the BCH relation, it is easy to obtain the analytical expression for the time evolution operator

$$\hat{U}(t) = \exp\left[ik^2(t - \sin(t))\right] \exp\left[k\hat{\sigma}_z(\eta\hat{a}^\dagger - \eta^*\hat{a})\right] \exp\left[-i\hat{a}^\dagger\hat{a}t\right] \tag{2.24}$$

where,

$$\eta = 1 - \exp\left[-it\right]. \tag{2.25}$$

Therefore, the time evolution for the initial state (Eq. (2.18)) corresponds to

$$|\psi(t)\rangle = \frac{1}{\sqrt{2}}|\uparrow\rangle \otimes \hat{D}(k\eta)\hat{D}(\alpha e^{-it})\,|0\rangle + \frac{1}{\sqrt{2}}|\downarrow\rangle \otimes \hat{D}(-k\eta)\hat{D}(\alpha e^{-it})\,|0\rangle\,, \tag{2.26}$$

taking into account that $\hat{D}(\alpha_1)\hat{D}(\alpha_2) = \exp\left[(\alpha_1\alpha_2^* - \alpha_1^*\alpha_2)/2\right]\hat{D}(\alpha_1 + \alpha_2)$, we can finally obtain

$$|\psi(t)\rangle = \frac{1}{\sqrt{2}}(e^{ik\alpha\sin(t)}|\uparrow\rangle \otimes |\alpha_\uparrow\rangle + e^{-ik\alpha\sin(t)}|\downarrow\rangle \otimes |\alpha_\downarrow\rangle) \tag{2.27}$$

where

$$|\alpha_\uparrow\rangle = \left|\alpha e^{-it} + k\eta\right\rangle, \tag{2.28}$$

$$|\alpha_\downarrow\rangle = \left|\alpha e^{-it} - k\eta\right\rangle \tag{2.29}$$

The above solution implies that the wave function is periodic and, in particular, the initial separable state is recovered at times $2\pi n$, n being an integer. On the other hand, for $0 < t < 2\pi$, the oscillator is entangled with the qubit — this hybrid entanglement reaching its maximum at time $t = \pi$. In order to quantify the entanglement we use the negativity (see Section 1.3.2). The time dependence is shown in Fig. 2.4 for a fixed coherent state ($\alpha = 2$) and different couplings k. A similar dynamics has been reported in analogous optomechanical settings (see *e.g.* Ref. [Bose1999a]). It is of relevance to notice at this stage that the

entanglement generated so far is due only to the interlinked dynamics of the qubit and the oscillator, as generated by the conditional displacement of Eq. (2.13). In the next section we will add another type of entanglement source to the system when a non-linearity is added.

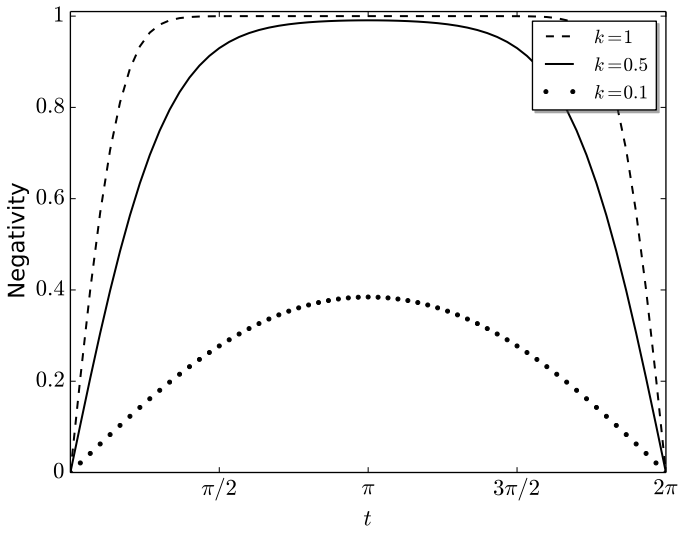

FIGURE 2.4: Time dependence of the Entanglement negativity for different values of k in absence of non-linearities in the NLO potential. Starting from the separated state given by Eq. (2.18) ($\alpha = 2$) the system becomes entangled ($0 < t < 2\pi$), reaching a maximum at $t = \pi$. Finally, at $t = 2\pi$ the system return to its original state, thus the negativity is zero. In this and all the figures, t is a scaled time, corresponding to the actual time multiplied by ω_o.

The periodicity of the system can be also appreciated from the reduced density matrix for the qubit $\hat{\rho}_q = \mathrm{Tr}_{osc}(|\psi(t)\rangle\langle\psi(t)|)$:

$$\hat{\rho}_q = \frac{1}{2}\left[|\uparrow\rangle\langle\uparrow| + \mathrm{e}^{4k^2(\cos(t)-1)}(|\uparrow\rangle\langle\downarrow| + |\downarrow\rangle\langle\uparrow|) + |\downarrow\rangle\langle\downarrow|\right] \tag{2.30}$$

given that $\langle\hat{\sigma}_z\rangle = 0$, we can easily plot in Fig. 2.5 the Bloch sphere top-view of the Bloch vector of $\hat{\rho}_q$.

Another feature immediately evident from the solution in Eq. (2.27) is that the dynamics of each qubit eigenstate is linked to that of a coherent state during the evolution (*e.g.*, the eigenstate $|\uparrow\rangle$ is linked to $\left|\alpha e^{-it} + k\eta\right\rangle$). In order to better appreciate this behavior, as well as the oscillator dynamics, we have calculated the Wigner function of the reduced density operator for the oscillator $\hat{\rho}_{osc} = \mathrm{Tr}_q\left[|\psi(t)\rangle\langle\psi(t)|\right]$. In Fig. 2.6 we plot the Wigner function of the reduced density operator for the NLO associated with the Eq. (2.27). As we can see, if the initial state is $|\downarrow, \alpha\rangle$ the

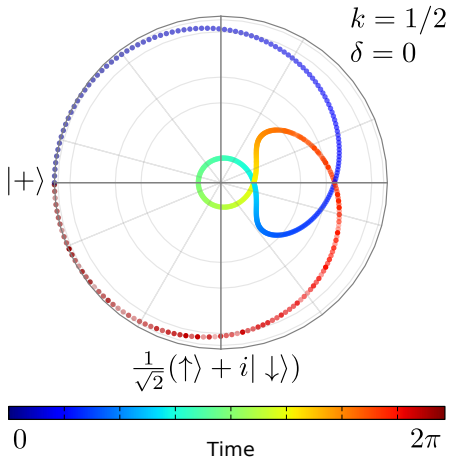

FIGURE 2.5: Dynamics of the reduced density operator for the qubit state in the Bloch Sphere (top-view) with $k = 0.5, \alpha = 2, \delta = 0$. We can see that in absence of non-linearities the qubit dynamics remains periodically for the whole evolution. Here, the leftmost (lowermost) point of the $x-$axis ($y-$axis) represents the state $|+\rangle = \frac{1}{\sqrt{2}}(|\uparrow\rangle + i|\downarrow\rangle)$.

oscillator's Wigner function rotates in a larger circle with respect to the $|\uparrow, \alpha\rangle$ initial state.

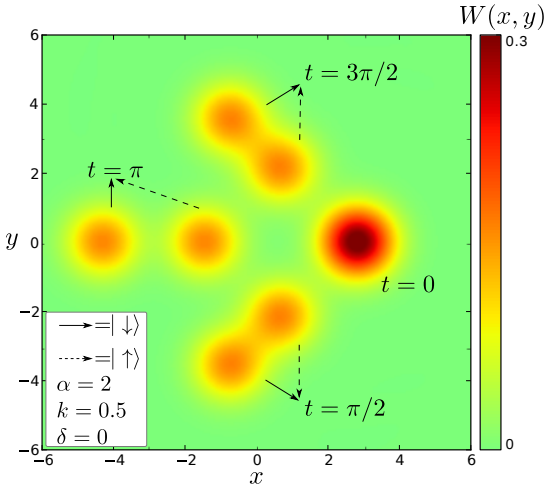

FIGURE 2.6: The figure shows the Wigner function $W(x, y)$ of the reduced density operator for the NLO associated with the Eq. (2.27). The single peak of the initial coherent states separates into two components, each associated with a different qubit eigenstate. Specifically, the solid line arrow (dashed line arrow) indicates the component associated with $|\downarrow\rangle(|\uparrow\rangle)$. The Wigner function is defined as $W(x,y) = \frac{1}{\pi\hbar}\int_{-\infty}^{\infty} \langle x + x'|\hat{\rho}_{osc}|x - x'\rangle\, e^{-2iyx'/\hbar} dx'$.

2.6 Non-linear Dynamics

We will now derive the central results of this work. In particular, in Sec. 2.6.1 we study the evolution for the weak coupling regime ($\{k, \delta\} \ll 1$), where an approximated analytical expression for the wave-function can be obtained. In Sec. 2.6.2 we present the general results in the strong coupling regime ($i.e., k \approx 1, \delta \ll 1$), considering as well the detrimental effects of noise.

2.6.1 Weak qubit-NLO coupling regime : Approximated analytical solution for k $\ll 1, \delta \ll 1$

We will refer to the weak coupling regime when the rescaled qubit-NLO coupling strength is much lower than the qubit and oscillator free energies. In order to investigate the perturbation in the NLO we rewrite the quartic term as follows

$$(\hat{a}^\dagger + \hat{a})^4 = \hat{\mathcal{A}}_4 + \hat{\mathcal{A}}_2 + \hat{\mathcal{A}}_{ns}, \tag{2.31}$$

where we have emphasized the phonon process contributions; namely, $\hat{\mathcal{A}}_{i=2,4,ns}$ correspond to the operators identifying two- and four-phonon transitions and the number-state contribution (ns), respectively. Considering the commutation rule $[\hat{a}, \hat{a}^\dagger] = 1$ one obtains

$$\hat{\mathcal{A}}_4 = \hat{a}^{\dagger 4} + \hat{a}^4, \tag{2.32}$$

$$\hat{\mathcal{A}}_2 = 6(\hat{a}^{\dagger 2} + \hat{a}^2) + 4(\hat{a}^{\dagger 2}\hat{a}^\dagger\hat{a} + \hat{a}^\dagger\hat{a}\hat{a}^2), \tag{2.33}$$

$$\hat{\mathcal{A}}_{ns} = 6((\hat{a}^\dagger\hat{a})^2 + \hat{a}^\dagger\hat{a}), \tag{2.34}$$

and the Hamiltonian in Eq. (2.14) reads as

$$\hat{H} = (1 + 6\delta)\hat{a}^\dagger\hat{a} + 6\delta(\hat{a}^\dagger\hat{a})^2 - k\hat{\sigma}_z(\hat{a}^\dagger + \hat{a}) + \delta(\hat{\mathcal{A}}_2 + \hat{\mathcal{A}}_4).$$

In the equation above, the terms $\{\hat{\mathcal{A}}_2, \hat{\mathcal{A}}_4\}$ are the two- and four-phonon transitions respectively, and they can both be neglected by invoking a rotating wave approximation. By considering a frame rotating with the free oscillator Hamiltonian, one

can recast Eq. (2.35) as

$$\begin{aligned}\hat{H}_{\rm int} = 6\delta\hat{a}^\dagger\hat{a} + 6\delta(\hat{a}^\dagger\hat{a})^2 \quad &- \quad k\hat{\sigma}_z\left(\hat{a}^\dagger e^{+it} + \hat{a}e^{-it}\right) \\ &+ \quad \delta\left(6e^{+2it}\hat{a}^{\dagger^2} + 4e^{+2it}\hat{a}^{\dagger^2}\hat{a}^\dagger\hat{a} + e^{+4it}\hat{a}^{\dagger^4} + H.c.\right)\end{aligned} \tag{2.35}$$

Among the terms proportional to the non-linearity strength δ, the oscillating ones can be approximately neglected. Thus, transforming back to the Schrödinger picture, one has the following Hamiltonian:

$$\hat{H}_{\rm RWA} \approx (1+6\delta)\hat{a}^\dagger\hat{a} + 6\delta(\hat{a}^\dagger\hat{a})^2 - k\hat{\sigma}_z(\hat{a}^\dagger + \hat{a}) \tag{2.36}$$

Using the same techniques as before we obtain the following solution for the wave function, where we have neglected the terms proportional to $\{k\delta, k^2\delta, k^3\delta\}$ (for simplicity we have considered real amplitudes for the coherent state).

Let us consider the following approximation

$$\hat{T}\hat{U}(t)_{app}\hat{T}^\dagger \approx \exp[-it(1+6\delta)\hat{a}^\dagger\hat{a} - 6i\delta t(\hat{a}^\dagger\hat{a})^2], \tag{2.37}$$

where we have neglected products proportional to $\{k\delta, k^2\delta, k^3\delta\} \ll 1$. Taking into account that

$$\exp[-it(1+6\delta)\hat{a}^\dagger\hat{a}]\hat{T} = \exp[-k\hat{\sigma}_z(\hat{a}^\dagger e^{-i(1+6\delta)t} - \hat{a}e^{i(1+6\delta)t})]\exp[-i(1+6\delta)t\hat{a}^\dagger\hat{a}]. \tag{2.38}$$

Multiplying on the left by $\hat{T}^\dagger$ and on the right by $\hat{T}$ the Eq. (2.37), we can finally obtain the time evolution operator

$$\begin{aligned}\hat{U}_{app} \quad &= \quad \exp[-k\hat{\sigma}_z(\hat{a} - \hat{a}^\dagger)\exp[-6\delta it(\hat{a}^\dagger\hat{a})^2]\exp[-k\hat{\sigma}_z(\hat{a}^\dagger e^{-i(1+6\delta)t} - \hat{a}e^{i(1+6\delta)t})] \\ &\times \quad \exp[-i(1+6\delta)t\hat{a}^\dagger\hat{a}].\end{aligned} \tag{2.39}$$

Using the above, it is straightforward obtain the wave function for this case

$$\begin{aligned} |\psi(t)\rangle &= \frac{e^{k(\hat{a}^\dagger-\hat{a})}}{\sqrt{2}}\exp\left[-6it\delta(\hat{a}^\dagger\hat{a})^2\right]\exp\left[\frac{k}{2}(\alpha-\alpha^*)\right]|\uparrow\rangle\otimes\left|e^{-i(1+6\delta)t}(\alpha-k)\right\rangle \\ &+ \frac{e^{k(\hat{a}-\hat{a}^\dagger)}}{\sqrt{2}}\exp\left[-6it\delta(\hat{a}^\dagger\hat{a})^2\right]\exp\left[\frac{k}{2}(\alpha^*-\alpha)\right]|\downarrow\rangle\otimes\left|e^{-i(1+6\delta)t}(\alpha+k)\right\rangle \end{aligned} \tag{2.40}$$

In general we have taken a real amplitude for the coherent state ($\alpha = 2$), hence the phase appearing in Eq. (2.40) vanishes giving us the Eq. (2.41).

$$\begin{aligned} |\psi(t)\rangle &= \frac{1}{\sqrt{2}}\hat{D}(+k)\exp\left[-6it\delta(\hat{a}^\dagger\hat{a})^2\right]|\uparrow\rangle\otimes|\tilde{\alpha}_\uparrow\rangle \\ &+ \frac{1}{\sqrt{2}}\hat{D}(-k)\exp\left[-6it\delta(\hat{a}^\dagger\hat{a})^2\right]|\downarrow\rangle\otimes|\tilde{\alpha}_\downarrow\rangle \end{aligned} \tag{2.41}$$

where,

$$|\tilde{\alpha}_\uparrow\rangle = \left|e^{-i(1+6\delta)t}(\alpha-k)\right\rangle, \tag{2.42}$$

$$|\tilde{\alpha}_\downarrow\rangle = \left|e^{-i(1+6\delta)t}(\alpha+k)\right\rangle. \tag{2.43}$$

A comparison between the approximate analytical results in Eq. (2.41) versus a numerical computation using the full original Hamiltonian in Eq. (2.14) is shown for short times in Fig. 2.7-a, where we plot the negativity for $k = 1/100$ and $\delta = 1/1000$ (for $\alpha = 2$). As we can see, the analytical approximation agrees reasonably well with the numerical results (the dotted line corresponds to the dynamics of the system in absence of non-linearity). More importantly, the presence of a non-linear Kerr-like term proportional to $(\hat{a}^\dagger\hat{a})^2$ represents a new source for entanglement and non-classical effects, allowing to grasp the main features associated with the full Hamiltonian. The first of these features is the lack of a periodic behavior for short times which implies, in particular, that the entanglement does not decrease to zero. In addition, the actual values of the negativity show a clear *enhancement of the entanglement* with respect to linear case ($\delta = 0$). Remarkably, as shown in Fig. 2.7-b, after few cycles the negativity reaches a plateau, implying a *time-stabilization of the entanglement* at values higher than the maximum attained for $\delta = 0$. For longer time-scales ($t \gg 120\pi$), the expected collapses and revivals appear only assuming both the rotating-wave approximation and small $k\delta$. On the

other hand, the full numerical solution of the evolution does not show any collapse nor revival—in fact, the negativity never drops to zero. Due to the establishment of a stabilization window, we can define the width of the time plateau (Δ) as the region in which the negativity does not show significant oscillations; e.g., in Fig. 2.7-b a plateau is approximately achieved for $30\pi \leq t \leq 70\pi$, being its width $\Delta \approx 40\pi$. The dependence between Δ and δ eludes analytical calculations, however a straightforward numerical evaluation (under the constraints of $\{k, \delta\} \ll 1$) shows the dependence to be inversely proportional to the non-linearity strength—in fact, for $10^{-4} < k < 10^{-2}$ and $10^{-4} < \delta < 10^{-2}$, one can show that $\Delta \approx 0.1/\delta$.

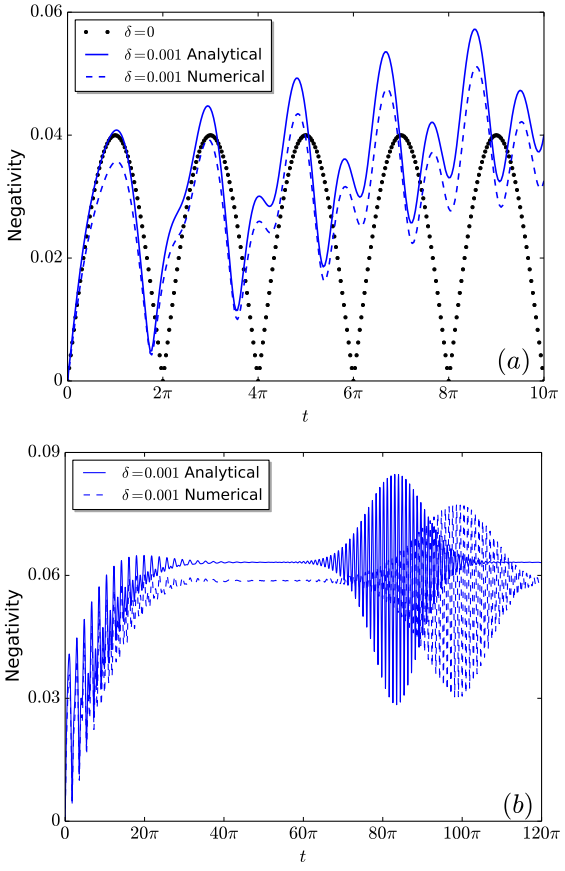

FIGURE 2.7: (a) negativity as function of time t for $k = 1/100$ and $\delta = 1/1000$ ($\alpha = 2$). We compare the entanglement using an analytical expression (solid line) (Eq. (2.41)) and the numerical one (dashed line) using Eq. (2.35). The dotted line is the evolution in absence of non-linearity. As we can see the inclusion of the non-linear term increases the entanglement reaching a time-plateau or stabilization zone. (b) We compare the analytical expression with the numerical solution for the same set of parameters for larger times.

We plot in Fig. 2.8-a the Wigner function for the NLO. For short times, we see that due to the weak coupling the two components of the Wigner function associated with

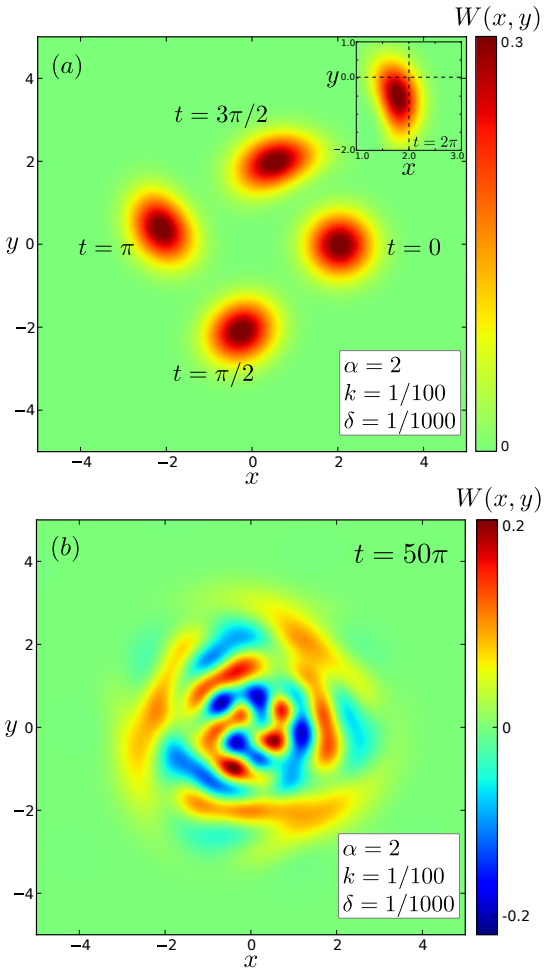

FIGURE 2.8: (a) The above figure shows the Wigner function ($W(x,y)$) for the oscillator state for $t = 0, \pi/2, \pi, 3\pi/2, 2\pi$. The state considered here is the one in Eq. (2.41). As we can see, in the first cycle, due to the small values of k and δ both components of the qubit remains superposed during all time, showing squeezing in the quadratures $\{x, y\}$. (b) The below figure shows the state at $t = 50\pi$, as we see the state becomes complex evidencing negatives values during the dynamics.

the qubit eigenstates are superposed (*i.e.* $|\tilde{\alpha}_\uparrow\rangle \approx |\tilde{\alpha}_\downarrow\rangle$). As anticipated, in contrast with the linear case we can see that the presence of the additional Kerr-like term gives rise to non-classical features. In particular Fig. 2.8-a shows the emergence of quadrature squeezing, with squeezing axes that rotate clockwise in the xy-plane. Defining two arbitrary canonical quadratures (ϕ is the angle of rotation measured from the x-axis to x_r-axis)

$$\hat{x}_r = \frac{1}{2}\left(\hat{a}e^{-i\phi} + \hat{a}^\dagger e^{i\phi}\right), \tag{2.44}$$

$$\hat{y}_r = \frac{1}{2i}\left(\hat{a}e^{-i\phi} - \hat{a}^\dagger e^{i\phi}\right). \tag{2.45}$$

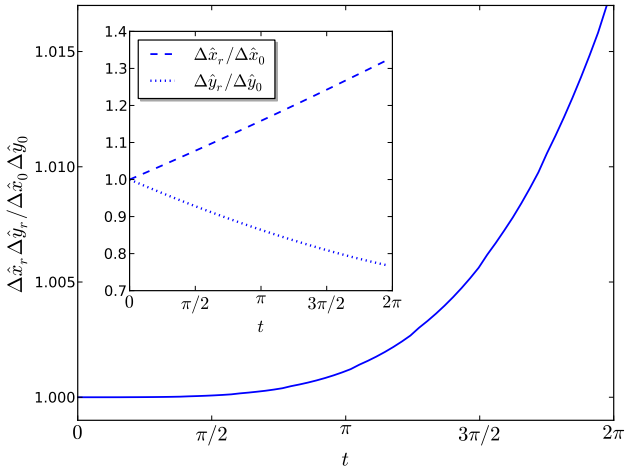

FIGURE 2.9: The main plot shows $(\Delta\hat{x}_r\Delta\hat{y}_r/\Delta\hat{x}_0\Delta\hat{y}_0)$ the normalized uncertainty relation for the first cycle in the weak coupling regime. The sudden increasing in time shows the short period in which the squeezing remains valid. The subplot shows the individual normalized variance, the quadrature x_r (y_r) becomes linearly increasing (decreasing).

we numerically find for each time t the angle ϕ that minimize the uncertainty of $\Delta\hat{y}_r$ (where $\Delta\hat{O} = \langle\hat{O}^2\rangle - \langle\hat{O}\rangle^2$). The results are given in Fig. 2.9 and quantitatively demonstrate the presence of squeezing for short times (the results are normalized with respect to the coherent state uncertainty $\Delta\hat{x}_0 = \Delta\hat{y}_0 = 1/2$).

Another interesting feature is that whereas for short times the Wigner function remains positive, for longer times it assumes negative values. Interestingly, the appearance of relevant negative regions corresponds to the stabilization zone of the negativity — for example at $t = 50\pi$ (see Fig. 2.8-b).

2.6.2 Strong qubit-NLO coupling regime : Numerical solution for $\mathbf{k \approx 1, \delta \ll 1}$.

In this section, we solve numerically the full dynamics involving the Hamiltonian in Eq. 2.14 without restricting to the weak coupling regime. In order to do that, we have expanded the oscillator state in the Fock basis, properly truncated to obtain a sufficient numerical accuracy as it is shown in Fig. 2.10.

Regarding the generation of entanglement between the qubit and the NLO, the effects of a strong coupling are that the two main features that we have individuated in the previous section are further enhanced. First, the entanglement negativity reaches higher values with respect to the absence of non-linearities. Second, the

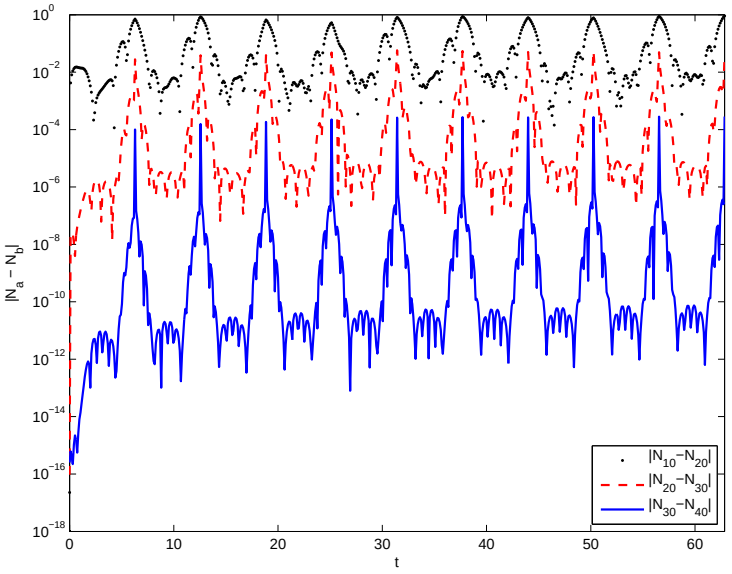

FIGURE 2.10: The figure shows $|N_a - N_b|$ (in logarithmic scale) as a function of time, where N_x corresponds to the negativity truncated to a maximal Fock basis given by x. For instance, N_3 means that the oscillator's field is expanded as $\{|0\rangle, |1\rangle, |2\rangle, |3\rangle\}$. In our calculations we have considered 50 as the maximum Fock state expansion (N_{50}).

entanglement reaches the stabilization region faster then for the weak coupling regime. As an example, we have plotted in Fig. 2.11 the negativity for $k = 0.5, \alpha = 2$, and two values for $\delta = \{1/100, 1/1000\}$. We can see that the negativity stabilizes already for $t \approx 5\pi$ ($\delta = 1/100$) close to the maximal reachable value of 1. This stability is sustained quite well in a window of time from $t = 5\pi$ to $t = 10\pi$, after which it starts to oscillate. Remarkably, in this regime the collapse and revival dynamics is entirely absent. The combination of a high amount of entanglement and the suppression of negativity oscillations provides a long time window in which the entanglement is maximal or near-maximal, in strong contrast to the linear case where maximal negativity is achieved only at defined times (odd multiples of $t = \pi$). Here timing selection is no longer a concern in order to achieve high negativity, representing in turn a relevant practical advantage.

Furthermore, it is important to note in the subplot in Fig. 2.11, that we have also considered the contribution of approximated Hamiltonian regarding to only number-state contribution and up to two-phonon transitions in the dynamics (see Eq. 2.31). As we can see in solid line, the full dynamics —i.e including up to four-phonon transitions— provides an entanglement plateau in time domain better than the other approximated cases.

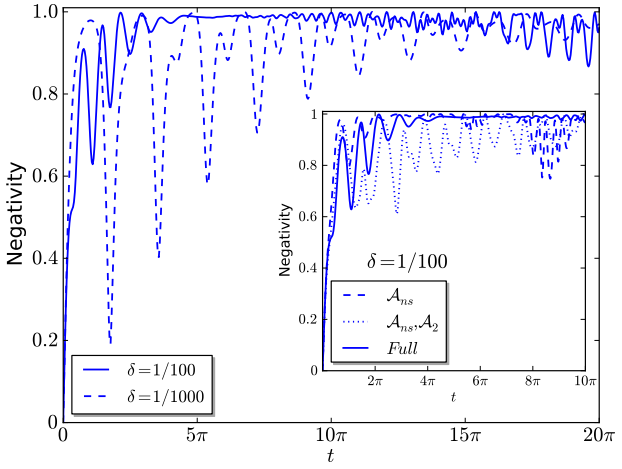

FIGURE 2.11: In the main plot we show the numerical results for the negativity for $k = 0.5, \alpha = 2$ and varying δ. In contrast with $\{k, \delta\} \ll 1$, here we have achieved a higher entanglement as well as a faster stabilization zone. In the subplot we compare the entanglement generated for $k = 0.5, \alpha = 2, \delta = 1/100$ using approximated Hamiltonian, the solid line is for a full Hamiltonian without approximation. The dashed line consider only number states in the quartic potential, and finally the dotted line consider up to four-phonon transitions in the quartic potential.

In order to better understand the enhancement of the qubit-NLO entanglement we have calculated the Wigner function of the oscillator state conditioned to the two qubit eigenstates *i.e.*, $\hat{\rho}(t)^{osc}_{\uparrow} = \langle\uparrow|\,\hat{\rho}(t)\,|\uparrow\rangle$ (or $\hat{\rho}(t)^{osc}_{\downarrow} = \langle\downarrow|\,\hat{\rho}(t)\,|\downarrow\rangle$). In Fig. 2.12, we have plot $W_{\uparrow,\downarrow}(x,y) = \frac{1}{\pi\hbar}\int_{-\infty}^{\infty}\left\langle x+x'\right|\hat{\rho}^{osc}_{\uparrow,\downarrow}\left|x-x'\right\rangle e^{-2iyx'/\hbar}dx'$ at $t = 2\pi, 4\pi, 6\pi, 10\pi, 15\pi$ for each qubit component, together with their product. We can see that the overlap between the two functions sensibly decades already after the first cycle ($t = 2\pi$). In order to show this quantitatively we illustrates in Fig. 2.12-c the overlap of the product $W_{\uparrow}(x,y)W_{\downarrow}(x,y)$ together with its integration over all $xy-$phase space

$$w_p = \int_{-\infty}^{+\infty}\int_{-\infty}^{+\infty} W_{\uparrow}(x',y')W_{\downarrow}(x',y')dx'dy'. \tag{2.46}$$

In other words, this shows that the conditioned Wigner functions $W_{\uparrow,\downarrow}(x,y)$ correspond to two almost orthogonal states which implies that maximally entanglement can be established between the qubit and the oscillator. The quasi-orthogonality is quantified using Eq. (2.46) and shown in Fig. 2.12-c.

As before, we also calculated numerically the reduced density matrix for the qubit. In the presence of non-linear coupling, the qubit exhibits an open cycle whose precession depends on the strength of the non-linearity. For $\delta \ll 1/1000$ the reduced qubit evolution tends to the quantum harmonic potential case, and therefore each cycle is closed. On the other hand, as δ increases, the qubit reaches a stationary point at times comparable to the entanglement stabilization region (see Fig. 2.13).

Finally, we considered the detrimental effects of noise in the dynamics of the NLO. We modeled the system with the following master equation in Lindblad form at zero temperature

$$\dot{\hat{\rho}}(t) \;=\; -i[\hat{H}_s,\hat{\rho}(t)] + \frac{\gamma}{2}(2\hat{a}\hat{\rho}(t)\hat{a}^{\dagger} - \hat{a}^{\dagger}\hat{a}\hat{\rho}(t) - \hat{\rho}(t)\hat{a}^{\dagger}\hat{a}) \tag{2.47}$$

where γ is the oscillator damping rate. In Fig. 2.14 we show the main effects of the losses. We can see that in the strong coupling regime the presence of the environment degrades the qubit-NLO entanglement but the main features observed in the previous sections are still present. In particular, both the enhancement of entanglement with respect to the linear case and the entanglement stabilization are robust for small losses.

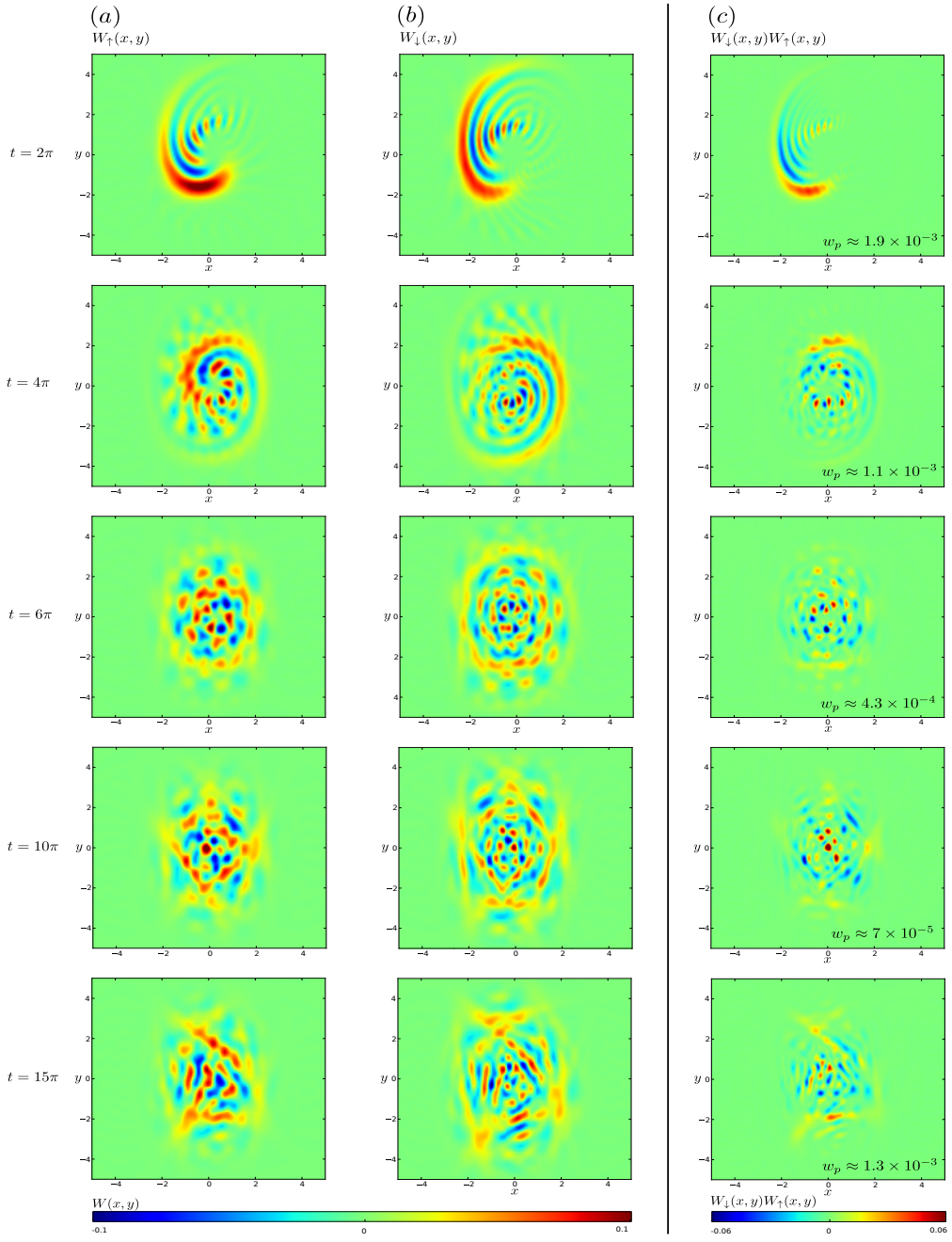

FIGURE 2.12: Here we provide a pictorial explanation for the entanglement enhancement for $k = 0.5, \alpha = 2, \delta = 1/100$ at different times $t = 2\pi, 4\pi, 6\pi, 10\pi, 15\pi$. In Figs. (a) and (b), we plot the Wigner function for the oscillator state for each spin component $W_{\uparrow,\downarrow}(x, y)$. In column (c), we show the product between $W_\uparrow(x, y)$ and $W_\downarrow(x, y)$. The number w_p in the corner corresponds to the integration of the product over all the $xy-$phase space (Eq. 2.46). The small overlap between $W_\uparrow(x, y)$ and $W_\downarrow(x, y)$ then shows that the states corresponding to the latter are quasi-orthogonal, thus allowing for the establishment of maximal entanglement.

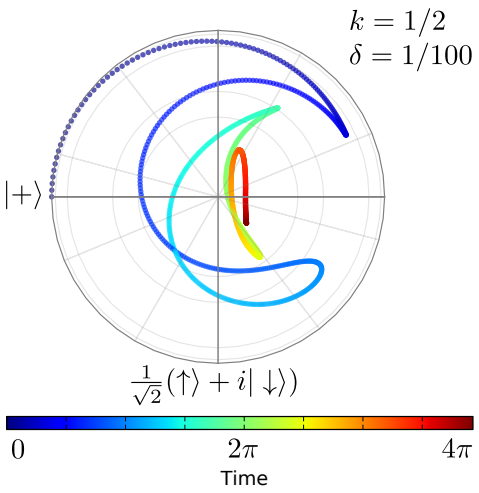

FIGURE 2.13: We illustrate the reduced density qubit operator in Bloch Sphere (top-view) for two cycles $0 \leq t \leq 4\pi$. The qubit shows a strong precession in the dynamics.

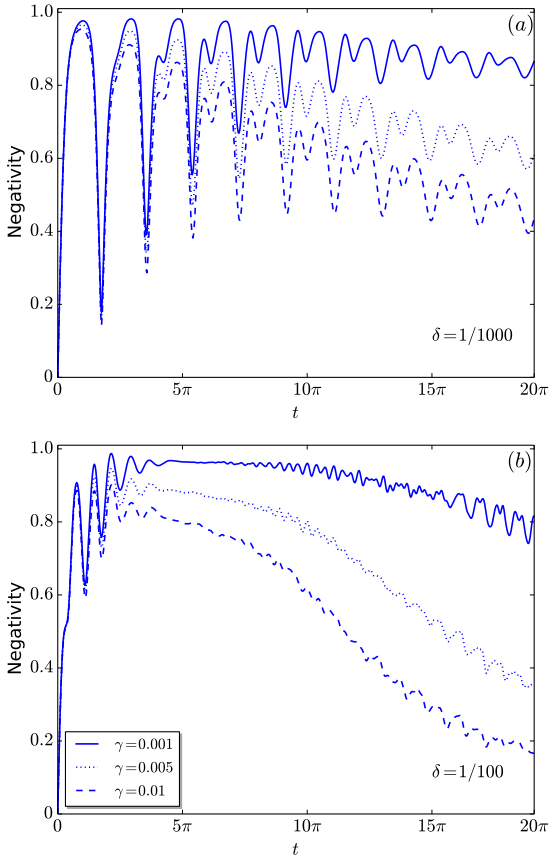

FIGURE 2.14: Negativity for the open quantum system for different values of the dissipation ratio γ, and different values of δ. Here, $k = 0.5, \alpha = 2$.

We have already mentioned some of the primary experimental setups in the introduction, let us now briefly examine some of those. The strong-coupling regime can be achieved using a qubit encoded in an electron on a quantum dot or a Cooper pair on a small superconducting island, coupled to an oscillator consisting of a vibrating gate electrode. In Ref. [Armour2002] the authors consider a micromechanical resonator capacitively coupled to a Cooper pair box (CPB). Here, a substantial coupling in the range of $g = 5 - 50$ MHz can be reached, and with the current technology $k \approx 1$ can be performed. Following with this regime, a qubit can also be modeled in clockwise and anti clockwise circulating currents in a superconducting loop. For instance, in Ref. [Rabl2009] the authors accomplish a strong coupling between a single electronic spin qubit associated with a nitrogen-vacancy impurity in diamond and the quantized motion of a magnetized nanomechanical resonator tip. Here, the dimensionless coupling is approximately $k \approx 0.1$ (For further details related with the full set of parameters see Ref. [Rabl2009]). On the other hand, the weak coupling regime can be realized in systems where a quantum dot is coupled to a mechanical oscillator, where this resonator is modulated by changing the local lattice of the host material [Kolkiran2006].

Another candidate setting for the implementation is given by trapped ions, where the strong coupling between hyperfine internal states of an ion and its motional degree of freedom has been shown in a variety of configurations [Blatt2008]. Moreover, the ion internal state can also be coupled to a cantilever under realistic conditions, for example, for a doubly clamped cantilever frequency of 19.7 MHz [LaHaye2004]. The coupling strength —which can be switched on and off— for a cadmium ion is given by $g \approx 52.5$ kHz [Nizamani2011], and therefore $k \approx 10^{-3}$.

Concerning possible implementations of non-linear quantum oscillators, various experimental platforms can be envisaged. As said, trapped ions can host qubit-oscillator systems. These platforms can also implement non-linear oscillators and in fact, by using a tunable set of parameters, the authors of Ref. [Nizamani2011] showed how to encompass both linear and non-linear potentials (anharmonic and double-well)—in order to achieve the efficient separation and re-combination of ions in surface ion-trap geometries using effective potentials. Furthermore, non-linearities can be generated as a result of static and longitudinal compressive force in suspended nanomechanical beams [Kolkiran2006] (see Fig. 2.15). For instance, for values of the length (L), thickness (d), and width (w) of the nanomechanical beam in the range of $L \approx 200 - 400$nm, $d \approx 5 - 10$nm, and $w \approx 10 - 20$nm a non-linear strength of the order of $\delta \approx 10^{-2}$ can be obtained. Finally, non-linearities can

be achieved in a mechanical oscillator in the form of a nano-cantilever cooled to its ground state. There, a ferromagnetic impurity in the cantilever tip (nano-magnets) can induce non-linear potentials via high homogeneous external magnetic fields in Helmholtz coil configuration [Joshi2011] (for an overview of quantum mechanical systems see Ref. [Poot2011]). All the mentioned systems are promising candidates in order to achieve the non-linearity we have considered in this work. In combination with the qubit-oscillator coupling, these schemes points at the actual possibility of implementing the qubit-NLO coupling, being the non-linearity the most challenging task to achieve in an experiment.

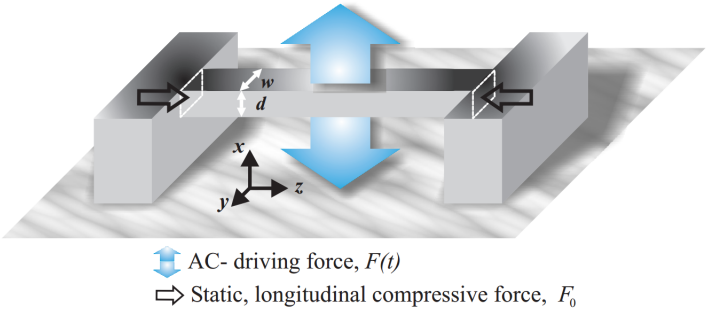

FIGURE 2.15: A nanomechanical beam of length L, width w, and thickness d is subject to a static longitudinal mechanical force F_0 to generate non-linearities. An external AC-driving transverse force $F(t)$ might be applied to drive the oscillator. **This figure was taken from the original paper "Quantum Properties of a Nanomechanical Oscillator" [Kolkiran2006]**

2.7 Entanglement Witness

In this final section, we will show the violation of the Bell function for the strong qubit-NLO regime ($k \approx 0.4$ and $\delta \leq 1/1000$). The Bell function ($\mathcal{B}$) can give us a full benchmark of quantum entanglement.

Any local theory will be restricted to a Bell value between $0 \leq \mathcal{B} \leq 2$, meanwhile a non-local theory (such as quantum mechanics) will take a number above that, i.e., $2 < \mathcal{B} < 2\sqrt{2}$, where the upper value is known to be the Cirel'son's bound. The Bell function is defined as:

$$\mathcal{B} = \max|E(\zeta, \beta) + E(\zeta', \beta) + E(\zeta, \beta') - E(\zeta', \beta')| \tag{2.48}$$

where $E(i,j) = \langle \hat{E}_A(i) \otimes \hat{E}_B(j) \rangle$ is the correlation function of two distinct measurements acting on subsystem A and B. In our particular case, we will follow the protocol investigated in Ref. [Park2012], where the authors can obtain a value above 2 for the Bell function in a qubit-field system.

As a first step, we will introduce the measurement for the qubit subsystem $\hat{E}_q(\zeta) = \hat{U}_q^\dagger(\zeta)\hat{\Gamma}_q\hat{U}_q(\zeta)$. Here, $\hat{\Gamma}_q = \hat{\sigma}_z$ corresponds to a dichotomic measurement combined with a unitary operation $\hat{U}_q(\zeta) = \exp[\zeta^*\hat{\sigma}^- - \zeta\hat{\sigma}^+]$ (single qubit rotation) parametrized by a complex value ζ. Therefore, the qubit measurements is ($\zeta(\theta,\phi) = \theta e^{-i\phi}$):

$$\hat{E}_q(\zeta) = \hat{U}_q^\dagger(\zeta)\hat{\Gamma}_q\hat{U}_q = \begin{pmatrix} \cos 2|\zeta| & -\frac{\zeta}{|\zeta|}\sin 2|\zeta| \\ -\frac{\zeta^*}{|\zeta|}\sin 2|\zeta| & -\cos 2\zeta \end{pmatrix} \tag{2.49}$$

On the other hand, even though in Ref. [Park2012] two field measurements are considered, namely "on/off measurements" and "parity measurements". For our purpose, it will enough to consider the first kind. Therefore, let us introduce the displaced on/off measurement for the oscillator field as:

$$\hat{O}_o(\beta) = \hat{D}(\beta)\left(\sum_{n=1}^{\infty}|n\rangle\langle n| - |0\rangle\langle 0|\right)\hat{D}^\dagger(\beta). \tag{2.50}$$

where $\hat{D}(\beta)$ is the displacement operator with displacement parameter β. Furthermore, an imperfect photodetector with efficiency ν is routinely modeled as a perfect photodetector preceded by a beam splitter (BS) of transmissivity $\sqrt{\nu}$ with one of the ports in the vacuum state $|0\rangle_{BS}$. The beam splitter operator then reads as : $\hat{B}_{o-BS} = \exp[0.5\cos^{-1}\sqrt{\nu}(\hat{a}_o^\dagger\hat{a}_{BS} - \hat{a}_o\hat{a}_{BS}^\dagger)]$.

After passing through the beam splitter, the qubit-oscillator outcome corresponds to:

$$\hat{\rho}_{qo}^\nu = \mathrm{Tr}_{BS}\left[\hat{B}_{o-BS}\hat{\rho}(t)_{qo} \otimes |0\rangle_{BS}\langle 0|_{BS}\hat{B}_{o-BS}^\dagger\right]. \tag{2.51}$$

The correlation function with the photon detection efficiency ν is the expectation value:

$$E(\zeta,\beta;\nu) = \mathrm{Tr}\left[\hat{\rho}_{qo}^\nu\hat{E}_q(\zeta) \otimes \hat{O}_o(\beta)\right] \tag{2.52}$$

Now, we have all the ingredients to maximize Eq. 2.48. As said, we based our results in Ref. [Park2012]. In that paper, the initial state corresponds to an equally superposed qubit-field state as $1/\sqrt{2}(|e\rangle|\alpha\rangle + |g\rangle|-\alpha\rangle)$. Under this state, the Bell

violation occurs for $\zeta = \pi/2, \zeta' = 0, \beta = -\beta' = |\beta|$, where $|\beta|$ satisfies:

$$2|\beta|e^{2(\eta-1)|\alpha|^2} = e^{-2|\alpha||\beta|\sqrt{\eta}}(|\beta| + |\alpha|\sqrt{\eta}) - e^{2|\alpha||\beta|\sqrt{\eta}}(|\beta| - |\alpha|\sqrt{\eta}) \tag{2.53}$$

However, our state differs from their initial state. In fact, in the weak qubit-oscillator coupling regime, the oscillator's amplitudes are $|\tilde{\alpha}_\uparrow\rangle = \left|e^{-i(1+6\delta)t}(\alpha - k)\right\rangle$, and $|\tilde{\alpha}_\downarrow\rangle = \left|e^{-i(1+6\delta)t}(\alpha + k)\right\rangle$. Also, even in the case in absence of non-linearity, the wave-function exhibits an extra phase. Therefore, to maximize the Bell function we consider the following i) the set of $\{\zeta, \zeta'\}$ parameters do not involve a major restriction as they corresponds to a qubit rotation, therefore we set $\zeta' = 0$ and $\zeta = 3\pi/4$. ii) The values of $|\beta|$ are taken from the expression in Eq. 2.53, being a deviation from the dynamics in absence of non-linearity (see Fig. 2.16).

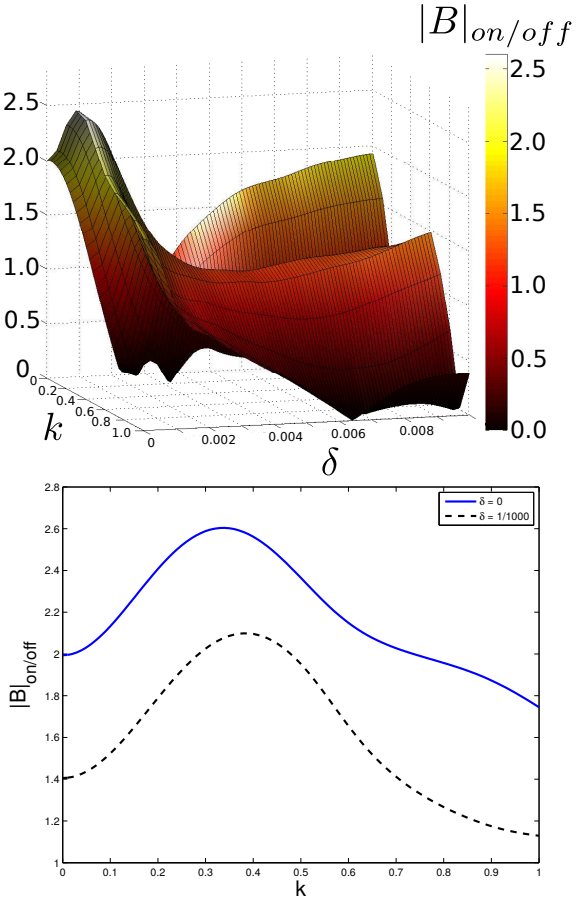

FIGURE 2.16: In the left panel we plot the Bell function as a function of the qubit-oscillator coupling (k) and the non-linearity strength (δ) for $t = \pi$. In the right panel, we compare the Bell function for $\delta = 0$ and $\delta = 1/1000$, in this last case a modest violation is achieved ($\mathcal{B} > 2$). In both cases we consider $\zeta' = 0, \zeta = 3\pi/4, \beta = -\beta' = |\beta|$, where $|\beta|$ satisfies Eq. 2.53, $\eta = 0.9$

2.8 Concluding Remarks

We have investigated a qubit (spin) coupled to a quartic non-linear oscillator through a conditional displacement Hamiltonian. The dynamics begins from a separable initial state composed of a qubit superposition state $(|\uparrow\rangle + |\downarrow\rangle)/\sqrt{2}$ and a coherent state $|\alpha\rangle$ for the oscillator. Throughout this Chapter we have used two relevant parameters, namely, the qubit-NLO coupling k and the non-linearity δ. We first recalled the results for the case $\delta = 0$. Here, the entanglement generation is due to the superposition principle of the hybrid system and it shows a periodic dynamics. On the other hand, when $\delta \neq 0$ and in the *weak coupling* regime we analytically show that a new Kerr-like term appears in the dynamics leading to *i)* quadrature squeezing of the oscillator state, *ii)* the suppression of the entanglement decay by the appearance of a stabilization region, and *iii)* an enhancement of the entanglement negativity compared to the linear case of $\delta = 0$.

The most interesting case corresponds to the *strong coupling regime*, when we see that two- and four-phonon transitions play a relevant role both in the entanglement stabilization and in its enhancement. In particular, the entanglement negativity can reach its maximal value by virtue of the orthogonalization of the oscillator states relevant to the present dynamics. Furthermore, solving numerically the corresponding master equation, we have shown that these effects remain robust to the presence of decoherence in the oscillator system.

Finally, we have considered in some details different possible experimental implementations for each regime considered here. Witnessing this type of hybrid entanglement is a hard task, however following the protocol in Ref. [Park2012] we can give a full proof of the violation of a Bell inequality for $\delta = 0$, and for the strong coupling regime.

Chapter 3

Entanglement Concentration in Optomechanics

On the one hand, the rapidly growing field of quantum cavity optomechanics give us a theoretical avenue to deeply investigate the interaction between quantized light and macroscopic oscillators, where —for example— the generation of non-classical states for macroscopic mechanical oscillators might be achieved within the quantum/mesoscopic limit. On the other hand, quantum cavity optomechanics allows us to build highly sensitive optical detectors of small forces, displacements, masses, and accelerations. Thus, becoming a promising field of research to explore, manipulate, and control mechanical motion using light.

Thus, due to the remarkable progress of this field over the last years, we will present a novel technique to concentrate/distill two-mode squeezed vacuum states using optomechanics, where our scheme relies essentially on quantum cavity optomechanics and homodyne detection.

To illustrate the final results of this chapter we will start with a brief summary on the progress on how the quantum cavity optomechanics has developed and evolved (review based on the manuscript by M. Aspelmeyer, T. J. Kippenberg, and F. Marquardt [Aspelmeyer2014]*, where the reader can find further details). Subsequently, we will give a relevant introduction on entanglement concentration/distillation, and finally, we will present the entanglement concentration via unsharp measurements.*

3.1 Cavity Quantum Optomechanics

Classical optomechanics was investigated back in the year 1619 when Kepler noted that the tails of the comets near to the Sun were always pointed away to its radial direction. This phenomena was understood as the pressure exerted on a material surface by electromagnetic fields, the so-called radiation pressure. As light carries momentum, then the radiation pressure force is classically stated as the temporal rate of the light momentum, i.e., $\mathbf{F} = d\mathbf{p}(t)/dt$.

In 1970s [Hansch1975, Wineland1975], the non-conservative nature of the radiation pressure force was pointed out opening a window for the foundations of laser cooling, an outstanding technique allowing, for example, to cool down ions to their motional ground state.

Other related works on feedback cooling were investigated in the same decade [Ashkin1978,Ashkin2006]. For instance, Braginsky [Braginsky1967, Braginsky1970] studied the radiation pressure on a suspended movable mirror of a cavity, where the mechanical oscillator might shows damping or anti-damping. Additionally, Braginsky [Braginsky1995] studied the quantum fluctuations of the radiation pressure force and how they set a limit for position measurement resolution. Future works based on this research [Caves1980] established the quantum standard limit for continuous position detection, which is essential for gravitational wave detectors [Abbott2009] (where, in order to measure the position of the mirror, one measures the optical phase shift).

In Fig. 3.1 we give a typical cavity optomechanics architecture, where the top panel shows an optical cavity driven by an external laser coupled to a mechanical mode. The bottom panel shows an analogue for a capacitive coupling.

Over the past few decades, the radiation pressure interaction in the quantum domain has been extensively explored both theoretically and experimentally. For instance, within the Fabry-Perot cavity configuration with a movable mirror due to radiation pressure, the authors present a model for quadrature squeezing [Mancini1994]. There, they achieved (for the open system) that the output light can be squeezed very close to the incident light, and therefore does not vanished by the thermal fluctuations. In contrast to previous works where i) the thermal fluctuations on the movable mirror were not taken into account [Stenholm1993], and ii) a semiclassical approach showed that squeezing is only feasible for extremely low temperatures [Hilico1992].

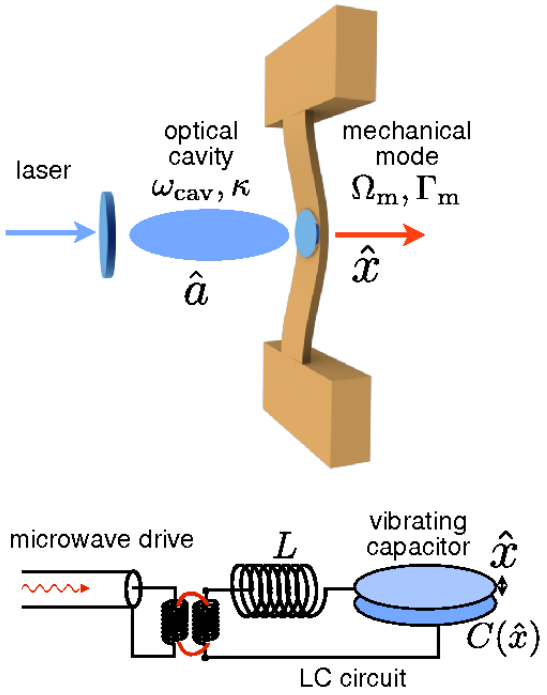

FIGURE 3.1: A typical optomechanical configuration. Above, an optical single cavity mode driven by an external laser is coupled to a mechanical single mode. Below, we show an analogue for a capacitive coupling. **This figure was taken from its original source** [**Aspelmeyer2014**]

Following with the mechanical effects of light on macroscopic objects, the fact that the radiation pressure coupling of the electromagnetic field to a oscillatory mirror shows bistability (experimentally showed in the optical [Dorsel1983] and the microwave regimes [Gozzini1985]). K. Jacobs *et. al.,* [Jacobs1994] shows a field-oscillatory system through radiation pressure in the adiabatic limit. In that proposal, the authors can obtain both the amplitude quadrature of the external field, as well as the photon number using the momentum fluctuations of the mirror as a *meter*.

Another example is the generation of non-classical states due to radiation pressure [Bose1997]. There, the authors were interested not only in the non-classical states of the light cavity field (which can be shown to produce entangled states of two or more cavity modes), but also in the non-classicality of the mechanical oscillator, a state which should be interesting in itself. To generate non-classical states of the cavity field you might follow i) multicomponent cat states generated due to dynamics alone, ii) entangled states of two or more light modes generated due to the dynamics

alone, and iii) nonclassical states produced due to conditional measurements on the mirror.

On the other hand, optical feedback cooling based on radiation pressure of light was first demonstrated in [Cohadon1999] for the vibrational modes of a macroscopic end-mirror. In this seminal work, an external laser beam exerted a radiation pressure force on the reflected mirror controlling in this way the mechanical motion. Here, cooling or heating of the mirror can be produced, depending on the gain of the feedback laser. Furthermore, the thermal motion of a $mm-$scale mirror was monitored in a LHe-cryogenic optical cavity [Tittonen1999]. In that experiment, the optomechanical sensor reads out the vibrations of a micro-mechanical oscillator (Fabry-Pérot cavity configuration), where the mechanical quality factor increases up to $Q = 4 \times 10^6, @4\text{K}$ ($Q = 3 \times 10^5, @300\text{K}$). Other examples on the experimental side are the optical spring effect [Vogel2003], feedback damping [Mertz1993], self-induced oscillations [Hohberger2004a], and cavity cooling due to dynamical backaction of retarded photothermal light forces [Hohberger2004b].

Currently, exhaustive work is being carried out on quantum cavity optomechanics with several new systems such as membranes [Thompson2008] and nanorods [Favero2009] inside Fabry-Pérot resonators. In those cases, the cavity corresponds to a standard Fabry-Pérot configuration with an external element placed in the middle of the cavity, e.g., a dielectric membrane, or a nanorod. Additionally, in the standard single-sided optomechanical Fabry-Pérot setup (when a single mirror is allow to move) is hard to achieve good optical properties (high F) and good mechanical properties (high Q) simultaneously. With the introduction of the membrane scheme this difficulty is removed, because the coupling between the membrane and light depends upon where the membrane is placed relative to the nodes and antinodes of the cavity mode. Other examples are whispering gallery microdisks [Jiang2009] and microspheres [Ma2007], photonic crystals [Eichenfield2009], and evanescently coupled nanobeams [Anetsberger2009]. In Fig. 3.2 we present a list of different optomechanical architectures arranged by mass.

3.2 Radiation Pressure — *The Quantum Case*

As mentioned in the introduction, the *classical* radiation pressure force was investigated in Kepler's times. A modern classical treatment of this force can be derived from Maxwell equations from classical electrodynamics, thus completing

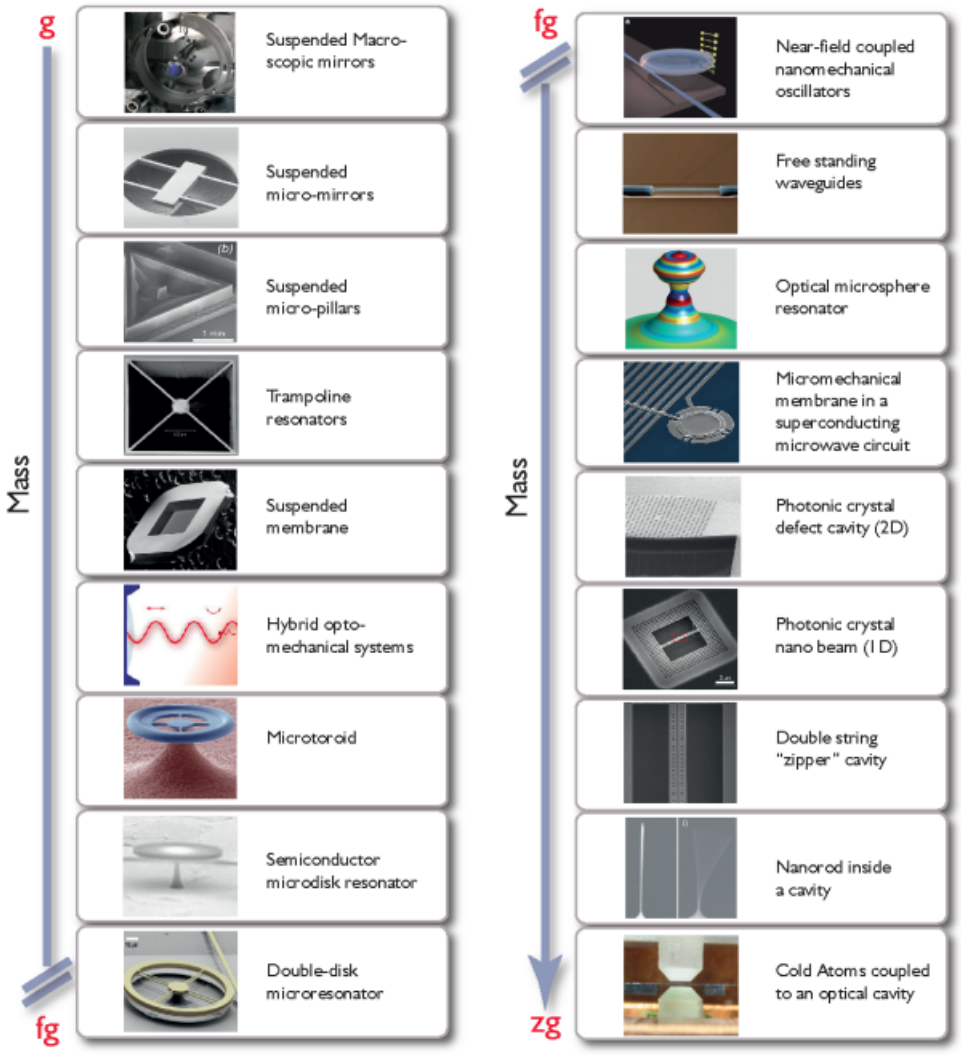

FIGURE 3.2: Several optomechanical architectures arranged by mass, from $g - zg$ (10^{-3} - 10^{-24} kg). **Figure taken from [Aspelmeyer2014].**

this picture. However, the quantum case is not a trivial task. For our purpose, we will present a brief derivation of the non-relativistic Hamiltonian under a linear approximation [Law1995].

Let us consider a one-dimensional Fabry-Pérot cavity configuration under ideal conditions, where one of the mirrors is allowed to move harmonically. This system with dynamical boundary conditions is quite challenging, because the field inside the cavity depends on the position of the movable mirror, and viceversa. The procedure derived in Ref. [Law1995] is the following. Starting from the Wave equation for the vector potential $A(x,t)$ with time-dependent boundary conditions $A(0,t) = A(q(t),t) = 0$, where $q(t)$ is the classical position of the mirror, we write

down the Newton's equation of motion. In principle, the set of above equations (not shown here), namely the equations for $\{q(t), A(x,t)\}$ specify completely the dynamics of the system. Next, we can construct a Lagrangian for the system, and finally a classical Hamiltonian as following:

$$H = \frac{1}{2m}\left(p + \frac{1}{q}\sum_{j,k} g_{kj} P_k Q_j\right)^2 + V(q) + \frac{1}{2}\sum_k P_k^2 + \omega_k^2 Q_k^2, \tag{3.1}$$

where p is the mirror's canonical momentum, Q_k is a set of generalized coordinates, P_k is the canonical conjugate of Q_k, $V(q)$ is the potential well, $g_k j$ are dimensionless coefficients, $\omega_k = k\pi/q$, and m being the mass of the mirror.

To quantize the classical Hamiltonian in Eq. 3.1, we follow the standard quantization procedure, i.e., we let the variables p, q, P_k, Q_k be operators, which obey the commutation relations $[\hat{q}, \hat{Q}_j] = [\hat{q}, \hat{P}_k] = [\hat{p}, \hat{Q}_j] = [\hat{p}, \hat{P}_k] = 0; [\hat{q}, \hat{p}] = i\hbar; [\hat{Q}_j, \hat{P}_k] = i\delta_{jk}\hbar$. To present the Hamiltonian using the boson operators, we use the relations shown in Ref. 1.17, but for cavity-length-dependent:

$$\hat{a}_k(\hat{q}) = \frac{1}{\sqrt{2\hbar\omega_k(\hat{q})}}(\omega_k(\hat{q})\hat{Q}_k + i\hat{P}_k). \tag{3.2}$$

The final quantized Hamiltonian corresponds to:

$$\hat{H} = \frac{(\hat{p} + \hat{\Gamma})^2}{2m} + \hat{V}(\hat{q}) + \hbar\sum_k \omega_k(\hat{q})\hat{a}_k^\dagger(\hat{q})\hat{a}_k(\hat{q}) - \frac{\hbar\pi}{24q}, \tag{3.3}$$

where,

$$\hat{\Gamma} \equiv \frac{i\hbar}{2q}\sum_{k,j} g_{kj}\sqrt{\frac{k}{j}}(\hat{a}_k^\dagger(\hat{q})\hat{a}_j^\dagger(\hat{q}) - \hat{a}_k(\hat{q})\hat{a}_j(\hat{q}) + \hat{a}_k^\dagger(\hat{q})\hat{a}_j(\hat{q}) - \hat{a}_j^\dagger(\hat{q})\hat{a}_k(\hat{q})). \tag{3.4}$$

In Eq. 3.3, the operator Γ is quadratic, which contributes to two-photon emission and absorption processes. Additionally, we have replaced the vacuum energy by the Casimir energy $-\hbar\pi/24q$ [Plunien1986]. The above general Hamiltonian is an adequate approximation for quantum optics purposes, in which the cavity field is dominant. Another final consideration is the linear case, in general we will deal with mirrors oscillating around a certain equilibrium position l_0. Thus, let us consider

$x_m \equiv q - l_0$ is small compared with l_0, therefore we can expand:

$$\hat{a}_k(\hat{q}) \approx \hat{a}_{k0} - \frac{x_m}{2l_0}\hat{a}^\dagger_{k0}, \tag{3.5}$$

$$\omega_k(\hat{q}) \approx \omega_{k0}\left(1 - \frac{x_m}{l_0}\right) \tag{3.6}$$

here, $\hat{a}_{k0}$ and ω_{k0} are the boson annihilation operator and the frequency associated with l_0, respectively. Using a unitary transformation, we finally get:

$$\hat{H}_{\text{linear}} \approx \frac{\hat{p}^2}{2m} + \hat{V}(\hat{q}) - \frac{\hbar\pi}{24q} + \hbar\sum_k \omega_{k0}\hat{a}^\dagger_{k0}\hat{a}_{k0} - \hat{x}_m\hat{F}_0. \tag{3.7}$$

In the special case where the cavity field is contributed dominantly from a single cavity mode k_0, then:

$$\hat{x}_m\hat{F}_0 \approx x_m\frac{\hbar\omega_{k0}}{l_0}\hat{a}^\dagger_{k0}\hat{a}_{k0}. \tag{3.8}$$

For a single cavity mode, and neglecting both retardation effects due to the oscillating mirror, as well as the the Casimir energy ($\omega_{\text{cav}} \gg \omega_{\text{osc}}$), the above linear Hamiltonian becomes:

$$\hat{H} = \frac{\hat{p}^2}{2m} + \frac{m\omega^2_{\text{osc}}}{2}\hat{x}^2 + \hbar\omega_{\text{cav}}\hat{a}^\dagger\hat{a} - \hbar\frac{\omega_{\text{osc}}}{l_0}\sqrt{\frac{\hbar}{2m\omega_{\text{osc}}}}\hat{a}^\dagger\hat{a}(\hat{b} + \hat{b}^\dagger) \tag{3.9}$$

where we have used Eq. 1.19, and we have considered a harmonic oscillation for the movable mirror. The Eq. 3.9 constitutes the relevant radiation pressure Hamiltonian studied below.

3.3 Entanglement Distillation

The aim of quantum processing is to perform some tasks that might be impossible (or hard) to realize in the classical domain. To achieve these quantum tasks it is required to have highly entangled states. However, because of the system-environment unavoidable coupling, the state could not have the entanglement needed to fulfill the quantum protocol.

To solve this bottleneck, Bennett *et. al.,* [Bennett1996] proposed the following protocol (originally for a qubit system). Let us consider two distant parties or subsystems labeled A and B, or *Alice* and *Bob*, as referred usually in quantum

information. Here, each one share a supply of many copies of a mixed and weakly (low) entangled state, subsequently they could *distill* a small number of copies of states arbitrarily close to a maximally entangled state by two-qubit operations, measurement and classical communication.

To extend Bennet's protocol we consider a particular class of states called Gaussian states. These states are interesting in two ways i) they have found many applications in quantum information science, and ii) they are easy to generate in the laboratory. *Unfortunately* [Eisert2002, Fiurasek2002, Giedke2002], it is not possible to distill Gaussian states using solely Gaussian operations, i.e., any joint operations, measurements and classical communication between Alice and Bob will leave them with a state with either the same or less entanglement than the initial state. However, we can still distill Gaussian states using a non-Gaussian operation, namely Photo-detection. On the one hand, one advantage of using Photo-detection is that this operations is quite topical and accessible in the laboratory. On the other hand, although we can generate states which will be more entangled than their initial supply, the Gaussian profile is lost. To solve this issue we can use a protocol called "Gaussification", which we will cover in Section 3.3.2.

3.3.1 Entanglement distillation using photo-detection

As an example we will refer to [Browne2005], where a simple way to distill a two-mode squeezed vacuum state —with squeezing parameter r— using photo-detection is presented. Let us consider that one of the light beams is mixed with a single photon state $|1\rangle$ into an ideal beam splitter with transmissivity T and reflectivity R, such as $R^2 + T^2 = 1$. Subsequently, one of the outputs of the beam splitter is measured via an ideal photo-detector.

The state after m photons are registered is:

$$|\psi\rangle = \sqrt{\frac{1}{\sum_{n=m-1}^{\infty} |\alpha_n(m)|^2}} \sum_{n=m-1}^{\infty} \alpha_n(m) \, |n\rangle \, |n+1-m\rangle \,, \tag{3.10}$$

where,

$$\alpha_n(m) = -\tanh^n(r) T^{n-m} R^{m-1} \left[-R^2 \sqrt{\binom{n}{m}(n+1-m)} + T^2 \sqrt{\binom{n}{m-1} m} \right] \tag{3.11}$$

and $\binom{n}{k} = 0$ if $k > n$; and T and R are real.

It is straightforward to compute the von Neumann entropy from Eq. 3.10 (see Ref. [Browne2005] for details). Here, using solely this non-Gaussian operation, it is possible to obtain a higher entanglement in contrast to their initial supply, but at cost of very low probability. This last point is a clear advantage of our protocol, in which a considerable probability (up to 25% of entanglement concentration success) is achieved for high distilled entangled states.

3.3.2 From a non-Gaussian state to a Gaussian state

As we briefly describe in the above section, it is possible to distill Gaussian states using a non-Gaussian operation, namely photon-detection. However the outcome state will not keep the Gaussian profile. As these states are currently quite topical in quantum optics/information and easy to prepare experimentally, it is important to solve this problem towards real quantum processing implementations using Gaussian states. A way to solve this issue consists in an iterative protocol called "Gaussification" [Browne2003a, Eisert2004]. As in the case of distillation explored previously, we need to have a supply of many copies, in this case copies of a non-Gaussian two-mode entangled state. After several non-deterministic iterations, it produces a small number of states that are arbitrarily close to Gaussian states and which are often more entangled than the input.

In the following, we will list the iterative procedure under ideal conditions for Gaussification, see Fig. 3.3 for a single iteration scheme (In Ref. [Browne2005] the authors consider the main imperfections in a real implementation, for our purpose it will enough to consider the ideal case)

- Initially, Alice (A) and Bob (B) share a two-mode entangled state $\left|\psi_{AB}^{(0)}\right\rangle$. Subsequently, in the next iteration they will use pairs of states generated by a previous successful iteration.
- Secondly, they prepare two copies of the state (in that iteration), i.e., $\left|\psi_{AB}^{(0)}\right\rangle_1 \otimes \left|\psi_{AB}^{(0)}\right\rangle_2$, and they mix their half of two copies of the state on a 50:50 beam splitter.
- They measure one of the outputs with a photo-detector.
- If no photons are registered, the iteration was a success (otherwise they drop that copy), and the resultant state is saved for the next iteration $\left|\psi_{AB}^{(1)}\right\rangle$.

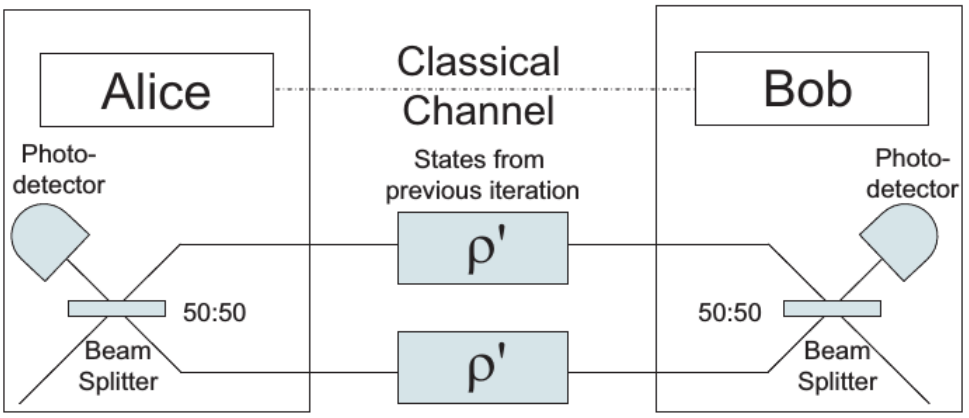

FIGURE 3.3: The figure shows a single iteration of the "Gaussification" protocol. **This figure was taken from Ref. [Browne2005].**

3.3.2.1 "Gaussification" example

As an example, let us consider the following input state:

$$\left|\psi_{AB}^{(0)}\right\rangle = |0\rangle_A |0\rangle_B + \eta |1\rangle_A |1\rangle_B \tag{3.12}$$

where, $A(B)$ stands for Alice (Bob). The two copies can be easily write down as $\left|\psi_{AB}^{(0)}\right\rangle_1 \otimes \left|\psi_{AB}^{(0)}\right\rangle_2$:

$$\begin{aligned}\left|\psi_{AB}^{(0)}\right\rangle_1 \otimes \left|\psi_{AB}^{(0)}\right\rangle_2 &= |0\rangle_A^1 |0\rangle_B^1 |0\rangle_A^2 |0\rangle_B^2 + \eta |1\rangle_A^1 |1\rangle_B^1 |0\rangle_A^2 |0\rangle_B^2 \\ &+ \eta |0\rangle_A^1 |0\rangle_B^1 |1\rangle_A^2 |1\rangle_B^2 + \eta^2 |1\rangle_A^1 |1\rangle_B^1 |1\rangle_A^2 |1\rangle_B^2 .\end{aligned} \tag{3.13}$$

It is straightforward to obtain the state after passing through the 50:50 beam splitter transformation. After measuring the second mode in zero photons for Alice and Bob, we get:

$$\left|\psi_{AB}^{(1)}\right\rangle = |0\rangle_A |0\rangle_B + \eta |1\rangle_A |1\rangle_B + \frac{\eta^2}{2} |2\rangle_A |2\rangle_B . \tag{3.14}$$

A generalization of the above example can be made, where for an infinite number of iterations a general input state $\left|\psi^{(0)}\right\rangle = \sum_n \alpha_n^{(0)} |n, n\rangle$ tends to a two-mode squeezed state, i.e., a Gaussian state.

3.4 Introduction to Entanglement Concentration in Optomechanics via Unsharp Measurements

Recent experiments with quantum optical systems have demonstrated the generation of entanglement across several hundred of modes and partitions [Yokohama2013, Chen2014, Gerke2015], thus offering unprecedented opportunities for quantum networking [Kimble2008]. However, the states generated in these systems (Gaussian states of light) suffer from the drawback that entanglement distillation — a pivotal primitive for long distance quantum communication and networking [Bennett1996] — is not readily available. This is due to the fact that the interactions naturally occurring in these systems are Gaussian and a "no-go theorem" prevents Gaussian operations to distill Gaussian entanglement [Eisert2002, Fiurasek2002, Giedke2002]. To overcome this, purely optical methods involving non-Gaussian operations have been suggested [Duan2000, Fiurasek2003, Browne2003b, Datta2012, Bartley2013], with the dominant scheme relying on photon subtraction [Opatrny2000, Olivares2003]. In particular, it has been shown that memory can sufficiently improve such schemes [Humphreys2014], including enabling quantum computation. The implementation of such schemes is currently topical but remains technologically challenging [Wenger2004, Franzen2006, Takahashi2010, Kurochkin2014, Ourjoumtsev2009] and [Dong2008]. We introduce here an alternative route based on hybrid opto-mechanical systems that naturally possess non-Gaussian radiation-pressure interactions.

In this context, quantum optomechanics is rapidly opening up new avenues for the manipulation of optical states [Aspelmeyer2010, Aspelmeyer2014]. Regarding quantum communications, the usage of optomechanical systems for teleportation and establishing Gaussian entangled states of distant systems have been studied (see, *e.g.* Refs. [Mancini2002, Pirandola2006, Chang2010, Asjad2014]). However the quantum communication enabling protocol of entanglement distillation has thus far been left untouched as the majority of the applications considered the linearized (therefore Gaussian) regime of opto-mechanical interaction. On the other hand, the bare optomechanical radiation pressure interaction is non-Gaussian (tri-linear) [Law1995]. Can this coupling be useful for quantum communication, namely, for entanglement distillation? While it has been known for a while that the trilinear coupling enables the probing of macroscopic superpositions [Bose1999a, Marshall2003], only recently it has started drawing serious attention [Nunnenkamp2011, Stannigel2012b, He2012, Liao2012, Xu2013a, Kronwald2013,

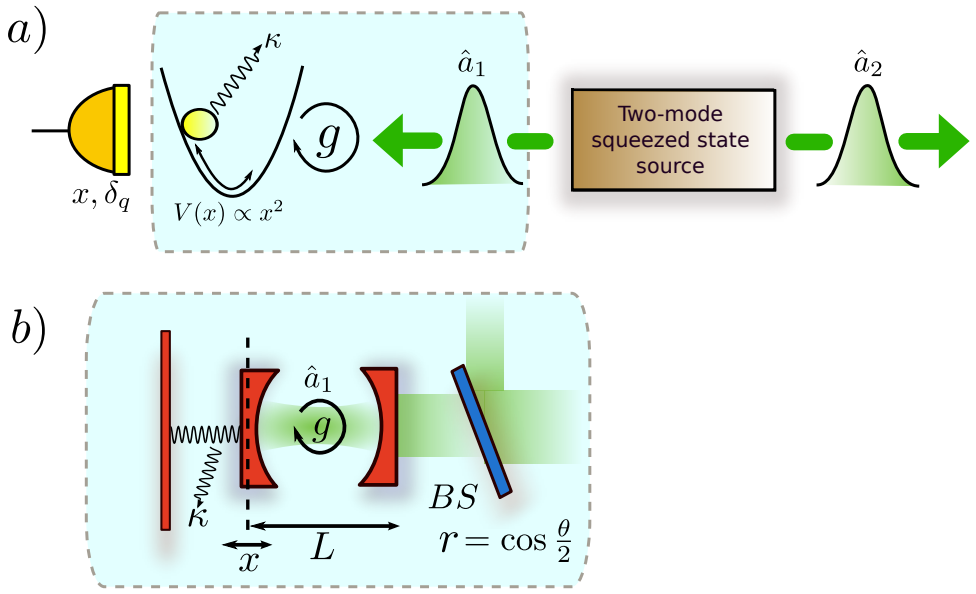

FIGURE 3.4: Concentration procedure for two-mode squeezed vacuum (TMSV). In a) we show the general scheme, where a source generates a TMSV, the first mode $\hat{a}_1$ interacts with a damped (κ) mechanical harmonic oscillator $V(x) \propto x^2$ (g is the scaled coupling strength). After this interaction, and conditioned on unsharp measurements of the position x of the mechanical oscillator with resolution δ_q, the initial TMSV entanglement between $\hat{a}_1$ and $\hat{a}_2$ can be increased. In b) we show the explicit realization of the same procedure: here we substituted the oscillator with a single sided Fabry-Pérot cavity with a movable mirror, modeling the injection of the mode $\hat{a}_1$ into the cavity via BS of reflectivity r. The position of the mirror is to be measured by pulsed optomechanics [Vanner2011].

Xu2013b, Akram2013, Liao2014] as it is becoming physically significant in certain setups [Safavi-Naeini2011, Chan2011, Teufel2011, Murch2008, Xuereb2012] and [Kaviani2014]. Here we show that the bare "tri-linear" optomechanical radiation pressure interaction can enable the concentration of the entanglement of two mode squeezed vacua by local operations. In particular, "snap-shot" position detections of a mechanical oscillator, whose technology has been developed recently [Vanner2011, Vanner2013, Sekatski2014], serve as the alternative to photo-detection. Our proposal also demonstrates that sometimes the usage of weak (in the sense of "coarse-grained" or unsharp) measurements can be more fruitful for enacting a quantum information protocol in comparison to fine grained ones.

This Chapter continues as following, in Section 3.5 we introduce the two-mode squeezed vacuum state which constitutes the initial input for our protocol. Next, in Section 3.6 we derive the dynamics of the density matrix in presence of detrimental effects, such as the injection of the light beam into the cavity, as well as the damping of the mechanical oscillator. Subsequently, we proceed to measure the position of

the mechanical oscillator in Section 3.7, achieving in this way the entanglement concentration for some optimal values. In addition, in order to give a full benchmark of the distilled output state, we use this state as a resource for the standard quantum teleportation protocol in Section 3.8. Finally, we give the experimental feasibility of our scheme in Section 3.9 and the final remarks in Section 3.10.

3.5 Two-Mode Squeezed Vacuum State

In general, the squeezed states experimentally generated are not single mode. A first approach is to consider the two-mode squeezed state (TMSV), being a highly entangled state. TMSV states are generated in an Optical Parametric Amplifier, currently they can be prepared as follows : A pumping laser light ($\hat{c}$) with angular frequency given by Ω is focused onto a non-linear crystal, which absorbs a pump photon and emits two photons, with frequencies ω_1 and ω_2 (being the idler and the signal of the amplifier), therefore $\Omega = \omega_1 + \omega_2$. The Hamiltonian for this non-linear process is:

$$\hat{H} = i\hbar\lambda(\hat{c}^\dagger \hat{a}_1 \hat{a}_2 - \hat{c}\hat{a}_1^\dagger \hat{a}_2^\dagger), \tag{3.15}$$

for an intense laser field, we can approximate the quantized boson operator $\hat{c}$ as a classical amplitude E

$$\hat{H} = i\hbar\lambda(E^* \hat{a}_1 \hat{a}_2 - E\hat{a}_1^\dagger \hat{a}_2^\dagger). \tag{3.16}$$

The time evolution for Eq. 3.16 is the generator of TMSV states, and it can be written as following ($\eta = \lambda E(t - t_0)$):

$$\begin{aligned} \exp(\eta^* \hat{a}_1 \hat{a}_2 - \eta \hat{a}_1^\dagger \hat{a}_2^\dagger) &= \frac{1}{\cosh s} \exp\left[-\hat{a}_1^\dagger \hat{a}_2^\dagger \tanh s e^{i\theta}\right] \\ &\times \exp\left[-(\hat{a}_1^\dagger \hat{a}_1 + \hat{a}_2^\dagger \hat{a}_2) ln(\cosh s)\right] \\ &\times \exp\left[-\hat{a}_1 \hat{a}_2 \tanh s e^{-i\theta}\right]. \end{aligned} \tag{3.17}$$

It is easy to prove that for a two-mode vacuum state $|\psi\rangle_{\text{TMSV}} = \exp(-\eta^* \hat{a}_1 \hat{a}_2 + \eta \hat{a}_1^\dagger \hat{a}_2^\dagger) |0\rangle_1 \otimes |0\rangle_2$, the TMSV state reads as:

$$|\psi\rangle_{\text{TMSV}} = \frac{1}{\cosh s} \sum_{n=0}^{\infty} \tanh^n s e^{in\theta} |n\rangle_1 \otimes |n\rangle_2 . \tag{3.18}$$

As seen in the Chapter 1, the above state is in the Schmidt form written in the two-mode bi-orthogonal Fock basis. Hence, the reduced density matrices are diagonal:

$$\hat{\rho}_{1,2} = \sum_{n=0}^{\infty} \frac{1}{\cosh^2 s} \tanh^{2n} s \, |n\rangle_{1,2} \langle n|_{1,2} \tag{3.19}$$

describing a thermal state, with $\bar{n} = \sinh^2 s$.

3.6 System Dynamics

Let us commence by considering two light-modes (with corresponding annihilation operators $\hat{a}_1$ and $\hat{a}_2$ satisfying $[\hat{a}_j, \hat{a}_j^\dagger] = 1$ for $j = 1, 2$) in a two-mode squeezed vacuum (TMSV)

$$|\psi(0)\rangle_{\text{TMSV}} = \sqrt{1-\lambda^2} \sum_{n=0}^{\infty} \lambda^n \, |n, n\rangle_{12} \tag{3.20}$$

with $\lambda = \tanh s$ and s being the squeezing parameter. One light beam ($\hat{a}_1$) is coupled to a mechanical harmonic oscillator (m), whereas mode $\hat{a}_2$ propagates freely [a general scheme is illustrated in Fig. (3.4-a)]. As said, we focus our attention on a Fabry-Pérot configuration [see Fig. (3.4-b)] where the mode $\hat{a}_1$ is injected into a cavity. Such injection of a freely propagating optical mode into a cavity is standard in LIGO [Abbott2009], and is considered quite standard in the study of cavity-based quantum networks [Chang2010, Parkins2000]. Obviously, the injection itself entails a loss and decoherence of the optical field, which we will duly take into account.

After mode $\hat{a}_1$ is injected into the cavity it starts interacting with the mechanical oscillator via an optomechanical Hamiltonian. In a frame rotating at the frequency ω_1 of mode $\hat{a}_1$, this is given by :

$$\hat{H}_{int} = \hat{b}^\dagger \hat{b} - g \hat{a}_1^\dagger \hat{a}_1 (\hat{b}^\dagger + \hat{b}), \tag{3.21}$$

where $g = g_0/\omega_m$ is the scaled coupling parameter, ω_m is the angular frequency of the mechanical oscillator ($\hat{b}$), $g_0 = x_{zpf}\omega_1/L$ is the radiation-pressure interaction strength, L is the cavity length at equilibrium, and x_{zpf} is the zero-point fluctuation amplitude (we set $\hbar = 1$) [Bose1999a]. In most experimental scenarios, the mechanical oscillator will initially be in a thermal state. However, given the recent possibilities of ground state cooling [Chang2010, Teufel2011, Machnes2012, Vanner2010]

and without loss of generality, we will consider the initial state of the oscillator as a coherent state with $\alpha = |\alpha|e^{i\phi_\alpha}$. The temporal evolution in the absence of any source of decoherence can be solved straightforwardly [Bose1997, Mancini1997]. In this ideal case, the dynamics is characterized by a displacement of the mirror position, conditioned on the photon number n, and a Kerr-like evolution of the light beam: $\lambda^n |n\rangle_1 |\alpha\rangle_m \rightarrow \lambda^n \exp(ig^2n^2(t-\sin t))\exp(ign\mathrm{Im}[\alpha\eta])\,|n\rangle_1 \left|\alpha e^{-it} + gn\eta\right\rangle_m$. Here $|n\rangle$ is a photonic Fock state, $\eta = 1-e^{-it}$, and t represents a scaled time, being the actual time multiplied by ω_m.

However, in realistic experimental conditions the state will be affected by unavoidable sources of decoherence. In order to give a full analytical solution we have neglected the photon leakage from the cavity (in other words, we require cavity decay $\kappa_c/\omega_m < g$). We solve the standard Markovian master equation at zero temperature for the decoherence of the oscillator. In this case, the master equation reads as: $d\hat{\rho}(t)/dt = -i[\hat{H}_{int}, \hat{\rho}(t)] + (2\hat{b}\hat{\rho}(t)\hat{b}^\dagger - \hat{b}^\dagger\hat{b}\hat{\rho}(t) - \hat{\rho}(t)\hat{b}^\dagger\hat{b})\kappa/2$, being κ the mechanical energy damping rate. Another inevitable source of decoherence is the attenuation due to the injection of the light beam into the cavity. To model this, we consider a beam splitter (BS) in front of the fixed cavity-mirror, such that one port of the latter is fed with mode $\hat{a}_1$ and the other with a vacuum field [Kim2002, Kim1998, Agarwal2012]. Under these sources of decoherence, the full analytical solution for the evolved density matrix reads

$$\begin{aligned}\hat{\rho}(t) &= |1-\lambda^2| \sum_{n,m=0}^{\infty} \mathcal{C}_{nm} e^{-D^\kappa_{nm}(t)} \sum_{k=0}^{\min[n,m]} G^k_{nm}(\theta)\,|n-k,n\rangle_{12}\,\langle m-k,m|_{12} \\ &\otimes |\phi_n(\kappa,t)\rangle_m \langle\phi_m(\kappa,t)|_m \end{aligned} \tag{3.22}$$

where the θ angle is related with the reflection coefficient of the BS as $r = \cos(\theta/2)$. The other terms are

$$\begin{aligned}\mathcal{C}_{nm} &= \lambda^{n+m} e^{ig^2[t-\sin t](n^2-m^2)} e^{ig\mathrm{Im}[\alpha\eta](n-m)} \\ G^k_{nm}(\theta) &= \sqrt{\binom{n}{k}\binom{m}{k}} \cos^{2k}\frac{\theta}{2} \sin^{n-k}\frac{\theta}{2} \sin^{m-k}\frac{\theta}{2} \\ \phi_n(\kappa,t) &= \frac{ign\left(1-e^{-(i+\kappa/2)t}\right)}{i+\kappa/2} + \alpha e^{-(i+\kappa/2)t} \\ D^\kappa_{nm}(t) &= \frac{\kappa}{2}\int_0^t \Big(|\phi_n(\kappa,t')|^2 + |\phi_m(\kappa,t')|^2 - 2\phi^*_n(\kappa,t')\phi_m(\kappa,t')\Big)dt'. \end{aligned} \tag{3.23}$$

The above expressions $\phi_n(\kappa,t)$ and $D^\kappa_{nm}(t)$ can be obtained from the step procedure

method derived in the appendix of Ref. [Bose1997]. Basically, this methodology alternates small time steps Δt between the unitary and the non-unitary dynamics. In other words, we consider an initial small time step where only the unitary dynamics take place. Subsequently, another small time step is considered only for the non-unitary part. Then, we iterate the procedure.

For the first unitary step, we know how the coherent amplitude for the mechanical oscillator evolves:

$$\phi_n(\kappa,t) \to \phi_n(\kappa,t)e^{-i\Delta t} + gn(1-e^{-i\Delta t}) \approx (1-i\Delta t)\phi_n(\kappa,t) + ign\Delta t. \tag{3.24}$$

For the non-unitary step dynamics, is known to transform [Walls1985]

$$\phi_n(\kappa,t) \to \phi_n(\kappa,t)e^{-\frac{\Delta t}{2}\kappa} \approx \phi_n(\kappa,t)\left(1-\frac{\Delta t}{2}\kappa\right). \tag{3.25}$$

Therefore, the full dynamics will be the contribution of both giving us the following differential equation

$$\frac{d}{dt}\phi_n(\kappa,t) = -i\phi_n(\kappa,t) - \frac{\kappa}{2}\phi_n(\kappa,t) + ign. \tag{3.26}$$

Starting from an initial complex amplitude α, it is straightforward to obtain the solution of Eq. 3.26 being the coherent amplitude shown in Eq. 3.23.

On the other hand,

$$\rho_{nm}(t) \to \rho_{nm}(t)e^{ig^2(n^2-m^2)(1-\cos t)\Delta t}e^{igr\Delta t(n-m)\cos(t-\phi)} \tag{3.27}$$

and,

$$\rho_{nm}(t) \to \rho_{nm}(t)\langle\phi_n(\kappa,t)|\phi_m(\kappa,t)\rangle^{(1-e^{-\kappa\Delta t})} \tag{3.28}$$

therefore,

$$\begin{aligned}
\rho_{nm}(t) &= \rho_{nm}(0)\exp\left(\int_0^t ig^2(n^2-m^2)(1-\cos t') + igr(n-m)\cos(t'-\phi)dt'\right) \\
&\times \exp\left(-\frac{\kappa}{2}\int_0^t |\phi_n(\kappa,t')|^2 + |\phi_m(\kappa,t')|^2 - 2\phi_n^*(\kappa,t')\phi_m(\kappa,t')dt'\right) \\
&= \rho_{nm}(0)e^{ig^2(n^2-m^2)(t-\sin t)}e^{ig\mathrm{Im}[\alpha\eta](n-m)}e^{-D_{nm}^{\kappa}(t)}
\end{aligned} \tag{3.29}$$

3.7 Entanglement Concentration via Radiation Pressure

To distill the initial TMSV we proceed to measure the quadrature position of the oscillator [Vanner2011] through an inefficient detector. This corresponds to the positive-operator valued measure (POVM):

$$\hat{\Pi}(q) = \frac{1}{\sqrt{2\pi\delta_q^2}} \int_{-\infty}^{\infty} \exp(-(q-y)^2/2\delta_q^2) \left|y\right\rangle \left\langle y\right| dy \tag{3.30}$$

where $q = x\sqrt{m\omega_m/\hbar}$ is the dimensionless position of the oscillator (with actual position x), m is the oscillator mass, and δ_q determines the measurement resolution [Ferraro2005]. The state (unnormalized) after the measurement, conditioned to an outcome q, is given by ($\mathrm{Tr}_m[\cdots]$ *stands for the trace operation with respect to the mechanical state*)

$$\begin{aligned}
\hat{\rho}(t)_{12} &= \mathrm{Tr}_m\left[\hat{\rho}(t)\hat{\Pi}(q)\right] \\
&= \int_{-\infty}^{\infty} dx \left\langle x\right| \hat{\rho}(t)\hat{\Pi}(q) \left|x\right\rangle \\
&= \int_{-\infty}^{\infty} dx \left\langle x\right| \hat{\rho}(t) \frac{1}{\sqrt{2\pi\delta_q^2}} \int_{-\infty}^{\infty} dy e^{-\frac{(q-y)^2}{2\delta_q^2}} \left|y\right\rangle \left\langle y|x\right\rangle \\
&= \frac{1}{\sqrt{2\pi\delta_q^2}} \int_{-\infty}^{\infty}\int_{-\infty}^{\infty} dxdy \left\langle x\right| \hat{\rho}(t) e^{-\frac{(q-y)^2}{2\delta_q^2}} \left|y\right\rangle \delta(y-x) \\
&= \frac{1}{\sqrt{2\pi\delta_q^2}} \int_{-\infty}^{\infty} dx \left\langle x\right| \hat{\rho}(t) e^{-\frac{(q-x)^2}{2\delta_q^2}} \left|x\right\rangle \\
&= \frac{|1-\lambda^2|}{\sqrt{2\pi\delta_q^2}} \sum_{n,m=0}^{\infty} \mathcal{C}_{nm} e^{-D_{nm}^{\kappa}(t)} \mathcal{I}_{nm} \sum_{k=0}^{\min[n,m]} G_{nm}^{k}(\theta) \left|n-k,n\right\rangle_{12} \left\langle m-k,m\right|_{12}
\end{aligned} \tag{3.31}$$

above, $D_{nm}^{\kappa}(t)$ corresponds to Eq. 3.23, being the damping term for the oscillator obtained following the alternate-step procedure previously discussed, and

$$\mathcal{I}_{nm} = \int_{-\infty}^{\infty} \psi_{\phi_n(\kappa,t)}(x) \psi^*_{\phi_m(\kappa,t)}(x) e^{-\frac{(q-x)^2}{2\delta_q^2}} dx \tag{3.32}$$

in which

$$\psi_\xi(x) \equiv \langle x\,|\xi\rangle = \frac{1}{\pi^{1/4}} e^{\frac{\beta^{*2}-\beta^2}{4}} e^{-\frac{1}{2}(q-\sqrt{2}\mathrm{Re}[\beta])^2} e^{iq\sqrt{2}\mathrm{Im}[\beta]} \tag{3.33}$$

is the position wave-function of an arbitrary coherent state $|\xi\rangle$. The probability density function (PDF) of the outcome q is

$$\mathrm{p}(q) = \frac{|1-\lambda^2|}{\sqrt{\pi(1+2\delta_q^2)}} \sum_{l=0}^{\infty} \lambda^{2l} \exp\left[\frac{(q-\sqrt{2}\mathrm{Re}[\phi_l(\kappa,t)])^2}{-(1+2\delta_q^2)}\right]. \tag{3.34}$$

To quantify the entanglement we use the negativity (see first Chapter), defined as $N(t) = \sum_i (|\varepsilon_i| - \varepsilon_i)$, where ε_i are the eigenvalues of the partial transposition of the normalized version of $\hat{\rho}(t)_{12}$ of Eq. (3.31).

A quick inspection of Eq. (3.34) reveals that a change in the initial amplitude from $|\alpha|e^{i\phi_\alpha}$ to $|\alpha'|e^{i\phi'_\alpha}$ entails a rigid shift of the outcome probability $p(q)$ by $\Delta q \approx |\alpha|\cos(\phi_\alpha - t) - |\alpha'|\cos(\phi'_\alpha - t)$. We verified numerically that also the entanglement negativity is subjected to the same shift, which implies that a change in α can be accounted for by selecting the measurement outcome q accordingly. Given this, we set for the rest of this work the initial coherent state to $\alpha = 0$.

We now have the ingredients to assess the validity of the concentration procedure. First, in Fig. 3.5 we plot the negativity as a function of the squeezing parameter λ for several scaled coupling strength g. For our concentration purposes, we will keep the squeezing parameter low $0 < \lambda < 0.5$ —when $\lambda \to 1$ the state approximates to an EPR (unphysical, we would require infinite energy to create it) entangled state. As we can notice we have fixed the amplitude of the coherent state $\alpha = 1$ and the negativity shows two regimes depending of g, for $0 < g < 0.3$ the states have always a higher entanglement compared with the input state ($g = 0$). On the other hand, when $g > 0.3$ the state is partially distilled.

For a fixed set of values ($\kappa = 0.01, \delta_q \approx 0.11, r = 0.1, t = \pi,\ \lambda = 0.3$) we plot in the left y-axis of Fig. (3.6-a) the ratio of the negativity N_D/N_0 (solid line) as a function of the outcome q of the measurement of the oscillator position, where $N_D(N_0)$ stands for the distilled (initial) negativity. In the right y-axis, we show its corresponding PDF (dashed line) as a function of q. The success probability of the concentration protocol, namely the probability of obtaining $N_D > N_0$, is given by

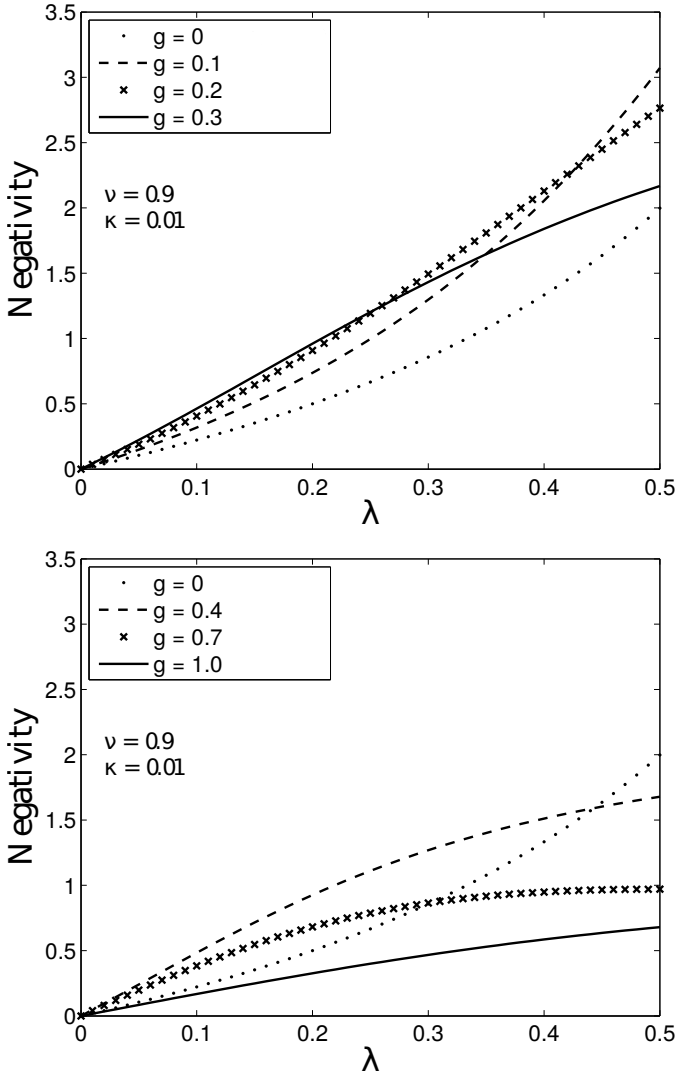

FIGURE 3.5: The plot shows the negativity as a function of the squeezing parameter λ for different scaled coupling strength g. We fixed $\nu = 0.9$, $q = 0$, and $\kappa = 0.01$. We obtain purification for the initial state when $0 < g < 0.3$. However, as g increases the purification is partially achieved. Other values are : $t = \pi, \alpha = 1$.

the shaded region and is defined as:

$$\Pr(g, \lambda)_s = \int_{N_D > N_0} p(q) dq, \tag{3.35}$$

In Fig. (3.6-a) we illustrate three representative cases. For weak optomechanical coupling ($g = 0.01$), one achieves a large success probability though at the cost of an almost negligible increase in negativity $N_D \approx N_0$. For intermediate coupling ($g = 0.2$) the negativity is significantly enhanced, still retaining a high success probability. On the other hand, for large coupling ($g = 1$), not only $N_D \lesssim N_0$ but

also the success probability is considerably small.

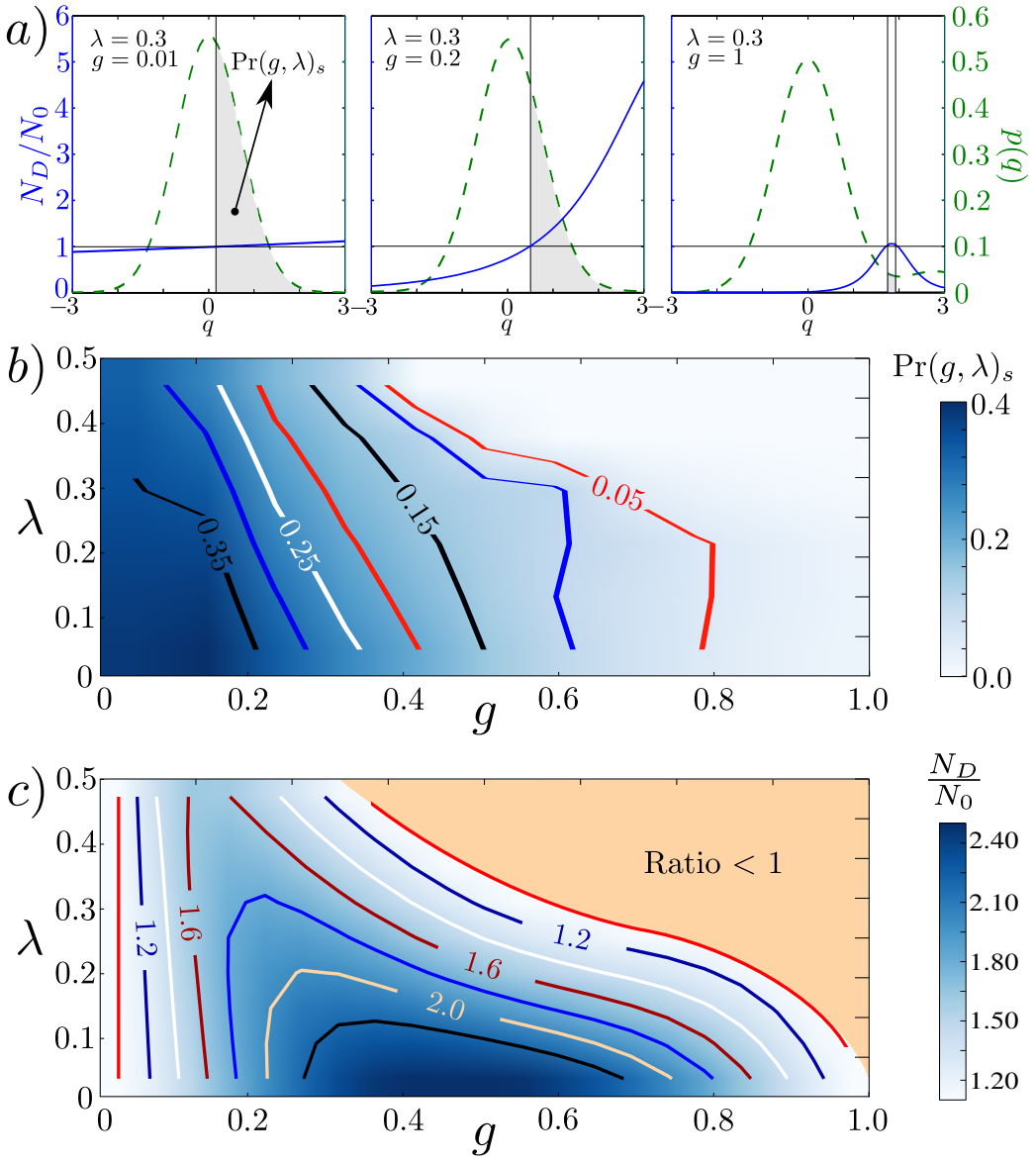

FIGURE 3.6: Upper panel a): We plot in the left y-axis the ratio of the negativity N_D/N_0 as a function of the oscillator's position q (solid line), where N_D (N_0) stands for the distilled (initial) negativity. In the right y-axis we show the PDF as a function of q (dashed line). In the middle panel b) we illustrate the concentration success probability ($\Pr(g,\lambda)_s$) corresponding to the shaded region in the upper panel. Finally, in the bottom panel c) we show the ratio of negativity as function of λ and g for a specific oscillator's position $q = 1.5$.

As a consequence, we see that an optimal region of the coupling value emerges, given that the entanglement concentration is predominantly achieved for *intermediate* radiation-pressure coupling. Similarly we can also see that entanglement concentration is achieved for intermediate values of the initial entanglement, implying

that concentration is optimal in the parameter region $0.2 < \{g, \lambda\} < 0.4$, for which $\Pr(g, \lambda)_s > 0.15$ and $N_D > N_0$.

The reason for this behaviour can be intuitively understood considering the structure of the TMSV state and its evolution under the concentration protocol. The states of the whole system (in absence of decoherence) before and after the optomechanical interaction are given by $|0\rangle_m \sum_n \lambda^n |n, n\rangle_{1,2}$ and $\sum_n \lambda^n e^{ig^2n^2\pi} |2gn\rangle_m |n, n\rangle_{1,2}$ respectively. The states $|2gn\rangle_m$ become more and more distinguishable for larger g. As a consequence, the measurement of the oscillator position effectively becomes a sharp measurement of Fock state inside the cavity [Jacobs1994] that projects the two light beams into a factorized state $|n, n\rangle_{1,2}$. This intuitively explains the failure of the concentration protocol for large g. The failure for large λ is instead due to the fact that the number of photon Fock states compatible with a specific outcome q is finite (for any non-zero g). For large enough λ, this finite superposition of a small set of Fock states $|n, n\rangle_{1,2}$ is not enough to exceed the entanglement of the initial TMSV.

As said, we are neglecting here the cavity decay and further losses in the extraction of the distilled state from the cavity. However, let us note that our results indicate that the concentration protocol is robust against large injection losses (in Fig. 3.6 we considered a beam-splitter reflectivity of $r = 0.1$), which in turn suggests robustness against cavity and extraction losses as well.

3.8 Quantum Teleportation with the Distilled State

It is of course, crucial to suggest both a method to verify the successful concentration/distillation of entanglement, as well as an application of the distilled state. In the following we will show how the teleportation of an arbitrary coherent state $|\beta\rangle$ by the distilled state can serve both purposes. Following the standard procedure [Braunstein1998], we combine mode $\hat{a}_1$ with the coherent state to teleport into a balanced beam splitter. Subsequently, we measure the position (momentum) quadrature of the transmitted (reflected) beam. The unnormalized state after the

joint $\{\bar{x},\bar{p}\}$-measurements corresponds to

$$\begin{aligned}\hat{\rho}(t)_2 &= \frac{|1-\lambda^2|e^{-(\bar{x}^2+\bar{p}^2)-|\beta|^2}}{\pi \mathrm{p}(q)\sqrt{2\pi\delta_q^2}} \sum_{n,m=0}^{\infty} \frac{\mathcal{C}_{nm}}{2^{n+m}} e^{-D^{\kappa}_{nm}(t)} \\ &\times \mathcal{I}_{nm} \sum_{n',m'=0}^{\infty} \frac{\beta^{n'}\beta^{*m'}}{2^{n'+m'}} \frac{1}{n'!m'!} \sum_{k=0}^{\min[n,m]} G^k_{nm}(\theta) \\ &\times \frac{4^k}{\sqrt{(n-k)!(m-k)!}} \sum_{j,j'=0}^{n-k,n'} \mathcal{D}(n-k,j,n',j') \\ &\times \sum_{l,l'=0}^{m-k,m'} \mathcal{D}^*(m-k,l,m',l') \,|n\rangle_2 \langle m|_2 \end{aligned} \tag{3.36}$$

where $\mathcal{D}(n-k,j,n',j') = \binom{n-k}{j}\binom{n'}{j'} e^{i\frac{\pi}{2}(2j'-n')} H_{j+j'}(\bar{x}) \times H_{n-k+n'-j-j'}(\bar{p})$, in which H_n the Hermite polynomial of degree n. The normalization of Eq. (3.36) gives us the probability of the joint measurement $p(\bar{x},\bar{p}) = \mathrm{Tr}\hat{\rho}(t)_2$. The success of the teleportation can be quantified by the fidelity which in our case reads as $f(\bar{x},\bar{p}) = \langle\beta|\hat{\rho}_2|\beta\rangle$, being $\hat{\rho}_2$ the normalized state appearing in Eq. (3.36) displaced by $\hat{D}(\sqrt{2}(\bar{x}+i\bar{p}))$. In particular, we consider the fidelity averaged over all possible outcomes:

$$\langle \mathcal{F}(\bar{x},\bar{p})\rangle_\beta = \int_{-\infty}^{+\infty} f(\bar{x},\bar{p})_\beta p(\bar{x},\bar{p})_\beta d\bar{x}d\bar{p}. \tag{3.37}$$

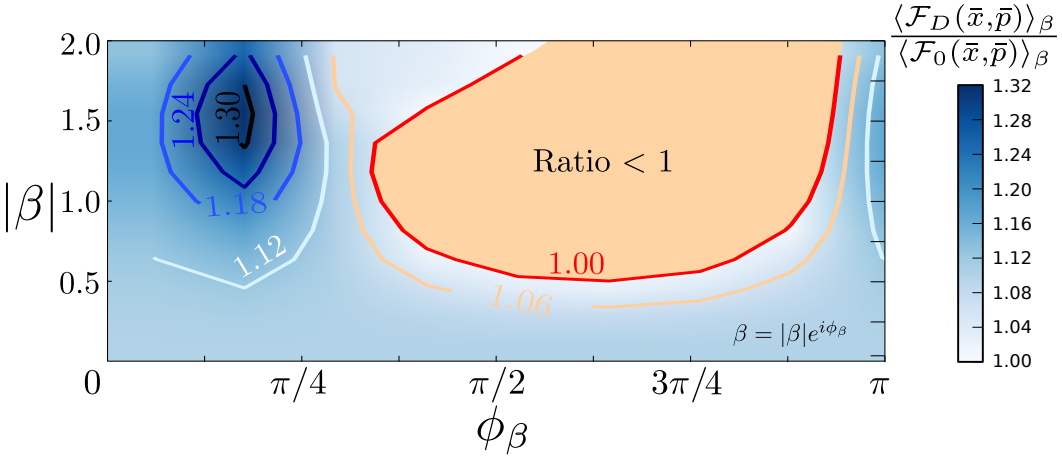

FIGURE 3.7: The figure shows $(\langle \mathcal{F}_D(\bar{x},\bar{p})\rangle_\beta / \langle \mathcal{F}_0(\bar{x},\bar{p})\rangle_\beta)$ the ratio of the average fidelity as a function of the amplitude (β) and phase (ϕ_β) of the coherent state to teleport. In this figure we have used the parameters $\alpha = 2e^i\pi/4$ and $q = 0$.

In Fig. (3.7), with parameters $\alpha = 2e^{i\pi/4}$ and $q = 0$, we clearly distinguish many instances in which the fidelity with the distilled state is greater then the one with the

original state, *i.e.*, $\langle \mathcal{F}_D(\bar{x},\bar{p})\rangle_\beta > \langle \mathcal{F}_0(\bar{x},\bar{p})\rangle_\beta$ [the subindex in $\mathcal{F}_D$ ($\mathcal{F}_0$) corresponds to the distilled (initial) state]. This shows that, for a wide range of β, the distilled state can be exploited to improve the performances of teleportation.

3.9 Experimental Feasibility

The generation of the TMSV state is routinely achieved in quantum optical laboratories, where our range of interests $0 < \lambda < 0.5$ can be fully realized. On the other hand, our protocol requires the initialization of the mechanical oscillator in its ground state or in a coherent state. The cooling of a mechanical oscillator to its quantum ground state has been recently achieved [Teufel2011, Machnes2012, Vanner2010]. Finally, typical values in optomechanics shown a wide range for the oscillator's damping rate κ [Verhagen2012, Chan2011, Murch2008] compatible with our assumptions. Therefore, the initial preparation does not involve a new experimental challenge. Our optimal g value of ~ 0.2 for the optomechanical interaction can now be achieved in several setups [Safavi-Naeini2011, Chan2011, Teufel2011, Murch2008, Xuereb2012, Kaviani2014].

The key stage of this work consists in measuring the oscillator. After the pulse $\hat{a}_1$ interacts with the mechanical oscillator under sufficiently weak radiation-coupling (e.g., using $g \approx 0.2$, $\omega_m/2\pi = 500$ kHz, and $g_0 \simeq 86$ kHz, as in [Vanner2011]), a second auxiliary pulse with a duration much smaller than the mechanical period is then injected into the cavity. The optical phase of the emerging field (correlated with the mechanical position) is then measured via balanced homodyne detection [Vanner2011].

3.9.1 Thermalized mechanical oscillator

To consider a more real experimental scenario, we treat the mechanical oscillator as a thermal state at some temperature T. The mechanics then corresponds to a collection of coherent states as following:

$$\hat{\rho}_m^{th}(0) = \frac{1}{\pi\bar{n}} \int |\alpha\rangle_m \langle\alpha|_m \, e^{-|\alpha|^2/\bar{n}} d^2\alpha \tag{3.38}$$

with $\bar{n}$ being the thermal occupation number.

The density matrix in absence of decoherence can be found easily as:

$$\begin{aligned}\hat{\rho}(t)_{12} &= \frac{1}{\sqrt{2\pi\delta_q^2}}\int_{-\infty}^{\infty} dx\,\langle x|\,\hat{\rho}(t)e^{-\frac{(q-x)^2}{2\delta_q^2}}\,|x\rangle \\ &= \frac{|1-\lambda^2|}{\pi\bar{n}\sqrt{2\pi\delta_q^2}}\sum_{n,m=0}^{\infty}\lambda^{n+m}e^{ig^2(t-\sin t)(n^2-m^2)}\,|n,n\rangle_{12}\,\langle m,m|_{12} \\ &\otimes \int d^2\alpha e^{-|\alpha|^2/\bar{n}}e^{ig\mathrm{Im}[\alpha\eta](n-m)}\int_{-\infty}^{\infty}\psi_{\phi_n}(x)\psi^*_{\phi_m}(x)e^{-\frac{(q-x)^2}{2\delta_q^2}}dx. \quad (3.39)\end{aligned}$$

Following the same alternate step procedure described above (see from Eq. 3.24), we can compute the dynamics in presence of the same detrimental effects considered in the coherent case, namely damping of the mechanical oscillator, and injection of the light beam into the cavity:

$$\begin{aligned}\hat{\rho}(t)_{12} &= \frac{|1-\lambda^2|}{\pi\bar{n}\sqrt{2\pi\delta_q^2}}\sum_{n,m=0}^{\infty}\lambda^{n+m}e^{ig^2(t-\sin t)(n^2-m^2)} \\ &\times \sum_{k=0}^{\min[n,m]}G^k_{nm}(\theta)\,|n-k,n\rangle_{12}\,\langle m-k,m|_{12} \\ &\times \int d^2\alpha e^{-|\alpha|^2/\bar{n}}e^{ig\mathrm{Im}[\alpha\eta](n-m)}e^{-D^{\kappa}_{nm}(t)} \\ &\times \int_{-\infty}^{\infty}\psi_{\phi_n(\kappa,t)}(x)\psi^*_{\phi_m(\kappa,t)}(x)e^{-\frac{(q-x)^2}{2\delta_q^2}}dx \quad (3.40)\end{aligned}$$

In Fig. 3.8 we plot in the left (right) $y-$axis the ratio of the negativity (the probability density function). In Fig. 3.9 we illustrate the negativity as a function of the squeezing parameter λ for different scaled coupling strength g.

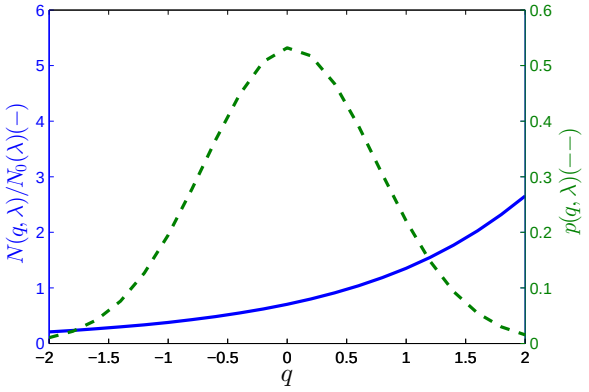

FIGURE 3.8: In the left (right) $y-$axis we plot the ratio of the negativity (the probability density function). Other values are ; $\nu = 0.95, \lambda = 0.3, g = 0.2, \bar{n} = 0.001, \kappa = 0.001$

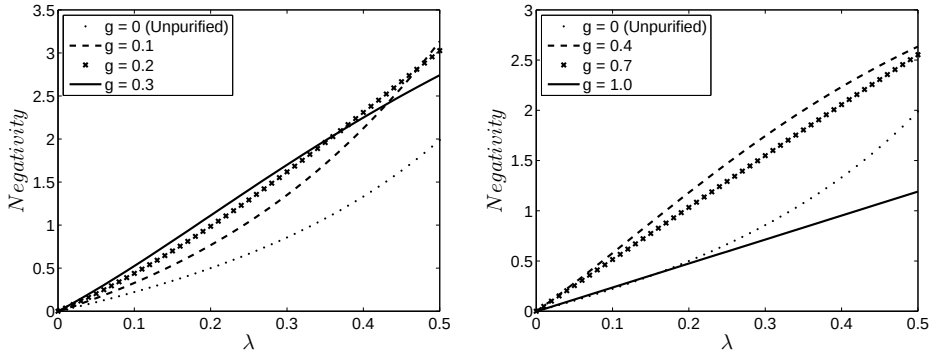

FIGURE 3.9: The plot shows the negativity as a function of the squeezing parameter λ for different scaled coupling strength g. Other values ; $\nu = 0.95, q = 1.5, \bar{n} = 0.001, \kappa = 0.001$.

3.10 Conclusion

In summary, we have presented a first application of optomechanics in entanglement concentration, which is arguably the most important protocol in long distance quantum communications. Our proposal uses an indirect measurement of the photon number of the electromagnetic field inside a cavity through the position measurement of a mechanical element coupled to it. For an optimal strength of the optomechanical coupling, the photon number is measured weakly or "unsharply" and this results in entanglement concentration conditioned to the position outcome. For a vacuum state inside the cavity, the position meter does not move, corresponding to a failed outcome of concentration. Thus our procedure has a degree of qualitative similarity with the known purely optical procedure of photon subtraction [Duan2000,

Fiurasek2003, Browne2003b, Datta2012, Bartley2013, Opatrny2000, Olivares2003], where also the vacuum component is essentially filtered, and we have comparable probabilities of success and entanglement enhancement on concentration. On the other hand, the position measurements of a mechanical oscillator can be highly precise, especially as we are not concerned about back-reaction as the measurement is at the end of our protocol (the oscillator can be reinitialized before performing concentration again). Other optimizations of our protocol may be attempted such as multiple modes in the cavity.

The state obtained through our protocol is non-Gaussian, and thus it can serve as the first step of Gaussification [Browne2003b, Campbell2012] (see Section 3.3.2) — which can enhance its entanglement further and act on multiple copies — or, more in general, for quantum computation purposes [Menicucci2006]. Moreover, the procedure here outlined could be useful also in a quantum repeater scenario for long distance communication, considering that there no further extraction of the distilled state from the optical cavity is needed.

Chapter 4

Mechanical Qubit-Light Entanglers in Nonlinear Optomechanics

Interfacing between matter qubits and light is a crucial requirement for scalable quantum networks. However, a generic qubit may not directly interact with a relevant optical field mode.

In Section 4.3, we show how a parametric coupling of the qubit with a mechanical object, in conjunction with the trilinear radiation pressure coupling of the same object with light, can induce near maximal qubit-light entanglement at an optimal time. Next, in Section 4.4, we show how this qubit-cavity entanglement can feasibly be used to entangle the qubit with light traveling through a linking optical fibre. Moreover we show the scenario can potentially be adapted to entangle a generic qubit with another atomic (resonant) qubit in a spatially separated cavity connected to the former through a single mode optical fibre (see Section 4.4). We also show in Section 4.3 how our method enables conditional non-classical state preparation of an optical field state through the measurement of a generic qubit, which might be more convenient to measure in comparison to the mechanics.

Our optomechanical transducer benefits from not requiring any cooling of the mechanical element, and not needing an adjusting of the detunings and transition frequencies so as to have perfect quanta-exchange Hamiltonians between any pairs of quantum systems.

4.1 Quantum Networks

A quantum network is composed of quantum nodes linked by classical or quantum channels. On the one hand, having n qubits connected by k classical channels the dimension of the state space is $2^n k$, meanwhile for the quantum case the dimension increases up to 2^{kn}, being exponentially larger [Kimble2008]. In general, the quantum nodes (usually a combination between fields and atomic qubit states due to their long storage times) are made to generate and to process (e.g. state selection via quantum measurements) quantum information, whereas the "flying qubits" or photons traveling through the quantum channels are made to distribute the quantum entanglement between nodes. In order to create a quantum network, it is a essential to efficiently control each node, and therefore all techniques used to protect or to improve the quantum entanglement are all crucially important. For example, quantum entanglement stability investigated in Chapter 2 and quantum concentration (or distillation for several copies) studied in Chapter 3 are important in these cases. Of course, the scalability of the network will contribute to the destruction of the coherence of the quantum information to propagate. It is then vital to consider the detrimental effects of the main sources of decoherence.

In Fig. 4.1 we show several schemes regarding quantum networks, where a special emphasis would be noted for the two quantum nodes linked through a quantum channel in Fig. 4.1-c. Although previous schemes are based on quantum state transfer and entanglement distribution between nodes within cavity quantum electrodynamics (QED) (e.g., see Refs. [Cirac1997, Pellizzari1997]), the main difference in our proposal lies within the undriven full dynamics (not linearized Hamiltonian) of a generic qubit coupled to an opto-mechanical system linked to a cavity QED system (Jaynes-Cummings interaction Hamiltonian) under cavity and mechanical losses. As far as I know, the above model under the full regime have not yet been explored.

4.2 Introduction

Over the last decades, the growing field of quantum information has become of paramount importance not only to test quantum mechanics, but also to achieve quantum algorithms towards the future universal quantum computer. Although some quantum algorithms have been successfully realized, it is still challenging

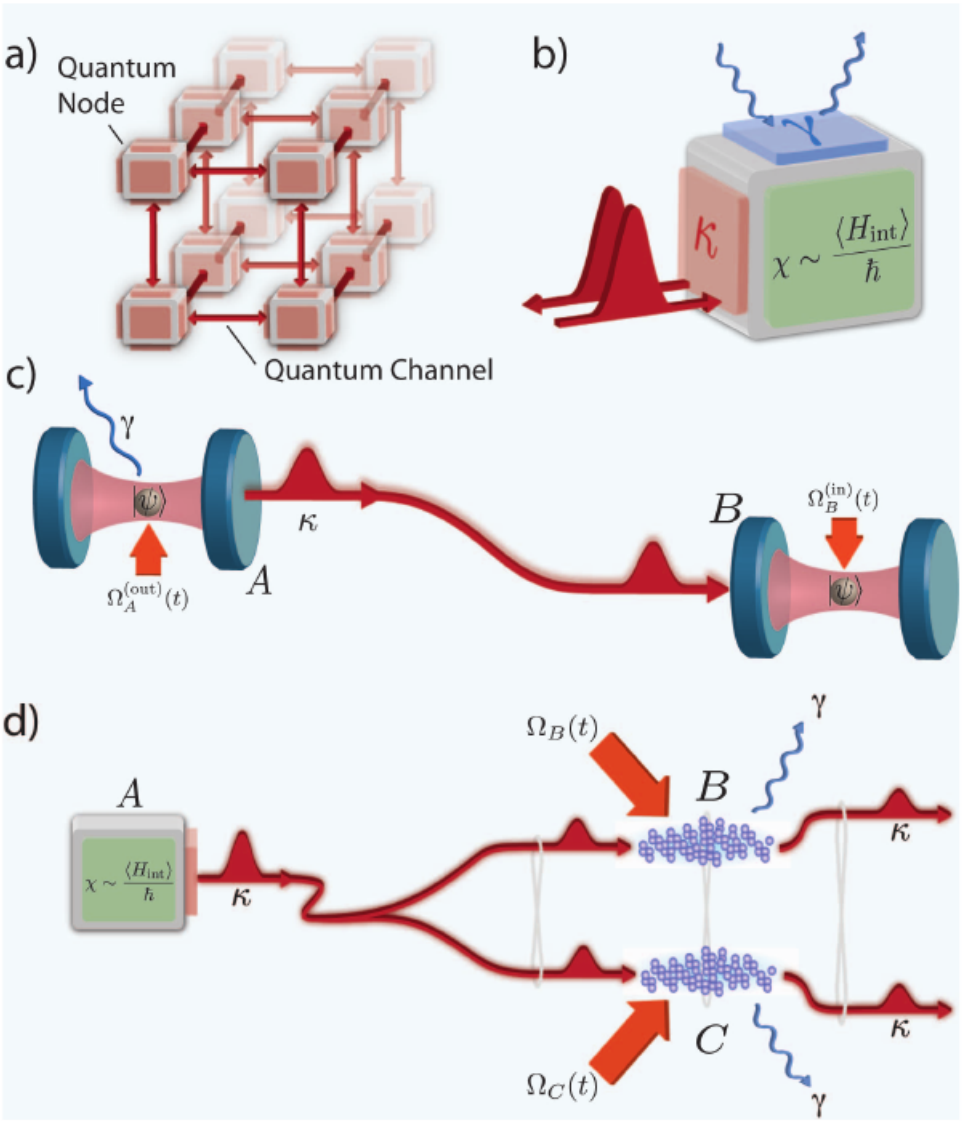

FIGURE 4.1: Several quantum networks scenarios. In (a) an array of quantum nodes linked to their neighbors through quantum channels. (b) The figure shows a matter-light interface. (c) Two nodes connected via an optical fibre, in particular two trapped atomic qubits are placed into two distant cavities within cavity QED operational regime. In (d) distribution of entanglement using ensembles of a large number of atoms. **This figure was taken from its original source, see Ref. [Kimble2008] for a more detailed description**

to deal against decoherence and scalability. To bypass these bottleneck, a solution has been proposed to distribute quantum entanglement over long distances with low losses rates, namely, a quantum network [Kimble2008]. In general, each quantum network node is built on single atoms due to their long storage/coherent time, whereas the "flying" qubits (optical photons) allow us to transfer information coherently between them. Central to these networks is to generate qubit-light entanglement for which would seem to require an interaction of a qubit and a cavity field. At least this was the standard scheme for very long as the qubits were generically assumed to be atomic in nature so that they could have a resonant interaction with cavity fields. The qubit-cavity direct coupling could be used to either map the qubit state to a cavity field so that it was carried and fed in to a distant cavity through the light [Cirac1997, Pellizzari1997, vanEnk1999], or to entangle maximally a qubit with the field in a cavity. Subsequent joint detections of fields from two separate cavities could be used to maximally entangle the qubits in a heralded manner [Bose1999b]. Crucial to all these is that the qubit interacts directly and resonantly with the optical field. In recent years a plethora of other qubits have surfaced which have frequencies in the microwave and radio-frequency range [Pla2012, Maragkou2015, Kolkowitz2012, Rabl2009, Rabl2010]. For these an alternate strategy has been suggested whereby both the qubit and the optics interact with a mechanical mediator. This is possible because a mechanical object generically interacts with a wide variety of physical systems. These systems have shown the successful linking of distant qubits through optomechanics [Stannigel2010, Stannigel2011, Stannigel2012a, Habraken2012]. However these schemes rely on an exchange of excitations between systems – between the qubit and the mechanics (a Jaynes-Cummings interaction) and between the mechanics and light (a beam-splitter interaction). Such an exchange is only ensured at the cost of an appropriate adjustment of detunings of the fields that drive the qubit and the optical field from their respective transitions by precisely the mechanical frequency. It is thereby be important to explore whether parametric interactions of qubits with mechanics (as in Chapter 2) as well as the parametric trilinear optomechanical interaction (as in Chapter 3) which are generic qubit-mechanics and radiation pressure interactions without any necessity for adjusting resonances, can be fruitfully used to entangle a qubit with light. In particular, this question is quite nontrivial as it is not apriori intuitive that the qubit and light can be entangled to a high degree by these means as the mechanical mediator needs to disentangle substantially from both of them in order for that to happen. In the previously studied case of Jaynes-Cummings combined with beam-splitter interaction, on the other

hand, it is quite intuitive that the former and latter Hamiltonians swap quantum states from the qubit to mechanics and mechanics to light respectively. They are thereby intuitively clear candidates for state transfer from qubits to optical fields. The nature of the parametric Hamiltonians, however, are clearly not of a state swapping type by nature. Thereby under these Hamiltonians the most sensible task perhaps is to look for an entanglement between the qubit and the optical fields mediated by the mechanical degree of freedom (obviously such entanglement suffices as a building block of optomechanical networks as discussed above). Even in this task, whether the entanglement will be "transitive" in nature is apriori not clear. The individual Hamiltonians do indeed entangle a qubit-mechanical oscillator pair and an optical field-mechanical oscillator pair, but whether also a qubit-optical field entanglement will result from this is hard to guess.

In this Chapter, we study essentially a feasible light-matter system, where a generic qubit (typically not having a resonance in the optical frequencies) is entangled to a single electromagnetic cavity mode, where both are mediated through a mechanical object (modeled as a harmonic oscillator for simplicity). Here we consider the qubit directly coupled to the mechanical oscillator position. Such a qubit-oscillator Hamiltonian can be synthesized in a variety of ways, notably through magnetic field gradients [Scala2013] or through capacitive couplings [Armour2002]. In other words, the actual mechanical position is essentially linked to two states of the qubit. On the other hand, for the oscillator-cavity subsystem we exploit the (intrinsically nonlinear) radiation pressure interaction. Very recently, such tripartite qubit-oscillator-optics systems have been found to be of interest fundamentally in giving rise to interesting polaritonic states involving mechanics [Restrepo2014] and tripartite entanglement [Abdi2015]. However, the practical applications of such systems in enabling quantum networking, specifically in the regime of the interactions we use remains unexplored.

In the following we divide our presentation into several sections. First, we fix our attention into the dynamics of quantum correlations for a tripartite system (qubit-oscillator-cavity). To study this case, we solve analytically the tripartite dynamics in absence of decoherence, and then we compute the negativity for the reduced bipartite subsystems respectively. Secondly, we study the conditional preparation of non-classical states of the optical field conditional on measuring the states of the qubit, which can, in principle, be done with a high fidelity. Subsequently, motivated for quantum networking, we coupled the single cavity mode to an output field (waveguide/optical fibre). In this case, we solve numerically the Markov-Born

master equation under oscillator energy losses and photon leakage from the cavity. Lastly we explore whether a generic qubit can be entangled with an atomic qubit in a distant cavity by using our mechanism in one of the cavities.

Our results are shown to be promising under actual experimental values. In our scheme, at a particular time (multiples of the mechanical oscillator cycle), a high amount of entanglement between the qubit-cavity subsystem is generated, independently of the qubit-oscillator and oscillator-cavity coupling parameters. Here, optimal entanglement between two subsystems is understood as the only non-zero negativity between relevant subsystems. This is because, at least when the whole tri-partite subsystem is assumed to be a closed system, then at this time, the relevant sub-systems are in an entangled pure state. Entangled pure states with substantial entanglement are, of course, the most useful type of entangled states. We have found that the mechanical oscillator state becomes disentangled from the rest of the system at each cycle so as to ensure (for optimally chosen couplings) that the qubit and the cavity field are in a highly entangled pure state. Furthermore, for some particular coupling values, we can also generate multicomponent Schrödinger-cats states for the cavity field. Additionally, a partial qubit-fibre entanglement is achieved for an optimal cavity-fibre coupling.

4.3 Tripartite Qubit-Oscillator-Cavity Evolution

At first we investigate the building block of our quantum network proposal towards the qubit-qubit correlation shown in Section 4.4, namely a single tripartite qubit-oscillator-cavity node. This first approach will show us —*among other things*— the optimal operational regime in which bipartite quantum entanglement between any pair of the systems can be generated. In subsequent sections, we will investigate how this basic node can be connected to another distant qubit-cavity node (under Jaynes-Cummings interaction) through an optical fibre.

Let us first commence considering a closed system as shown in Fig. 4.2 —*in a later Section we will solve the Born-Markov master equation when both the photon leakage from the cavities as well as the oscillator damping are considered.* As mentioned in the introduction, a generic qubit is indirectly coupled to a single cavity mode, where both are being mediated through a quantum mechanical oscillator (modeled as a harmonic oscillator for simplicity)

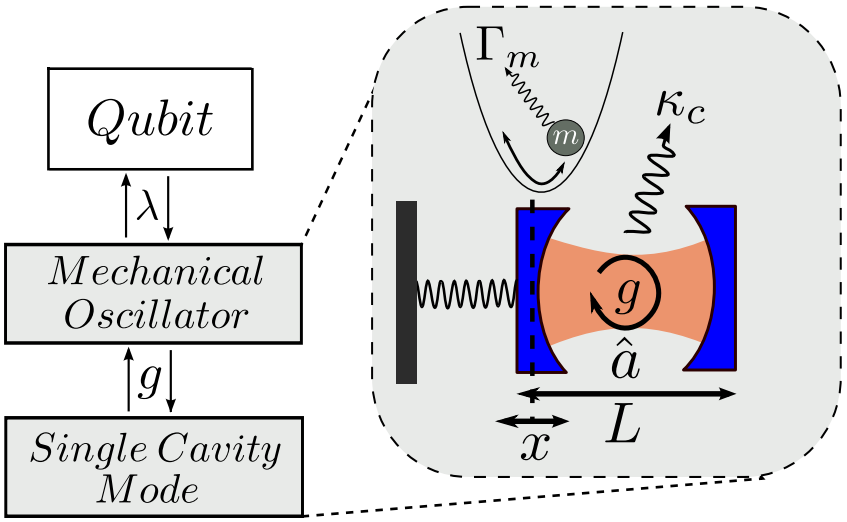

FIGURE 4.2: The figure shows a qubit-cavity bipartite system mediated through a mechanical oscillator. On the one hand, the mechanical mode ($\hat{b}$) is coupled to the cavity field ($\hat{a}$) with a strength g via radiation pressure interaction as in Chapter 3, whereas the qubit is coupled to the oscillator position with a strength λ as studied in Chapter 2. In Section 4.4 we will consider the quantum open system, where Γ_m and κ_c are the rates of mechanical loss and photon leakage respectively.

The interaction Hamiltonian considered here is a combination of previous couplings reported in this Thesis, namely the qubit-oscillator displaced conditioned Hamiltonian (see Chapter 2), and the radiation pressure interaction for the oscillator-field coupling (see Chapter 3). In principle, it is not obvious that the bipartite qubit-light system will be entangled dynamically. Because, in contrast to other proposals where they are mainly based on excitation exchange (Jaynes-Cummings like, and Beam-Splitter interactions), the qubit-light Hamiltonian considered here it is of a dispersive type, i.e. an interaction Hamiltonian that conserves the excitations of the qubit and the cavity field.

It is straightforward to write down the relevant Hamiltonian ($\hbar = 1$) in the interaction picture as following:

$$\hat{H}_{\text{int}} = -(g\hat{a}^\dagger\hat{a} + \lambda\hat{\sigma}^z)(\hat{b}e^{-i\omega_m t} + \hat{b}^\dagger e^{i\omega_m t}) \tag{4.1}$$

where, ω_m stands for the angular frequency of the mechanical oscillator; g is the cavity-oscillator radiation-pressure coupling, and λ is the qubit-oscillator coupling strength. Finally, $\hat{a}$ ($\hat{b}$) is the usual boson annihilation operator for the cavity (oscillator), and $\hat{\sigma}^z$ is the Pauli $z-$spin matrix for the spin qubit. Even in a bipartite optomechanical system it is known that measurements on the cavity field can

conditionally project the mechanical oscillator to interesting non-classical states [Bose1997]. However, in practice, a qubit (being a digital measurement of 0 or 1) may be measured much more faithfully in comparison to a continuous position degree of freedom. Thus it is important to find whether non-classical states of a cavity field can be prepared even when a qubit and the field are interfaced indirectly through the mechanical element. Here we show that it is indeed the case.

For a particular set of values of the coupling parameters g and λ we can generate non-classical states for the cavity mode (multimode Schrödinger cat states). The appropriate choice of $\{g, \lambda\}$ is shown in the regions denoted by i, ii, and iii in Fig. 4.3-top and coincides with the disentanglement between the qubit and the cavity mode at $t = 2\pi/\omega_m$ (particularly, in those regions the relation between g and λ corresponds to $g\lambda = k/4$, where $k = 1, 2, 3$, respectively).

The multimode Schrödinger cat states are achieved for $g^2 = \omega_m^2/2p$, where $p \geq 2$ gives the $p-$mode Schrödinger cat state generated. This can be quantitatively shown with the reduced cavity density matrix at $t = 2\pi/\omega_m$ (see Fig. 4.3-bottom for a gallery of multimode cat states).

$$\hat{\rho}(2\pi/\omega_m)_c = e^{-|\alpha|^2} \sum_{n,m=0}^{\infty} \frac{\alpha^n \alpha^{*m}}{\sqrt{n!m!}} e^{\frac{2i\pi g^2(n^2-m^2)}{\omega_m^2}} \cos(4\pi g\lambda(n-m)/\omega_m^2) \left|n\right\rangle \left\langle m\right| \quad (4.2)$$

4.4 Towards Quantum Networking: Qubit-fiber Entanglement and Quantum Correlations of Two Distant Qubits

In the following, we will address the quantum networking scenario in order to achieve this goal we will consider the network architecture shown in Fig. 4.4. Firstly, we will only aim for the bipartite qubit-fibre entanglement dynamics, i.e., in absence of the second node. Subsequently, we will solve the full qubit-qubit dynamics in presence of photon leakage from cavities and damping of the mechanical object.

Although the optical fibre can be modeled as a space-temporal operator into a continuum of modes, i.e., $\hat{f}(t,z) \approx \int_0^\infty \hat{f}_\omega e^{-i\omega(t-z/c)} d\omega$, where $[\hat{f}_\omega, \hat{f}_{\omega'}^\dagger] = \delta(\omega - \omega')$, we will use an approximation which takes into account the finiteness length l of the fibre. Let us consider the number of modes which would significantly interact

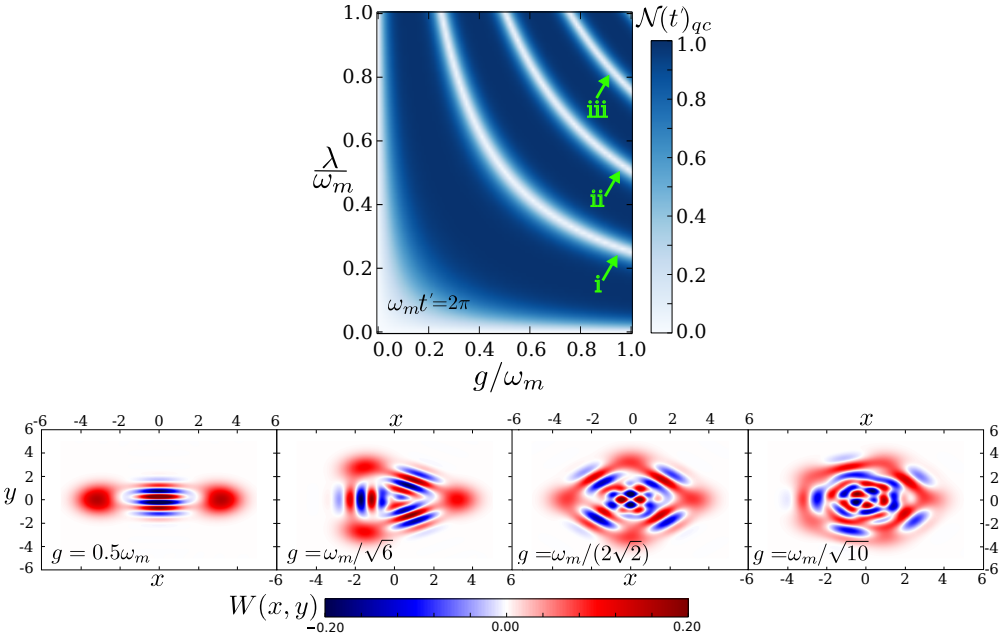

FIGURE 4.3: The top figure shows the negativity as a function of λ/ω_m and g/ω_m at $t = 2\pi/\omega_m$. As seen above, a high qubit-cavity entanglement can be reached for a wide set of coupling values. However, in regions *i*, *ii*, and *iii* the qubit-cavity might disentangle for some chosen parameters. Interestingly, in those regions we can achieve non-classical states (multimode Schrödinger cat states, see bottom figure) for $\lambda = 1/4g$. Other values are $\alpha = 1, \bar{n} = 0.1$.

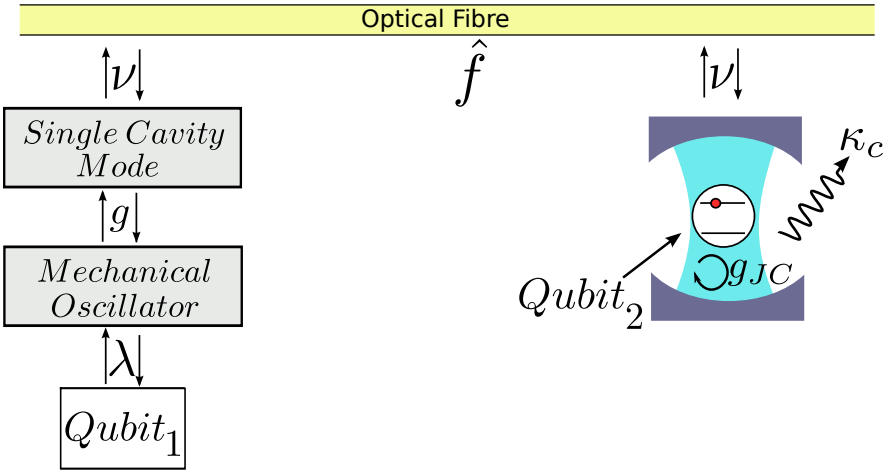

FIGURE 4.4: The figure illustrates the quantum open case for two distant qubits connected through an optical fibre. A tripartite qubit-mechanical-optics system is coupled to an output field by an interaction strength ν, a remote qubit is trapped inside a cavity (single-mode) interacting via Jaynes-Cummings coupling.

with the cavity mode as $n = (l\bar{\nu})/2\pi c$, where $\bar{\nu}$ is the decay rate of the cavity field into a *continuum* of fibre modes. For simplicity we will consider $n \leq 1$, i.e., essentially only one (resonant) mode of the fibre will interact with the cavity modes. This approximation is often called the short-fibre limit [Serafini2006]. Moreover, another fibreless situation can be considered, i.e., one can remove the optical fibre dependence. For example this can be achieved having in mind on-chip technologies, where the nodes are directly coupled next to each other, even though this case is quite interesting (and as far as I know it has not been treated under our particular model) it is not modeled here.

The Hamiltonian for the single node coupled to an output field then reads as — where we have considered cavity-fibre resonance:

$$\hat{H}_{\text{int}} = -(g\hat{a}^{\dagger}\hat{a} + \lambda\hat{\sigma}^{z})(\hat{b}e^{-i\omega_m t} + \hat{b}^{\dagger}e^{i\omega_m t}) + i\sqrt{2\kappa_f}(\hat{a}^{\dagger}\hat{f} - \hat{a}\hat{f}^{\dagger}). \tag{4.3}$$

In Fig. 4.5, we have computed the negativity for an initial coherent state for the cavity $\alpha = 0.8$, and other parameters that they were chosen to maximize the entanglement. In particular, we selected $\bar{n} = 0$ for simplicity, some cooling techniques for macroscopic objects can be found in [Teufel2011, Machnes2012] and also they were already discussed in Chapter 3. To reach a higher entanglement we prepare the cavity in a number state superposition:

$$|\psi(0)\rangle_{\text{cav}} = \frac{1}{\sqrt{2}}(|0\rangle - |1\rangle). \tag{4.4}$$

Even though this state superposition is hard to produce in the laboratory, there have been some experimental proposals to generate it, for instance see Ref. [Bose1999a]. In Fig. 4.5 we plot the entanglement generated dynamically for the initial cavity state shown in Eq. 4.4. After this stage, two qubit-fiber entanglement pairs can in principle be used to entangle distant qubits. The idea is that the light from two distinct fibers is jointly measured to entangle the qubits in a heralded manner. However, we are next going to consider the entanglement between two distant qubits in a pure dynamical manner (i.e., without measurements). The combined dynamics of two of our spin-opto-mechanical nodes connected by fiber becomes too complicated to handle in view of the growing Hilbert space and the fact that though each individual node can be analytically solved, the case when they are connected

by a fiber has to be handled numerically. We are thereby going to consider a somewhat simplified problem where one node has our spin-optomechanical setup, while the other node has a resonant qubit.

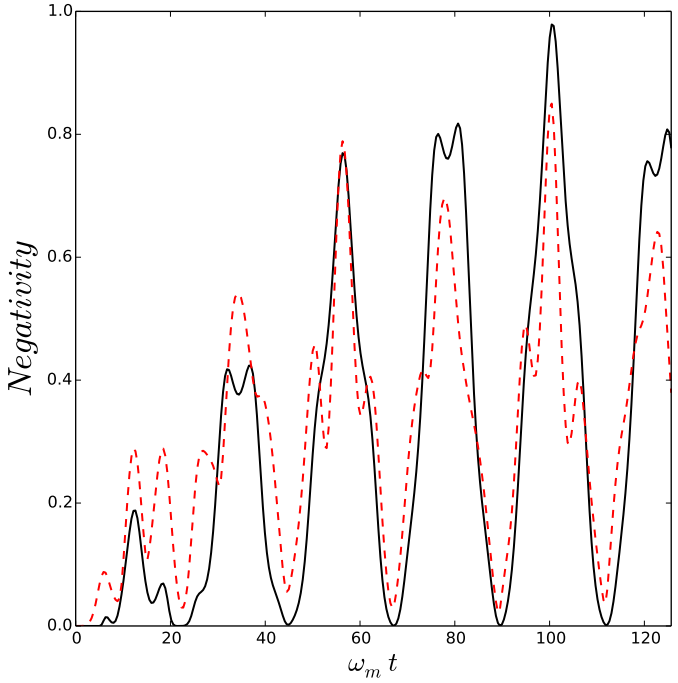

FIGURE 4.5: The figure shows the qubit-fibre entanglement dynamics for two different initial cavity states. We plot in red dashed line an initial coherent state for the cavity $\alpha = 0.8$, other parameters are : $g = 0.1\omega_m, \lambda = 0.2\omega_m, \bar{n} = 0, \nu = 0.1\omega_m$. In black solid line we consider an initial number state superposition for the cavity $|\psi(0)\rangle_{\text{cav}} = \frac{1}{\sqrt{2}}(|0\rangle - |1\rangle)$, other values are : $g = 0.1\omega_m, \lambda = 0.16\omega_m, \bar{n} = 0, \nu = 0.14\omega_m$.

Now, we have all the ingredients to explore the quantum entanglement dynamics generated between distant qubits. On the one hand, a generic qubit is placed as in Section 4.3. On the other hand, we will consider a second resonant qubit trapped inside a distant cavity through Jaynes-Cummings coupling interaction g_{JC}, where both cavities are connected via an optical fibre (see Fig. 4.4).

The Hamiltonian in the interaction picture (in units of $\hbar$) is:

$$\hat{H}_{\text{int}} = -(g\hat{a}_1^\dagger\hat{a}_1 + \lambda\hat{\sigma}_1^z)(\hat{b}e^{-i\omega_m t} + \hat{b}^\dagger e^{i\omega_m t}) + g_{JC}(\hat{\sigma}_2^+\hat{a}_2 + \hat{\sigma}_2^-\hat{a}_2^\dagger) \quad (4.5)$$

$$+ \sum_{j=1,2} i\sqrt{2\kappa_f}(\hat{a}_j^\dagger\hat{f} - \hat{a}_j\hat{f}^\dagger). \quad (4.6)$$

To consider a realistic scenario we will numerically solve the Markovian master equation under energy losses from the cavities, as well as the damping from the oscillator —for an initial number superposition state for the cavities. The master equation reads as following:

$$\begin{aligned}\dot{\hat{\rho}}(t) &= -i[\hat{H}_{\rm int},\hat{\rho}(t)] + \frac{\kappa_c}{2}\sum_{i=1,2}\mathcal{L}[\hat{a}_i]\hat{\rho}(t) \\ &+ (n_{\rm th}+1)\frac{\Gamma_m}{2}\mathcal{L}[\hat{b}]\hat{\rho}(t) + n_{\rm th}\frac{\Gamma_m}{2}\mathcal{L}[\hat{b}^\dagger]\hat{\rho}(t) \qquad (4.7)\end{aligned}$$

where, $\mathcal{L}[\hat{O}]\hat{\rho}(t) = 2\hat{O}\hat{\rho}(t)\hat{O}^\dagger - \hat{O}\hat{O}^\dagger\hat{\rho}(t) - \hat{\rho}(t)\hat{O}\hat{O}^\dagger$. In additions, κ_c is the rate of energy losses due to photon leakage from the cavity, and Γ_m corresponds to the damping of the mechanical oscillator. We solve Eq. 4.7 at zero temperature, i.e., $n_{\rm th} = 0$.

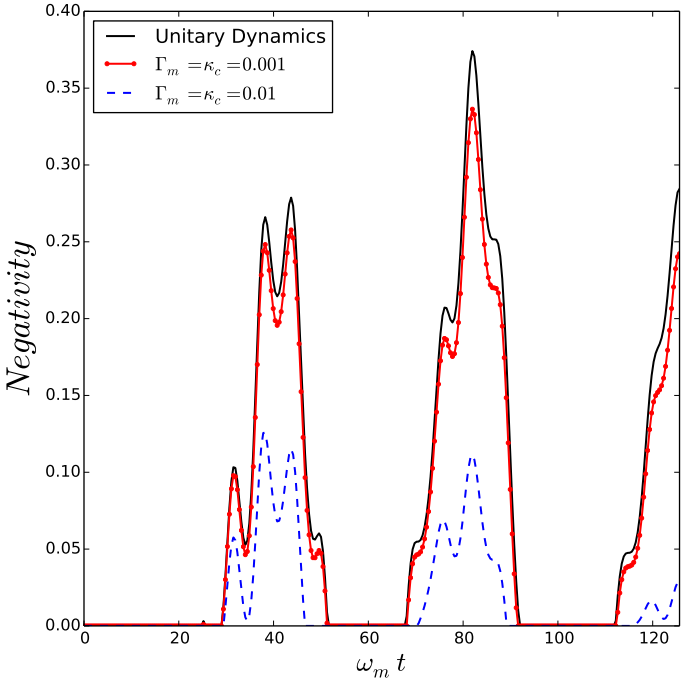

FIGURE 4.6: Qubit-qubit entanglement dynamics for the quantum open system. We consider equal losses rate for both the photon cavity leakage, as well as the damping of the mechanical oscillator. In red solid line (blue dashed line) $\Gamma_m = \kappa_c = 0.001$ ($\Gamma_m = \kappa_c = 0.01$). In black solid line we show the dynamics in absence of losses, i.e., the unitary evolution. Other values are : $g = 0.1\omega_m, \lambda = 0.16\omega_m, \bar{n} = 0, \nu = 0.14\omega_m$.

4.5 Concluding Remarks

In this Chapter, we have presented two main results i) a feasible interfacing between matter qubits and light, and ii) qubit-qubit quantum entanglement between two distant nodes.

Basically, for the first case, we have considered a physical model composed of a parametric coupling of the qubit with a mechanical object, together with the radiation pressure coupling of the same object with light. To explore the quantum entanglement dynamically generated between bipartite systems, we solve the negativity for the corresponding reduced density matrices, with special attention in the (indirect) qubit-light subsystem. As a result of the dispersive nature of the interaction Hamiltonian considered here, it is not straightforward to evidence quantum correlations between them. Our results shown to be quite promising under low qubit-mechanics and qubit-light coupling strength, for experimental values shown in Chapters 2 and 3 respectively. For instance, for optimal values $\alpha = 1, \bar{n} = 0.1, \lambda/\omega_m = 0.5, g/\omega_m = 0.1$ a high entanglement can be achieves for $\omega_m t = 2\pi$ ($\mathcal{N} \to 1$). Moreover, at that time (and multiples of the mechanical oscillator cycle), we have found that the mechanical oscillator state becomes disentangled from the rest of the system at each cycle so as to ensure (for optimally chosen couplings) that the qubit and the cavity field are in a highly entangled pure state, being of course, the most useful type of entangled states.

Furthermore, for some particular coupling values, we can also generate multicomponent Schrödinger-cats states for the cavity field when the qubit is measured. In practice, the advantage of a qubit projection is that a qubit may be measured much more faithfully in comparison to a continuous position degree of freedom as shown previously, e.g., see Ref. [Bose1997].

On the other hand, towards the remote qubit-qubit quantum entanglement between nodes. First, we shown (for a closed system) a partial qubit-fibre entanglement for an optimal cavity-fibre coupling. Secondly, we solved the master equation considering photon losses from the cavities, as well as energy losses from the mechanical object. The results shown that qubit-qubit entanglement can be generated between a generic and an atomic qubit.

Our proposal opens up the scope of quantum networking even when the interactions are not of the energy exchange type, such as purely Jaynes-Cummings type.

Furthermore, in our investigation we have not considered a linearized Hamiltonian nor an external field to drive the cavity mode —a regime unexplored so far.

Chapter 5

Quantum Correlations Driven by Thermal Environments

At first glance, this part of the Thesis might seems as the most different Chapter of this work. However, the physical system is closely related to quantum networks (as it is based on a well-known system, see for instance Ref. [Serafini2006]). Furthermore, we use this model to explore other ways to quantify quantum correlations, as well as to answer a more fundamental question regarding quantum open systems — whether the thermal quantum fluctuations of the environment can induce quantum correlations or not.

As said, this Chapter is devoted to the study of the evolution of an open quantum system within the Born-Markov microscopic master equation (MME). Particularly, our system of interests corresponds to two distant two-level atoms trapped in fibre-coupled cavities. In general, thermal effects on the relevant system have been usually treated as a destructive source of quantum correlations. However, a counterintuitive dynamics was found a few years ago [Krauter2011, Muschik2011, Kastoryano2011, Memarzadeh2011] where thermal fluctuations might indeed induce quantum correlations.

To study the quantum correlations driven by thermal fluctuations. First, we will consider that our system will start from its ground state, i.e., no excitations are present at $t = 0$ —atoms are in the ground state, and fields are in the vacuum state. Secondly, each (independent) reservoir will start at a non-zero temperature. Finally, under the approximation of one-excitation allowed in the atom-cavity-fibre

basis, we can obtain an induced quantum correlations for the transient evolution due to thermal fluctuations from the environment.

To quantify the quantum correlations, we will explore two new measures of quantum entanglement, namely Quantum Discord (see Sec. 5.1) and Concurrence.

5.1 Quantum Discord

Alternatively to entanglement, the quantum correlations can be also quantified by the quantum discord originally suggested in Refs. [Henderson2001, Ollivier2001], also see for instance [Luo2008, Ali2010, Lu2011, Qing2011, Fanchini2010]. Quantum discord corresponds to a measure of quantum correlation which does not involve quantum entanglement necessarily — *only for mixed states, for pure states quantum entanglement and quantum discord are equivalent.* In other words, the quantum entanglement can be zero, but there may be still quantum correlations due to quantum nature alone. In fact, non-zero quantum discord indicates the presence of correlations that are due to non-commutativity of quantum operators.

To define this measure of quantum correlations, we have to go back to classical information theory. As known, the Shannon entropy $\mathcal{H}(X)$ quantify the amount of information contained in a random variable X. If $\mathcal{H}(X) = 0$, then no new information can be obtained by measuring X, therefore we have complete knowledge about that variable. Thus, Shannon entropy can be related both to the degree of knowledge of an specific random variable or to the amount of information that it can be extracted via measurements. The mutual information is then define as following

$$\mathcal{I}(A;B) = \mathcal{H}(A) + \mathcal{H}(B) - \mathcal{H}(A,B), \tag{5.1}$$

where, $\mathcal{H}(A,B)$ is the joint conditional entropy, i.e., corresponds to the information content of the full system. The meaning of the mutual information is quite straightforward from its mathematical expression.

On the other hand, classical correlation is defined as:

$$\mathcal{C}(A;B) = \mathcal{H}(A) - \mathcal{H}(A|B), \tag{5.2}$$

above, $\mathcal{H}(A|B) = \mathcal{H}(A,B) - \mathcal{H}(B)$ stands for the conditional entropy, which quantifies the uncertainty in measurement the random variable A when B is known.

The quantum discord $\mathcal{QD}(\hat{\rho}^{(AB)})$ of a bipartite system A and B described by a density matrix $\hat{\rho}^{(AB)}$ is defined as the difference between the mutual information and the classical correlation

$$\mathcal{QD}(\hat{\rho}^{(AB)}) = \mathcal{I}(\hat{\rho}^{(AB)}) - \mathcal{C}(\hat{\rho}^{(AB)}), \tag{5.3}$$

where the quantum mutual information reads as:

$$\mathcal{I}(\hat{\rho}^{(AB)}) = S(\hat{\rho}^{A}) + S(\hat{\rho}^{B}) - S(\hat{\rho}^{(AB)}), \tag{5.4}$$

On the other hand, the classical correlation for a density matrix is given by:

$$\mathcal{C}(\hat{\rho}^{(AB)}) = \max_{\{\hat{\Pi}_k\}}[S(\hat{\rho}^{A}) - S(\hat{\rho}^{A}|\{\hat{\Pi}_k\})] \tag{5.5}$$

where $\{\hat{\Pi}_k\}$ is a complete set of projectors preformed locally on the B-subsystem, and $S(\hat{\rho}^{A}|\{\hat{\Pi}_k\}) = \sum_{k=1,2} p_k S(\hat{\rho}_q^{A(k)})$ stands for the quantum conditional entropy, being

$$\hat{\rho}_q^{A(k)} = \frac{1}{p_k}(\hat{\mathbb{I}} \otimes \hat{\Pi}_k)\hat{\rho}_q(\hat{\mathbb{I}} \otimes \hat{\Pi}_k), \tag{5.6}$$

above p_k corresponds to the probability of measuring the B-subsystem, thus $p_k = \mathrm{Tr}[(\hat{\mathbb{I}} \otimes \hat{\Pi}_k)\hat{\rho}_q(\hat{\mathbb{I}} \otimes \hat{\Pi}_k)]$.

The maximization shown in Eq. 5.5 is due to that classical correlations can vary according to the chosen basis $\{\hat{\Pi}_k\}$. Therefore, to compute the purely quantum correlations regardless $\{\hat{\Pi}_k\}$, it is necessary that $\mathcal{C}(\hat{\rho}^{(AB)})$ be maximized over the set of all possible projective measurements.

In addition, quantum discord might be a better measurements for quantum correlations than quantum entanglement as shown in Ref. [Datta2008]. In fact, in a DQC1 circuit [Knill1998] even though a small amount of entanglement is achieved, the quantum discord can be nonzero for typical instances of the DQC1 circuit. This could explain the speed-up in the DQC1 circuit when there is no quantum entanglement.

5.2 Microscopic Master Equation

In the following Section, we will introduce a different master equation derived from a microscopic point of view. In Ref. [Kryszewski2008] there is an excellent tutorial to obtain the final standard form of the microscopic master equation (MME) considered here. In the following, we will only highlight some important points for its derivation, it is not our intention to give an exhaustive treatment of the microscopic approach.

Let us commence from the von Neumann equation in the Schrödinger picture,

$$\frac{d}{dt}\hat{\rho}_{AB}(t) = -\frac{i}{\hbar}[\hat{H}_{AB}, \hat{\rho}_{AB}(t)], \tag{5.7}$$

where A stands for the system of interests, and B corresponds to the environment (being $A+B$ a closed system). The total Hamiltonian is $\hat{H}_{AB} = \hat{H}_0 + \hat{V}_{AB}$, where $\hat{H}_0 = \hat{H}_A \otimes \hat{I}_B + \hat{I}_A \otimes \hat{H}_B$, and $\hat{V}_{AB}$ is the system-environment interaction Hamiltonian. As usual, we proceed as following, *i*) we switch the Eq. 5.7 to the Interaction picture frame, *ii*) we solve formally the von Neumann differential equation in this rotating frame, and lastly *iii*) we iterate further to obtain the following solution:

$$\begin{aligned}\Delta\tilde{\hat{\rho}}_{AB}(t) &= -\frac{i}{\hbar}\int_t^{t+\Delta t} dt_1[\tilde{\hat{V}}_{AB}(t_1), \tilde{\hat{\rho}}_{AB}(t)] \\ &- \frac{1}{\hbar^2}\int_t^{t+\Delta t} dt_1 \int_t^{t_1} dt_2[\tilde{\hat{V}}_{AB}(t_1), [\tilde{\hat{V}}_{AB}(t_2), \tilde{\hat{\rho}}_{AB}(t)]],\end{aligned} \tag{5.8}$$

where, we have kept up to the second order in $\tilde{\hat{V}}_{AB}(t_j)$. Therefore, we have neglected earlier times of the dynamics. To obtain only the evolution of A we proceed to perform the partial trace on B,

$$\begin{aligned}\Delta\tilde{\hat{\rho}}_{A}(t) &= -\frac{i}{\hbar}\int_t^{t+\Delta t} dt_1 \mathrm{Tr_B}\{[\tilde{\hat{V}}_{AB}(t_1), \tilde{\hat{\rho}}_{AB}(t)]\} \\ &- \frac{1}{\hbar^2}\int_t^{t+\Delta t} dt_1 \int_t^{t_1} dt_2 \mathrm{Tr_B}\{[\tilde{\hat{V}}_{AB}(t_1), [\tilde{\hat{V}}_{AB}(t_2), \tilde{\hat{\rho}}_{AB}(t)]]\}.\end{aligned} \tag{5.9}$$

To compute the partial trace in the above equation, we consider

$$\tilde{\hat{\rho}}_{AB}(t) = \tilde{\hat{\rho}}_{A}(t) \otimes \tilde{\hat{\rho}}_{B}(t) + \tilde{\hat{\rho}}_{\mathrm{entangled}}(t). \tag{5.10}$$

The Born approximation allow us to approximate the above relation as following:

$$\hat{\tilde{\rho}}_{AB}(t) \approx \hat{\tilde{\rho}}_{A}(t) \otimes \hat{\tilde{\rho}}_{B}(t). \tag{5.11}$$

Additionally, we use the fact that the environment is at thermodynamic equilibrium, and therefore it can be replaced by $\hat{\tilde{\rho}}_{B}(t) = \hat{\sigma}_{B}$. On the other hand, in general, we can write the interaction operator in the Schrödinger picture as:

$$\hat{V}_{AB} = \sum_{\alpha} \hat{A}_{\alpha} \otimes \hat{X}_{\alpha} = \sum_{\alpha} \hat{A}_{\alpha}^{\dagger} \otimes \hat{X}_{\alpha}^{\dagger}, \tag{5.12}$$

where $\hat{A}_{\alpha}$ ($\hat{X}_{\alpha}$) acts on $\hat{H}_{A}$ ($\hat{H}_{B}$). Moreover, for simplicity we will use $\langle \hat{X}_{\alpha}(t) \rangle_{B} \equiv \mathrm{Tr_B}\{\hat{X}_{\alpha}\hat{\rho}_{B}(t)\} = \mathrm{Tr_B}\{\hat{X}_{\alpha}\hat{\sigma}_{B}\} = 0$. After some algebra, we get:

$$\begin{aligned} \frac{\Delta\hat{\tilde{\rho}}_{A}(t)}{\Delta t} &= \frac{1}{\hbar^2 \Delta t} \int_{t}^{t+\Delta t} dt_1 \int_{t}^{t_1} dt_2 \mathrm{Tr_B}\{\hat{\tilde{V}}_{AB}(t_2)\hat{\tilde{\rho}}_{A}(t) \otimes \hat{\sigma}_{B}\hat{\tilde{V}}_{AB}(t_1) \\ &- \hat{\tilde{V}}_{AB}(t_1)\hat{\tilde{V}}_{AB}(t_2)\hat{\tilde{\rho}}_{A}(t) \otimes \hat{\sigma}_{B}\} + H.C. \end{aligned} \tag{5.13}$$

At this point, there is no much difference between the usual master equation used in quantum optics/quantum information. In fact, this is a quite general approach of solving the open quantum case. In the next section we will introduce the so-called Davies operators, physically representing quantum jumps between the eigenstates of the full system of interests, being the main difference with the master equation routinely used in quantum open systems.

5.2.1 Quantum jumps between eigenstates of the system

For a non-degenerate spectrum, we can write the Hamiltonian of the system as following:

$$\hat{H}_{A} = \sum_{a} \hbar\omega_{a} \left|a\right\rangle \left\langle a\right|, \tag{5.14}$$

where, $\hbar\omega_{a}$ is the energy associated with the projector eigenstate $\left|a\right\rangle \left\langle a\right|$. We define the Davies operators as [Breuer-Book]:

$$\begin{aligned} \hat{A}_{\alpha}(\Omega) &\equiv \sum_{a,b} \delta(\omega_{ba} - \Omega) \left|a\right\rangle \left\langle a\right| \hat{A}_{\alpha} \left|b\right\rangle \left\langle b\right|, \\ \hat{A}_{\alpha} &= \sum_{\Omega} \hat{A}_{\alpha}(\Omega). \end{aligned} \tag{5.15}$$

In the following step, we consider the Markov approximation. As said in Chapter 1, we neglect the influence of the history of the physical system on its current state.

Switching to the Schrödinger picture, we readily get:

$$\begin{aligned}\frac{d\hat{\rho}_A(t)}{dt} &= -\frac{i}{\hbar}[\hat{H}_A, \hat{\rho}_A(t)] \\ &+ \frac{1}{\hbar^2}\sum_{\substack{\Omega \\ \alpha,\beta}} \Gamma_{\alpha\beta}(\Omega)(\hat{A}_\beta(\Omega)\hat{\rho}_A(t)\hat{A}^\dagger_\alpha(\Omega) - \frac{1}{2}\{\hat{A}^\dagger_\alpha(\Omega)\hat{A}_\beta(\Omega), \hat{\rho}_A(t)\}),\end{aligned} \tag{5.16}$$

above we have neglected the Lamb shift contribution $i/\hbar[\hat{H}_{LS}, \hat{\rho}_A(t)]$, where

$$\begin{aligned}\Gamma_{\alpha\beta}(\Omega) &= \int_{-\infty}^{\infty} d\tau e^{i\Omega\tau} G_{\alpha\beta}(\tau), \\ \Delta_{\alpha\beta}(\Omega) &= \frac{1}{2i}\int_0^{\infty} d\tau \left(e^{i\Omega\tau}\mathrm{Tr}_\mathrm{B}\{\hat{\tilde{X}}^\dagger_\alpha(\tau)\hat{X}_\beta\hat{\sigma}_B\} - e^{-i\Omega\tau}\mathrm{Tr}_\mathrm{B}\{\hat{X}^\dagger_\alpha\hat{\tilde{X}}_\beta(\tau)\hat{\sigma}_B\}\right), \\ G_{\alpha\beta}(t_1,t_2) &\equiv G_{\alpha\beta}(\tau = t_1 - t_2) = \mathrm{Tr}_\mathrm{B}\{\hat{\tilde{X}}^\dagger_\alpha(\tau)\hat{X}_\beta\hat{\sigma}_B\}, \\ \hat{H}_{LS} &= \frac{1}{\hbar}\sum_{\alpha,\beta,\Omega} \Delta_{\alpha\beta}(\Omega)\hat{A}^\dagger_\alpha(\Omega)\hat{A}_\beta(\Omega).\end{aligned} \tag{5.17}$$

Eq. 5.16 corresponds to the MME used below, this standard form preserves normalization, hermiticity, and positivity of the density matrix $\hat{\rho}_A(t)$. Other properties can be found in [Breuer-Book, Kryszewski2008].

5.2.2 On time-scales

Firstly, let us consider a fast time-scale regarding the decay of correlations in the environmental degrees of freedom τ_B. A second slower (compared with τ_B) time-scale, T_A is related with the dynamics of the system, where both are related as $\tau_B \ll t \ll T_A$. In other words, the environment does not change significantly when time $t \ll T_A$ elapses.

In Eq. 5.8, we have kept up to the second order in the interaction strength. To justify this truncation, it can be shown that the third order contribution reads as:

$$\frac{\Delta\hat{\tilde{\rho}}_A(t)}{\Delta t}^{(3)} \sim \frac{V\tau_B}{\hbar}\frac{\hat{\tilde{\rho}}_A(t)}{T_A} \ll 1 \tag{5.18}$$

where, we have used that $V\tau_B/\hbar \ll 1$. Therefore, third and higher orders can be neglected.

5.3 Introduction

Entanglement is a property hard to reach technologically and even when achieved, it is a very unstable quantum state, vulnerable under the effects of decoherence, any dissipative process as a result of the coupling to environment. Conventionally these effects are considered mainly destructive for entanglement, nevertheless some recent studies of this subject attest results different from the common conviction, appearing as counterintuitive at a first glance [Krauter2011, Muschik2011, Kastoryano2011, Memarzadeh2011].

An alternative approach to measure the entire correlations in a quantum system was originally suggested in [Henderson2001, Ollivier2001]. For example, by using the concepts of mutual information and quantum discord (QD) the quantum correlations may be distinguished from the classical ones. Further the QD could be compared to the entanglement of formation (E) [Wooters1998] in order to find if the system is in a quantum inseparable state (entangled), or in a separable state with quantum correlations like QD [Luo2008, Ali2010, Lu2011, Qing2011, Fanchini2010]. Such an analysis is considered in this Chapter.

The inclusion of the interaction of the system with the environment plays an important role in physics, implying a more realistic picture because the dissipation is always present in the real devices. In the proposed study we deal with atoms, cavities and a fibre in the framework of the physical model suggested in [Cirac1997] which attracted a high interest for quantum information applications and subsequently discussed detailed from different aspects [Pellizzari1997, Mancini2004, Serafini2006, Yang2011]. As a basic model, we consider the one recently analyzed in [Montenegro2011] and extend the calculations for a very special case, i.e. when the atoms are initially disentangled and in the ground states while the fields are in vacuum states and coupled to the reservoirs at finite temperatures. The entire system is considered open because of the leakage of the electromagnetic field from the cavities and fibre into their own thermal baths. Therefore, *Is it possible to generate atomic quantum correlations by the processes of absorption and exchanging excitations with the thermal reservoirs*? In the following we present the model and detailed analysis in search for an answer.

5.4 Trapped Atoms in a Fibre-Coupled Cavities

We present here the model schematically shown in Fig. 5.1 and recall the basic equations which lead us to the effect we are looking for. Hence, one considers two qubits (two-level atoms) interacting with two different and distant cavities, coupled by a transmission line, e.g. fibre, waveguide. For simplicity we consider the short-fibre limit, i.e., only one (resonant) mode of the fibre interacts with the cavity modes [Serafini2006].

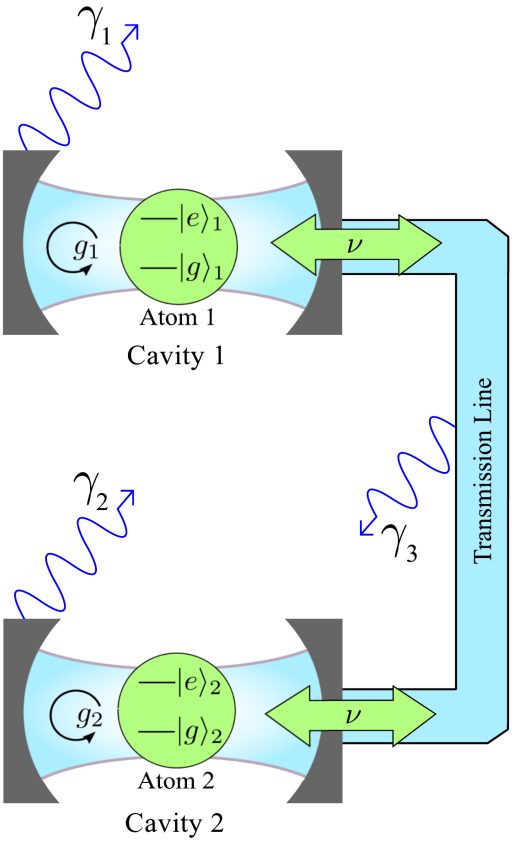

FIGURE 5.1: Two atoms trapped in distant coupled cavities. The cavities and transmission line exchange the energy at the rates γ_1, γ_2 and γ_3 with their baths having the temperatures T_1, T_2 and T_3, respectively.

Now, let us define a given state of the whole system by using the notation: $|i\rangle = |A_1\rangle \otimes |A_2\rangle \otimes |C_1\rangle \otimes |C_2\rangle \otimes |F\rangle \equiv |A_1 A_2 C_1 C_2 F\rangle$, where $A_{j=1,2}$ correspond to the atomic states, that can be $e(g)$ for excited(ground) state, while $C_{j=1,2}$ are the cavity states, and F corresponds to the state of the fibre. Both $C_{j=1,2}$ and F describe a 0 or 1 photon state. The Hamiltonian of the composite system under the RWA reads

(with $\hbar = 1$)

$$H_s = \omega_0 a_3^\dagger a_3 + \sum_{j=1}^{2} \left(\omega_a S_{j,z} + \omega_0 a_j^\dagger a_j \right) + \sum_{j=1}^{2} \left(g_j S_j^+ a_j + \nu a_3 a_j^\dagger + H.c. \right), \quad (5.19)$$

where a_3 is the boson operator defining the fibre mode, $a_1(a_2)$ is the boson operator for the cavity 1(2); ω_0 and ω_a are the fibre (cavity as well) and the atomic frequencies, respectively; g_j (ν) the atom-cavity (fibre-cavity) coupling constants; and S_z, $S^\pm$ are the usual atomic inversion and ladder operators, respectively.

The model is studied under the assumption of a single excitation in the system of atoms and fields, and using the above mentioned notation, the state-basis of the system becomes:

$$\begin{aligned} |1\rangle &= |eg000\rangle, \\ |2\rangle &= |gg100\rangle, \\ |3\rangle &= |gg001\rangle, \\ |4\rangle &= |gg010\rangle, \\ |5\rangle &= |ge000\rangle, \\ |6\rangle &= |gg000\rangle, \end{aligned} \quad (5.20)$$

where the last vector is required by the existence of the excitation's leakage to the reservoirs. Hence, it is straightforward to bring the Hamiltonian H_s in Eq. (5.19) to a matrix representation in the above state-basis [Montenegro2011].

$$\hat{H}_s = \begin{pmatrix} 0 & g_1 & 0 & 0 & 0 & 0 \\ g_1 & \Delta & \nu & 0 & 0 & 0 \\ 0 & \nu & 0 & \nu & 0 & 0 \\ 0 & 0 & \nu & \Delta & g_2 & 0 \\ 0 & 0 & 0 & g_2 & 0 & 0 \\ 0 & 0 & 0 & 0 & 0 & -\omega_a \end{pmatrix}, \quad (5.21)$$

where $\Delta = \omega_c - \omega_a$ is the atom-cavity detuning.

To simulate the dynamics of the given system, one considers the approach of the microscopic master equation (MME), developed in [Scala2007, Breuer-Book] in order to describe the system-reservoir interactions by a Markovian master equation.

This description considers jumps between eigenstates of the system Hamiltonian rather than the eigenstates of the field-free subsystems, which is the case in many approaches employed in quantum optics. Therefore, we assume that the system of interest, i.e. the atoms, cavities and fibre are parts of a larger system, composed by a collection of quantum harmonic oscillators in thermal equilibrium.

The external environment represents the part of the entire closed system other than the system of interest. Between each element of the system and its own bath one may identify different kind of dissipation channels. In CQED the main source of dissipation originates from the leakage of the cavity photons due to the imperfect reflectivity of the cavity mirrors. A second source of dissipation corresponds to the spontaneous emission of photons by the atom, however this kind of loss we consider small and they are neglected in the model. Following the common procedures [Scala2007, Breuer-Book], one obtains the MME for the system's reduced density operator $\rho(t)$

$$\frac{\partial \rho}{\partial t} = -i\left[H_s, \rho\right] + \mathcal{L}(\bar{\omega})\rho + \mathcal{L}(-\bar{\omega})\rho, \tag{5.22}$$

where $\bar{\omega} > 0$ with the dissipation terms defined as

$$\mathcal{L}(\bar{\omega})\rho = \sum_{j=1}^{3} \gamma_j(\bar{\omega}) \left(2A_j(\bar{\omega})\rho A_j^{\dagger}(\bar{\omega}) - \left\{ A_j^{\dagger}(\bar{\omega}) A_j(\bar{\omega}), \rho \right\} \right).$$

In the above equations we considered: $A_j(\bar{\omega}) = \sum_{\bar{\omega}_{\alpha,\beta}} |\phi_\alpha\rangle \langle\phi_\alpha| \left(a_j + a_j^{\dagger}\right) |\phi_\beta\rangle \langle\phi_\beta|$ fulfilling the properties $A_j(-\bar{\omega}) = A_j^{\dagger}(\bar{\omega})$, where $\bar{\omega}_{\alpha,\beta} = \Omega_\beta - \Omega_\alpha$ with Ω_k as an eigenvalue of Hamiltonian H_s and its corresponding eigenvector $|\phi_k\rangle$, denoting the k-th dressed-state. We should point out that the eigenfrequencies of Hamiltonian H_s are chosen in order to satisfy the following inequality $\Omega_6 < \Omega_5 < \Omega_4 < \Omega_3 < \Omega_2 < \Omega_1$.

Further in Eq. (5.22) one may use the so-called *Kubo-Martin-Schwinger* (KMS) condition [Breuer-Book], which gives a relation for the damping constants $\gamma_j(-\bar{\omega}) = \exp\left(-\bar{\omega}/T_j\right)\gamma_j(\bar{\omega})$, where T_j are the reservoir temperatures in the corresponding unit. The KMS condition ensures that the system tends to a thermal equilibrium for $t \to \infty$.

In order to solve Eq. (5.22) one may use a kind of formal solution, because in the most general case there is no an analytic solution for the eigenvalue equation based on Hamiltonian H_s. Once having the operators $A_j(\bar{\omega}_{\alpha\beta})$, it is easy to

write Eq. (5.22) for the density operator $\rho(t)$ decomposed in the eigenstates basis, $\langle\phi_m|\,\rho(t)\,|\phi_n\rangle = \rho_{mn}$, and we get

$$\begin{aligned}\dot{\rho}_{mn} &= -i\bar{\omega}_{n,m}\rho_{mn} + \sum_{k=1}^{5}\frac{\gamma_{k\to 6}}{2}\big(2\delta_{m6}\delta_{6n}\rho_{kk} - \delta_{mk}\rho_{kn} \\ &- \delta_{kn}\rho_{mk}\big) + \sum_{k=1}^{5}\frac{\gamma_{6\to k}}{2}\big(2\delta_{mk}\delta_{kn}\rho_{66} - \delta_{m6}\rho_{6n} - \delta_{6n}\rho_{m6}\big) \qquad (5.23)\end{aligned}$$

Here δ_{mn} is the Kronecker delta; the physical meaning of the damping coefficients $\gamma_{k\to 6}$ and $\gamma_{6\to k}$ refers to the rates of the transitions between the eigenfrequencies Ω_k downward and upward, respectively, defined as follows $\gamma_{k\to 6} = \sum_{j=\{1,2,3\}} c_i^2\gamma_j\left[\langle n(\bar{\omega}_{6,k})\rangle_{T_j} + 1\right]$ and $\gamma_{6\to k}$ results from the KMS condition, where c_i are the elements of the matrix for the transformation from the states $\{|1\rangle, ..., |6\rangle\}$ to the states $\{|\phi_1\rangle, ..., |\phi_6\rangle\}$ (see Eq. (14) and Appendix A in [Montenegro2011]). Here $\langle n(\bar{\omega}_{\alpha,\beta})\rangle_{T_j} = \left(e^{(\Omega_\beta - \Omega_\alpha)/T_j} - 1\right)^{-1}$ corresponds to the average number of the thermal photons. The damping coefficients play the central role in our model because their dependence on the temperature of the reservoirs imply a complex exchange mechanism between the elements of the system and the baths. Therefore, in the presence of the temperature we solve numerically the coupled system of the first-order differential equations (5.23) and compute the evolution of entanglement considering the atom-field system in the initial unexcited state $|gg000\rangle$.

In order to compute the atomic entanglement, we need to perform a measurement of the cavities-fibre field with a state $|000\rangle = |0\rangle_{C1} \otimes |0\rangle_{C2} \otimes |0\rangle_F$. The feasibility of such a measurement is discussed in the next section.

In the next section we present the calculations of the quantum correlations depending on the system characteristics: such as atom-cavity detuning, coupling constants and thermal reservoirs.

5.5 Measuring the quantum correlations

5.5.1 Entanglement

Once projected on the state $|000\rangle$ of the field subspace we find that the reduced atomic density matrix in the 2-qubit basis $\{|gg\rangle, |ge\rangle, |eg\rangle, |ee\rangle\}$ preserves during

the time evolution a symmetric X-form structure

$$\tilde{\rho}(t) = \begin{pmatrix} a & 0 & 0 & 0 \\ 0 & b & b & 0 \\ 0 & b & b & 0 \\ 0 & 0 & 0 & 0 \end{pmatrix}, \tag{5.24}$$

with the atoms initially in ground state, i.e. $a(0) = 1$ and $b(0) = 0$. This particularity of the density matrix results from the implicit symmetry on the interchanging of the undistinguished qubits in equivalent cavities. In the following we will compute the qubit-qubit entanglement using the concurrence [Wooters1998]. This quantum correlation measure is defined as $C(\rho) = \max(0, \lambda_1, \lambda_2, \lambda_3, \lambda_4)$, where $\lambda_{\{i+1\}} > \lambda_i$ for $i = \{1, 2, 3\}$ are the eigenvalues of the matrix $\sqrt{\sqrt{\rho}\tilde{\rho}\sqrt{\rho}}$, with $\tilde{\rho} = (\hat{\sigma}_y \otimes \hat{\sigma}_y)\rho^*(\hat{\sigma}_y \otimes \hat{\sigma}_y)$ is the spin-flipped state of ρ. For our particular case, the concurrence can be easily computed [Montenegro2011] and gives $C(t) = 2b/(a+2b)$.

In the following, we are mainly interested in studying the evolution of atomic entanglement, the concurrence (C), as a function of the temperatures of the thermal baths. The system under consideration refers to the atoms with long radiative lifetimes, each coupled to its own cavity. These two cavities are connected by a fibre with the damping rates $\gamma_1 = \gamma_2 = \gamma_3 \equiv \gamma = 2\pi \cdot 10\text{MHz}$, respectively, which are within the current technology [Serafini2006]. The transition frequency of the atom is chosen to be mid-infrared (MIR), i.e. $\omega_a/2\pi = 4\text{THz}$ and hence, for experimental purposes the coupling between the distant cavities can be realized by using the modern resources of IR fibre optics, e. g. hollow glass waveguides [Bowden2007], plastic fibres [Chen2006], etc. We choose the range of MIR frequencies in order to limit the thermal reservoir only up to room temperature (300K), that corresponds to a thermal photon. The values of the coupling constants and the atom-cavity detuning will be varied in order to search the optimal result. We must mention here that to satisfy the RWA we should have $2g \gg \gamma_{max}(\bar{\omega})$ [Scala2007]. Satisfying this condition we start with the case $g_1 = g_2 \equiv g = \nu = 5\gamma$, considering all the reservoirs at the same temperature, T, and study how the atomic entanglement evolves as a function of the atom-cavity detuning, Δ.

The result is shown in Fig. 5.2 from which we conclude that the atom-cavity detuning facilitate in this case the generation of a quasi-stationary atomic entanglement and for $\Delta = 0.1\omega_a$ the system reaches a long-lived entanglement state. Of course,

in the asymptotic limit the concurrence will vanish and the atoms eventually disentangle themselves due to the damping action of the reservoirs. The maximal value of the concurrence of ∼0.2 corresponds to the bath's temperature about 300 K, that is about one thermal excitation for the given frequency ω_a (i.e. $k_B T/\hbar\omega_a \simeq 1.5$).

In order to find the optimal relation between the coupling constants and damping rate we did the calculations for different situations as follows: (i) $g = \nu = 100\gamma$, (ii) $g = \gamma$ and $\nu = 100\gamma$, (iii) $g = 10\gamma$ and $\nu = \gamma$. For example, we present the case (ii) in Fig. 5.3, from which we see that the concurrence gets the same maximal value as in the previous case Fig. 5.2(c), but it takes a longer time for the quasi stationary entanglement to reach its plateau. The rest of the cases give worst results.

Now, let us analyze a more general situation, when all the independent baths have different temperatures. After performing the computations, we found an interesting effect that only the thermal bath of the fibre plays an important role in the generation of entanglement in the system, while the thermal baths of the cavities generate very little entanglement. This situation is represented in Fig. 5.4. Therefore, after analyzing all the calculations, we come to the conclusion that the case represented in Fig. 5.2(c) corresponds to the optimal one for the generation of entanglement.

5.5.2 Quantum Discord

Since in our case the 2-qubit density matrix has a simplified X-form (5.24), one can easily compute the quantum and classical correlations in the system by using a particular case for the algorithm discussed in [Ali2010]. Even if some recent studies as [Lu2011, Qing2011] found that the analytic approach of [Ali2010] could not be considered as a general one, in our case the computation of QD may follow this procedure without some divergences of the minimization approach. In the framework of the algorithm and notations used in [Ali2010], we have to optimize QD just by changing the parameters (k, l) in the range $(0, 1)$ and find easily the condition of the resultant minimum for (k, l)=1/2. For more accuracy we have compared the calculations with the approach proposed in [Fanchini2010], by using Eq. (6) of the later and obtained exactly the same result. Hence, we observe in Fig. 5.5 the time evolution of the QD similar to that of entanglement, but the initial growth is steeper in the discord, which implies the appearance of the quantum correlations in the system prior to the entanglement [Auyuanet2010]. For a better illustration of the thermal effect under discussion, in the inset is shown the

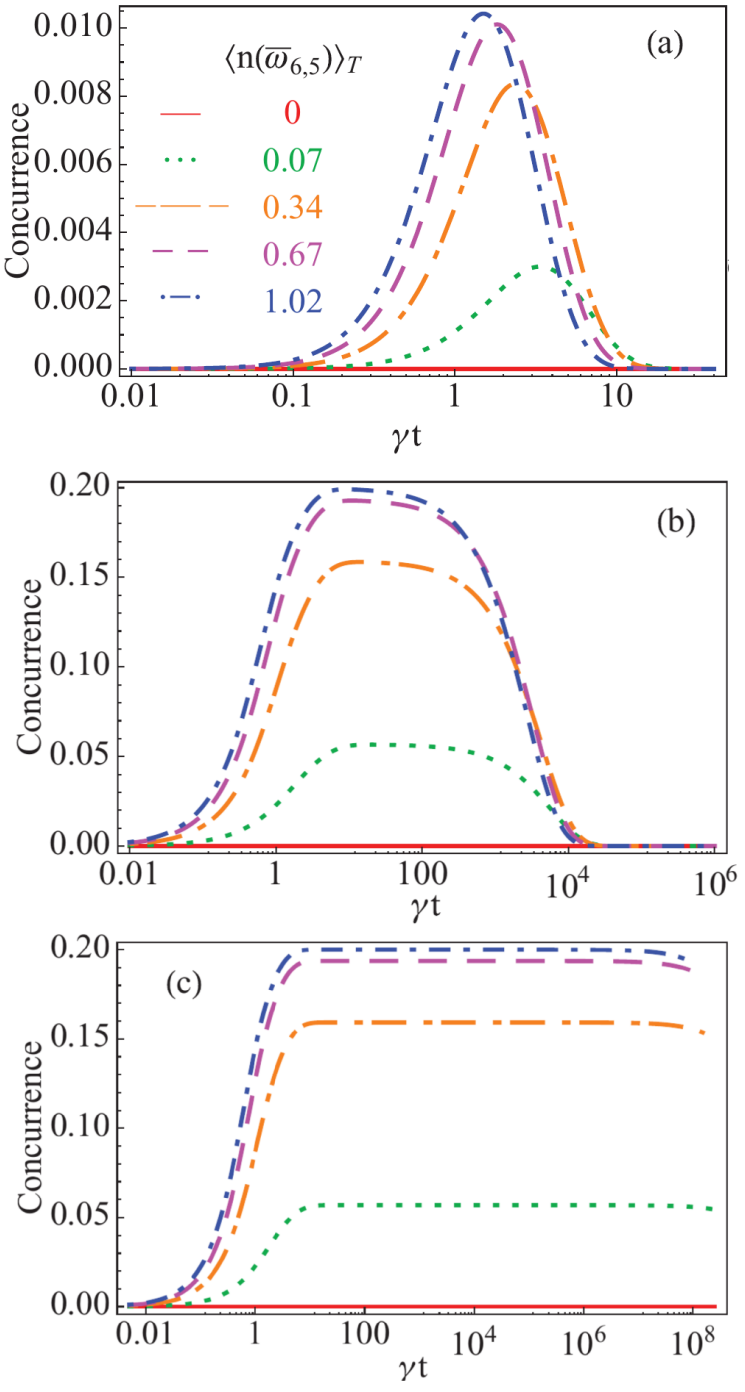

FIGURE 5.2: Evolution of the concurrence for $g = \nu = \gamma$ and different atom-cavity detunings: (a) $\Delta = 0$, (b) $\Delta = 10^{-4}\omega_a$ and (c) $\Delta = 0.1\omega_a$. The baths have the same temperature with the average number of thermal photons given by $\langle n(\bar{\omega}_{6,5})\rangle_T$. The abscissa axis of the dimensionless time, γt, is in a logarithmic scale.

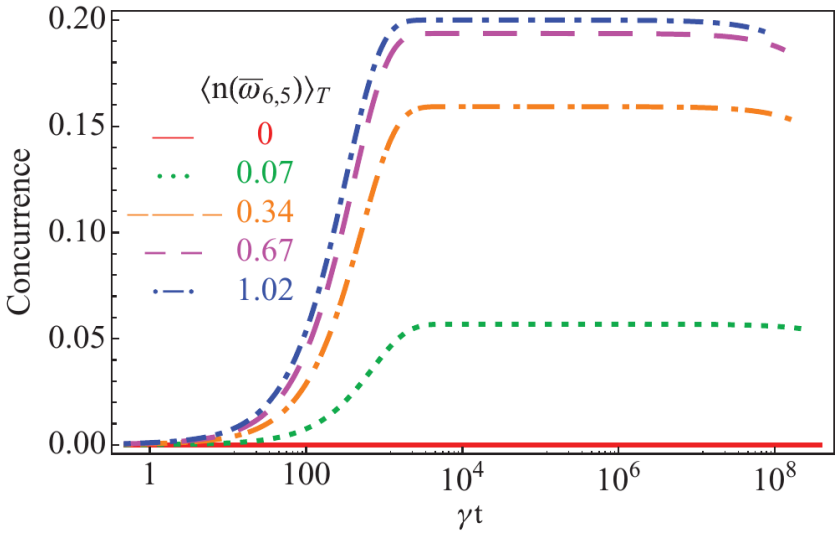

FIGURE 5.3: Concurrence for $\Delta = 0.1\omega_a$, $g = 5\gamma$ and $\nu = 100\gamma$.

temperature dependence of the steady values (flat time-plateau) of the quantum and classical correlations.

5.5.3 Experimental hint

In this section we discuss the tasks important for an experimental realization of the ideas discussed here. In our opinion, the most difficult is to realize a quantum non-demolition (QND) measurement of the photon states in the fibre-coupled cavities. However, currently there exists technological possibilities to realize experiments on QND photon counting, attaining single-quantum resolution, performed with optical or microwave photons [Guerlin2007], for an exhaustive review see [Grangier1998]. In the experiment discussed in [Guerlin2007] the cavity mode was coupled to Rydberg atoms or superconducting junctions and the QND method is based on the detection of the dispersive phase shift produced by the field on the wave function of non-resonant atoms crossing the cavity. This shift can be measured by atomic interferometry, using the Ramsey separated-oscillatory-field method. The advantages of QND experiments in radiometry and in particular applied for IR photons are suggested in [Castelleto2001].

In order to simulate a measurement on the fibre-cavity subsystem one may compute the field density operator and therefore monitoring the probability of the field state. As we are interested to preserve the field in the vacuum state, i.e. $\rho_{fib-cav}(t) = |000\rangle\langle 000|$, one tests the probability of this state during the temporal evolution of

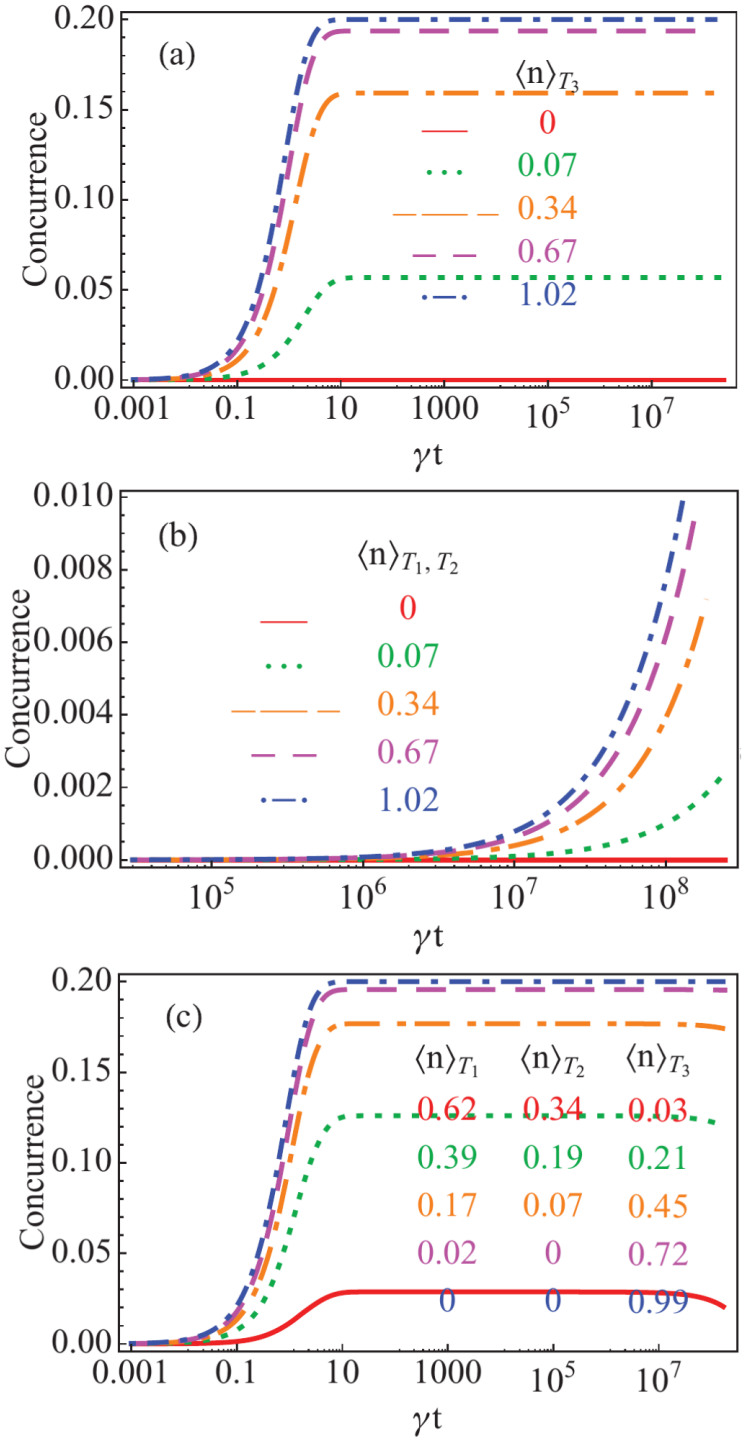

FIGURE 5.4: Evolution of the concurrence for arbitrary baths temperatures, (a) $T_1 = T_2 = 0$ and varying the fibre's bath temperature, (b) $T_3 = 0$ and varying equally the cavities' bath temperatures, and (c) varying differently all the temperatures. The rest of the parameters are the same as in Fig. 5.2(c).

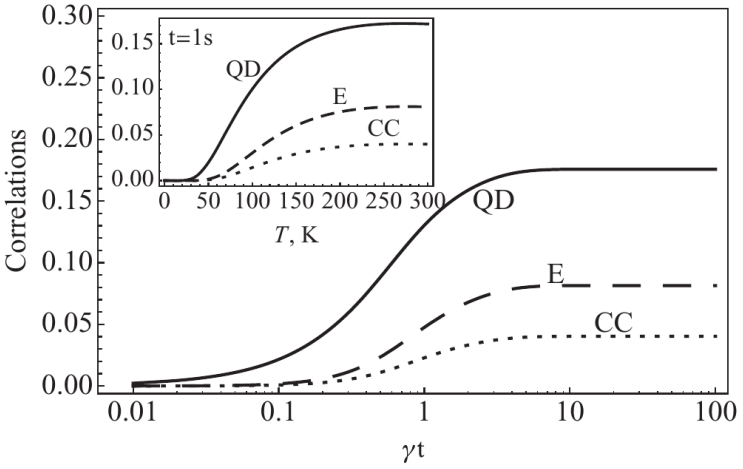

FIGURE 5.5: Evolution of the quantum discord (QD), entanglement of formation (E) and classical correlations (CC) for one thermal excitation and the parameters chosen as in Fig. 5.2(c). The inset represents the same quantities as a function of the temperatures of the reservoirs calculated for a late time, $t = 1$s.

the system. The dynamics of this probability for different schemes of engineering of the thermal reservoirs is shown in Fig. 5.6. Based on these results we conclude that the success to find the fibre-cavity field in a vacuum state after the measurement strongly depends on the managing of the thermal reservoirs. Hence, from this point of view, a more efficient variant to drive the qubits to long-lived quantum correlations is to increase the fibre's bath temperature while the baths of the cavities maintain at possible low temperature.

5.6 Concluding remarks

In this study we show a very interesting effect that the long-lived quantum correlations between the atoms trapped in separate cavities can be generated by the dissipative coupling to the thermal baths. This is an example that could give us a new insight into the effects of the system-environment exchange versus the quantum correlations. From the analysis of the obtained results, mainly Fig. 5.4 and 5.6, we conclude that the entanglement can be optimized by engineering the thermal bath of the fibre rather than the baths of each cavity, hence suggesting that the "quasi-local" manipulations produce little effect on the generation of entanglement. Furthermore, we found that our system evidences quantum correlations quantified by QD prior to the appearance of the entanglement. The model discussed here could be experimentally implemented by using a QND experiment in order to test

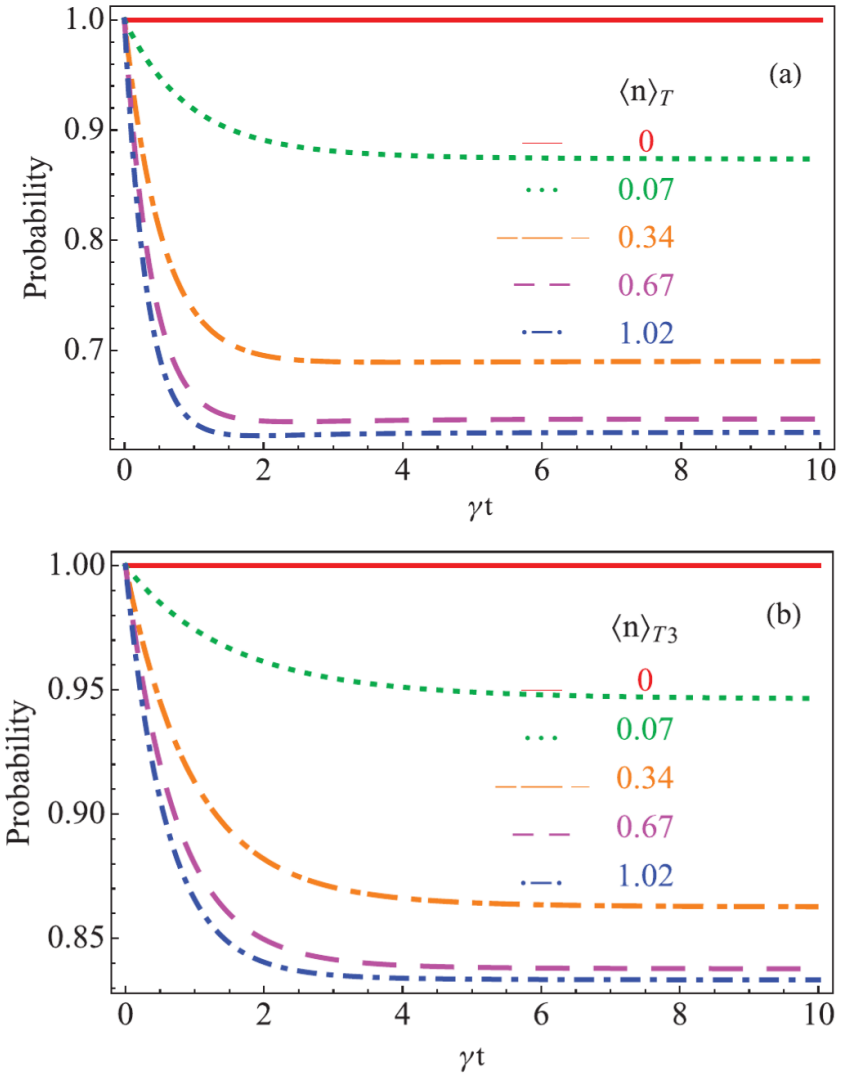

FIGURE 5.6: Probability to find simultaneously the fibre and the cavities in a vacuum state by engineering of the thermal baths as follows: (a) all the baths have the same temperature T, (b) varying the fibre's bath temperature T_3, while $T_1 = T_2 = 0$. The rest of the parameters are the same as in Fig. 5.2(c).

the fibre-cavity field state and evidences a sufficient high probability for a successful measurement.

Chapter 6

Monitoring the quantum correlations of two remotely-located atomic-mechanical systems

In this final Chapter, we present an ongoing investigation, where the physical system under consideration corresponds to a hybrid atomic-mechanical system formed from two initially entangled remote qubits (two-level atoms) interacting with individual harmonic oscillators. Therefore, we will bring together elements previously explored in this Thesis, such as the direct qubit-oscillator coupling studied in Chapter 2, and interesting applications towards quantum networking schemes (see Chapter 4).

We study thoroughly the dynamics of the main measures of quantum correlations (entanglement and discord, see Chapter 5) for different physical conditions of the entire system in order to control the generation, propagation, and preservation of the correlations. The system is investigated when any dissipation mechanism is neglected; and subsequently, we consider the mechanical losses of the oscillators. For both cases, the two qubits are initially prepared in a Bell-diagonal state, and consequently discover that the two-qubit correlations exhibit few interesting effects such as freezing, sudden changes and revivals in the evolution of the quantum entropic discord.

6.1 Non-dissipative dynamics

Essentially, the system is composed of two remote qubit-oscillator systems (denoted by A and B), where each qubit interact with its own oscillator — modeled harmonically for simplicity, see Fig. 6.1. First, we shall consider the system in absence of any source of decoherence, afterward (in Section 6.3) we will solve the system subject to mechanical losses.

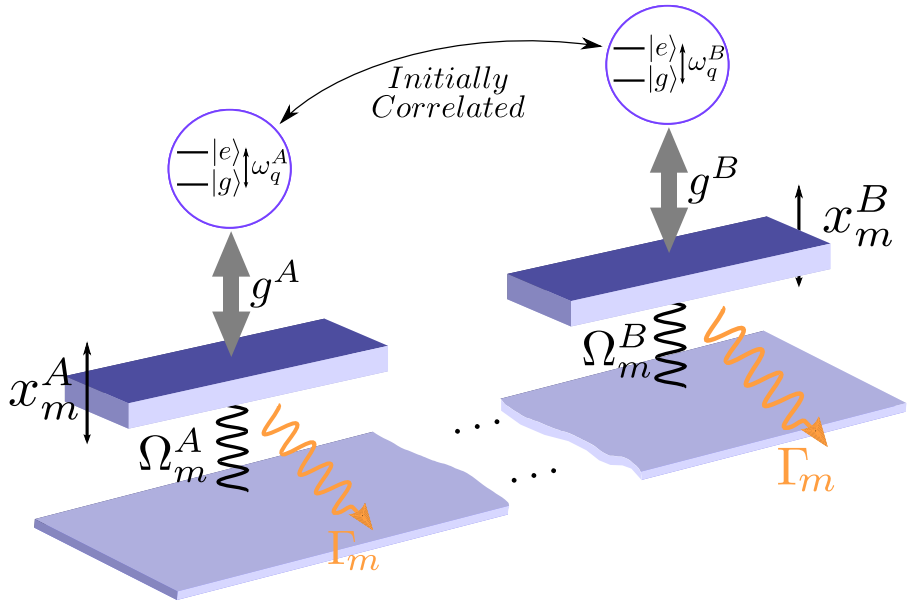

FIGURE 6.1: The figure illustrates two subsystems labeled A and B, where two initially correlated qubits are coupled to their independent distant quantum harmonic oscillator. On the one hand, the mechanical oscillator oscillates with an angular frequency Ω_m^i and amplitude x_m^i, $i = \{A, B\}$. On the other hand, the qubit (two-level atom) is characterized as usual by its excited (ground) state $|e\rangle$ ($|g\rangle$), with an energy gap given by $\hbar\omega_q^A$. In Section 6.3 we will consider the damping of the oscillator, being Γ_m the mechanical damping rate.

The Hamiltonian of the model in the Schrödinger picture is (in the units of $\hbar$),

$$\hat{H} = \sum_{i=\{A,B\}} \omega_q \hat{\sigma}_z^i + \Omega^i \hat{a}_i^\dagger \hat{a}_i - g^i \hat{\sigma}_z^i (\hat{a}_i^\dagger + \hat{a}_i). \tag{6.1}$$

Here, ω_q is the qubit energy gap (for simplicity, $\omega_q^A = \omega_q^B = \omega_q$), Ω^i is the angular frequency for the oscillator ($i = \{A, B\}$), and $g^i = x_{\text{zpf}}^i \omega_q / L$ corresponds to the qubit-oscillator strength coupling; being x_{zpf}^i the zero-point fluctuation oscillator amplitude, and L the oscillator equilibrium length. On the other hand, $\hat{\sigma}_z^i$ is the

usual z-Pauli operator for the qubit and $\hat{a}_i$ ($\hat{a}_i^\dagger$) is the annihilation (creation) boson operator for the oscillator.

The direct interaction in Eq. 6.1 ($\approx \hat{\sigma}_z^i \otimes \hat{x}_m^i$) is the conditioned displacement Hamiltonian (see Chapter 2 for more details), where each qubit eigenstate is being monitored via the oscillator's position quadrature throughout the dynamics.

To obtain the relevant Hamiltonian of our work, we switch from the Schrödinger picture to the Interaction picture as follows (in reference frame rotating at ω_q)

$$\hat{H}_{\rm int} = \hat{a}_A^\dagger \hat{a}_A - k^A \hat{\sigma}_z^A (\hat{a}_A^\dagger + \hat{a}_A) + \tilde{\Omega} \hat{a}_B^\dagger \hat{a}_B - k^B \hat{\sigma}_z^B (\hat{a}_B^\dagger + \hat{a}_B), \tag{6.2}$$

where $\hat{H}_{\rm int}$ is scaled by the mechanical frequency of the $A-$subsystem (Ω^A), so the scaled qubit-oscillator coupling, $k^i = g^i/\Omega^A$ ($i = \{A, B\}$) and the oscillator angular frequency ratio is $\tilde{\Omega} = \Omega^B/\Omega^A$.

From Eq. 6.2 it is clear that i) the Hamiltonian is analogous to an effective potential energy for the oscillator with its center shifted a quantity proportional to g, depending on the qubit eigenvalue ± 1. ii) It is straightforward to notice that $[\hat{H}_A, \hat{H}_B] = 0$, where a simple inspection show us; $\hat{H}_A = \hat{a}_A^\dagger \hat{a}_A - k^A \hat{\sigma}_z^A (\hat{a}_A^\dagger + \hat{a}_A)$ and $\hat{H}_B = \tilde{\Omega}_m \hat{a}_B^\dagger \hat{a}_B - k^B \hat{\sigma}_z^B (\hat{a}_B^\dagger + \hat{a}_B)$. Hence, the unitary operator evolution can be easily calculated as $\hat{U}(t) = \exp[-it\hat{H}_{\rm int}/\hbar] = \exp[-it(\hat{H}_A + \hat{H}_B)/\hbar] = \exp[-it\hat{H}_A/\hbar]\exp[-it\hat{H}_B/\hbar]$. The previous exponential has been derived in Chapter 2, given us for our case the final expression:

$$\begin{aligned} \hat{U}(t) &= \exp\left[k^A \hat{\sigma}_z^A (\eta(t)\hat{a}_A^\dagger - \eta^*(t)\hat{a}_A)\right] \exp\left[-i\hat{a}_A^\dagger \hat{a}_A t\right] \\ &\times \exp\left[k^B \hat{\sigma}_z^B (\eta(\tilde{t})\hat{a}_B^\dagger - \eta^*(\tilde{t})\hat{a}_B)\right] \exp\left[-i\hat{a}_B^\dagger \hat{a}_B \tilde{t}\right] \end{aligned} \tag{6.3}$$

Above, we defined $\eta(t) = 1 - \exp[-it]$ and $\tilde{\Omega}_m t \equiv \tilde{t}$.

Regarding the initial conditions, we prepare the oscillators as coherent states with different amplitudes, namely, $\left|\alpha^A\right\rangle$ and $\left|\alpha^B\right\rangle$ ($\{\alpha^A, \alpha^B\} \in \mathbb{C}$), and the qubits will be initialized in a state with maximally mixed marginals, i.e. Bell-diagonal (BD), described by a X-type density matrix. In the Bloch form reads $\hat{\rho}(0)_q^{AB} = [I \otimes I + \vec{c} \cdot (\hat{\boldsymbol{\sigma}}_A \otimes \hat{\boldsymbol{\sigma}}_B)]/4$, where $\vec{c} = \{c_1, c_2, c_3\}$ and $\hat{\boldsymbol{\sigma}} = (\hat{\sigma}_x, \hat{\sigma}_y, \hat{\sigma}_z)$ is the Pauli vector (see Chapter 1). On the other hand, in the two-qubit basis, the matrix form for the

maximally mixed marginals is:

$$\hat{\rho}(0)_q^{AB} = \frac{1}{4}\begin{pmatrix} 1+c_3 & 0 & 0 & c_1-c_2 \\ 0 & 1-c_3 & c_1+c_2 & 0 \\ 0 & c_1+c_2 & 1-c_3 & 0 \\ c_1-c_2 & 0 & 0 & 1+c_3 \end{pmatrix} \tag{6.4}$$

To derive the density matrix dynamics, we can easily notice that

$$\begin{aligned} \hat{U}(t)\left|e,e\right\rangle \otimes \left|\alpha^A,\alpha^B\right\rangle &= C_{+,+}\left|e,e\right\rangle \otimes \left|\Phi_+^A(t),\Phi_+^B(\tilde{t})\right\rangle, \\ \hat{U}(t)\left|e,g\right\rangle \otimes \left|\alpha^A,\alpha^B\right\rangle &= C_{+,-}\left|e,g\right\rangle \otimes \left|\Phi_+^A(t),\Phi_-^B(\tilde{t})\right\rangle, \\ \hat{U}(t)\left|g,e\right\rangle \otimes \left|\alpha^A,\alpha^B\right\rangle &= C_{-,+}\left|g,e\right\rangle \otimes \left|\Phi_-^A(t),\Phi_+^B(\tilde{t})\right\rangle, \\ \hat{U}(t)\left|g,g\right\rangle \otimes \left|\alpha^A,\alpha^B\right\rangle &= C_{-,-}\left|g,g\right\rangle \otimes \left|\Phi_-^A(t),\Phi_-^B(\tilde{t})\right\rangle. \end{aligned} \tag{6.5}$$

where,

$$C_{\pm,+} = e^{\pm ik^A \mathbb{I}m\left\{\alpha^A\eta(t)\right\}} e^{+ik^B \mathbb{I}m\left\{\alpha^B\eta(\tilde{t})\right\}}, \tag{6.6}$$

$$C_{\pm,-} = e^{\pm ik^A \mathbb{I}m\left\{\alpha^A\eta(t)\right\}} e^{-ik^B \mathbb{I}m\left\{\alpha^B\eta(\tilde{t})\right\}}, \tag{6.7}$$

$$\Phi_\pm^A(t) = \alpha^A e^{-it} \pm k^A\eta(t), \tag{6.8}$$

$$\Phi_\pm^B(\tilde{t}) = \alpha^B e^{-i\tilde{t}} \pm k^B\eta(\tilde{t}). \tag{6.9}$$

Finally, the initial state $\hat{\rho}(0)^{AB} = \hat{\rho}(0)_q^{AB} \otimes \left|\alpha^A\right\rangle\left\langle\alpha^A\right| \otimes \left|\alpha^B\right\rangle\left\langle\alpha^B\right|$ evolves as following:

$$\begin{aligned} \hat{\rho}(t)^{AB} &= \frac{1}{4}\Big[(1+c_3)\left|e,e\right\rangle\left\langle e,e\right| \otimes \hat{\rho}_m^{+,+,+,+} + (c_1-c_2)C_{+,+}^2\left|e,e\right\rangle\left\langle g,g\right| \otimes \hat{\rho}_m^{+,+,-,-} \\ &+ (1-c_3)\left|e,g\right\rangle\left\langle e,g\right| \otimes \hat{\rho}_m^{+,-,+,-} + (c_1+c_2)C_{+,-}^2\left|e,g\right\rangle\left\langle g,e\right| \otimes \hat{\rho}_m^{+,-,-,+} \\ &+ (c_1+c_2)C_{-,+}^2\left|g,e\right\rangle\left\langle e,g\right| \otimes \hat{\rho}_m^{-,+,+,-} + (1-c_3)\left|g,e\right\rangle\left\langle g,e\right| \otimes \hat{\rho}_m^{-,+,-,+} \\ &+ (c_1-c_2)C_{-,-}^2\left|g,g\right\rangle\left\langle e,e\right| \otimes \hat{\rho}_m^{-,-,+,+} + (1+c_3)\left|g,g\right\rangle\left\langle g,g\right| \otimes \hat{\rho}_m^{-,-,-,-}\Big] \end{aligned} \tag{6.10}$$

above we defined the mechanical operator as ($\hat{\rho}_m^{a,b,c,d} = \hat{\rho}_m^{a,b,c,d}(t)$):

$$\hat{\rho}_m^{a,b,c,d}(t) = \left|\Phi_a^A(t),\Phi_b^B(\tilde{t})\right\rangle\left\langle\Phi_c^A(t),\Phi_d^B(\tilde{t})\right| \tag{6.11}$$

here, $\{a, b, c, d\}$ can take the symbols $\{+, -\}$.

6.2 Dynamics of the Two-Qubit Correlations

To have access to the qubit evolution one traces over the degrees of freedom of both oscillators in Eq. 6.10, hence the reduced density matrix results

$$\begin{aligned}\hat{\rho}(t)_q^{AB} &= \frac{1}{4}\Big[(1+c_3)\,|e,e\rangle\langle e,e| + (c_1-c_2)C^2_{+,+}\phi^A_{-,+}\phi^B_{-,+}\,|e,e\rangle\langle g,g| \\ &+ (1-c_3)\,|e,g\rangle\langle e,g| + (c_1+c_2)C^2_{+,-}\phi^A_{-,+}\phi^B_{+,-}\,|e,g\rangle\langle g,e| \\ &+ (c_1+c_2)C^2_{-,+}\phi^A_{+,-}\phi^B_{-,+}\,|g,e\rangle\langle e,g| + (1-c_3)\,|g,e\rangle\langle g,e| \\ &+ (c_1-c_2)C^2_{-,-}\phi^A_{+,-}\phi^B_{+,-}\,|g,g\rangle\langle e,e| + (1+c_3)\,|g,g\rangle\langle g,g|\Big] \end{aligned} \tag{6.12}$$

where we have used $\mathrm{Tr}\left(|\alpha_1\rangle\langle\alpha_2|\right) = \langle\alpha_2|\,\alpha_1\rangle$, hence $\phi^A_{\pm,\mp} = \langle\Phi^A_{\pm}(t)|\Phi^A_{\mp}(t)\rangle$, and $\phi^B_{\pm,\mp} = \langle\Phi^B_{\pm}(\tilde{t})|\Phi^B_{\mp}(\tilde{t})\rangle$.

First let us compute the entropic quantum discord, $\mathcal{QD}(\hat{\rho}_q)$ (see Section 5.1 for further details), defined as the difference between the mutual information $\mathcal{I}(\hat{\rho}_q)$, and the classical correlation $\mathcal{C}(\hat{\rho}_q)$.

$$\mathcal{QD}(\hat{\rho}_q^{AB}) = S(\hat{\rho}_q^A) + S(\hat{\rho}_q^B) - S(\hat{\rho}_q^{AB}) - \max_{\{\hat{\Pi}_k\}}[S(\hat{\rho}_q^A) - S(\hat{\rho}_q|\{\hat{\Pi}_k\})]. \tag{6.13}$$

To compute the above Eq. 6.13, we require both the associated von Neumann entropies $\{S(\hat{\rho}_q^A), S(\hat{\rho}_q^B), S(\hat{\rho}_q^{AB})\}$ as well as the quantum conditional entropy defined by (see Chapter 5)

$$S(\hat{\rho}_q|\{\hat{\Pi}_k\}) = \sum_{k=1,2} p_k S(\hat{\rho}_q^{A(k)}), \tag{6.14}$$

where, $\hat{\rho}_q^{A(k)}$ is:

$$\hat{\rho}_q^{A(k)} = \frac{1}{p_k}(\hat{\mathbb{I}}\otimes\hat{\Pi}_k)\hat{\rho}_q(\hat{\mathbb{I}}\otimes\hat{\Pi}_k), \tag{6.15}$$

above, p_k is the probability ($p_k = \mathrm{Tr}[(\hat{\mathbb{I}}\otimes\hat{\Pi}_k)\hat{\rho}_q(\hat{\mathbb{I}}\otimes\hat{\Pi}_k)]$), and $\{\hat{\Pi}_k\}$ corresponds to a complete set of projectors pre-formed locally on the B-subsystem defined by : $\hat{\Pi}_k = |\pi_k\rangle\langle\pi_k|$, corresponding to a qubit rotation to cover all possible outcomes

$$\pi_1 = \cos\theta\,|e\rangle + e^{i\mu}\sin\theta\,|g\rangle\,, \tag{6.16}$$

$$\pi_2 = e^{-i\mu}\sin\theta\,|e\rangle - \cos\theta\,|g\rangle\,, \tag{6.17}$$

where the angles vary between $0 \leq \theta \leq 2\pi$, and $0 \leq \mu \leq 2\pi$.

It is straightforward to obtain the von Neumann entropy for the reduced operators $S(\hat{\rho}_q^A) = S(\hat{\rho}_q^B) = 1$. Moreover,

$$\begin{aligned}
\hat{\rho}_q^{A(1)} &= \frac{1}{2}\Big[(1+\cos(2\theta)c_3)\,|e\rangle\langle e| + f(\mu,\theta)\,|e\rangle\langle g| \\
&+ h(\mu,\theta)\,|g\rangle\langle e| + (1-\cos(2\theta)c_3)\,|g\rangle\langle g|\Big] \qquad (6.18)\\
\hat{\rho}_q^{A(2)} &= \frac{1}{2}\Big[(1-\cos(2\theta)c_3)\,|e\rangle\langle e| - f(\mu,\theta)\,|e\rangle\langle g| \\
&- h(\mu,\theta)\,|g\rangle\langle e| + (1+\cos(2\theta)c_3)\,|g\rangle\langle g|\Big]. \qquad (6.19)
\end{aligned}$$

where,

$$\begin{aligned}
f(\mu,\theta) &= \sin\theta\cos\theta[(c_1-c_2)C^2_{+,+}\phi^A_{-,+}\phi^B_{-,+}e^{i\mu} + (c_1+c_2)C^2_{+,-}\phi^A_{-,+}\phi^B_{+,-}e^{-i\mu}],\\
h(\mu,\theta) &= \sin\theta\cos\theta[(c_1+c_2)C^2_{-,+}\phi^A_{+,-}\phi^B_{-,+}e^{i\mu} + (c_1-c_2)C^2_{-,-}\phi^A_{+,-}\phi^B_{+,-}e^{-i\mu}].
\end{aligned} \qquad (6.20)$$

To calculate the quantum conditional entropy, we notice that the eigenvalues for the density matrices $(\{\varepsilon^{(k)}_{1,2}\}, k = 1,2)$ in Eqs. 6.18-6.19 are equivalent, and they correspond to:

$$\begin{aligned}
\varepsilon^{(k)}_{1,2} &= \frac{1}{2}\left[1 \pm \frac{1}{2}\sqrt{2(c_3^2 + 2f(\mu,\theta)h(\mu,\theta) + c_3^2\cos 4\theta)}\right]\\
&= \frac{1}{2}\left[1 \pm \Lambda(\mu,\theta)\right]. \qquad (6.21)
\end{aligned}$$

For instance, $\varepsilon^{(2)}_1$ stands for the first eigenvalue for $\hat{\rho}_q^{A(2)}$. Moreover, we can simplify the quantum conditional entropy expression as following:

$$\begin{aligned}
S(\hat{\rho}_q|\{\hat{\Pi}_k\}) &= -\frac{1}{2}\left[1+\Lambda(\mu,\theta)\right]\log_2\left[\frac{1}{2}(1+\Lambda(\mu,\theta))\right]\\
&- \frac{1}{2}\left[1-\Lambda(\mu,\theta)\right]\log_2\left[\frac{1}{2}(1-\Lambda(\mu,\theta))\right]\\
&= \mathcal{F}(\mu,\theta). \qquad (6.22)
\end{aligned}$$

Therefore, the classical correlation can be written as : $\mathcal{C}(\hat{\rho}_q) = \max_{\{\hat{\Pi}_k\}}[S(\hat{\rho}_q^A) - S(\hat{\rho}_q|\{\hat{\Pi}_k\})] = 1 - \min_{\{\mu,\theta\}}[\mathcal{F}(\mu,\theta)]$. Since the above function $\mathcal{F}(\mu,\theta)$ is a monotonically decreasing function, we can obtain the minimal value of $(\mathcal{F}(\mu,\theta))$ maximizing

the value of $\Lambda(\mu,\theta)$, this imply to optimize the angles $\{\mu,\theta\}$ in the expression: $c_3^2 + 2f(\mu,\theta)h(\mu,\theta) + c_3^2\cos 4\theta$.

Finally, we can give the following expression for the classical correlation:

$$\mathcal{C}(\hat{\rho}_q) = \sum_{j=1,2} \frac{1}{2}\left[1+(-1)^j m(t)\right]\log_2\left[\frac{1}{2}(1+(-1)^j m(t))\right] \tag{6.23}$$

being $m(t) = \max_{\{\mu,\theta\}}[\Lambda(\mu,\theta)]$. Therefore, the quantum discord reads as:

$$\mathcal{QD}(\hat{\rho}_q) = 2 + \sum_{i=1}^{4}\lambda_i \log_2\lambda_i - \sum_{j=1,2}\frac{1}{2}\left[1+(-1)^j m(t)\right]\log_2\left[\frac{1}{2}(1+(-1)^j m(t))\right] \tag{6.24}$$

where λ_i are the eigenvalues of the reduced qubit density matrix in Eq. 6.12, they can be easily found as:

$$\lambda_{1,2} = \frac{1}{4}\left(1 - c_3 \pm |\phi^A_{-,+}\phi^B_{-,+}(c_1+c_2)|\right), \tag{6.25}$$

$$\lambda_{3,4} = \frac{1}{4}\left(1 + c_3 \pm |\phi^A_{-,+}\phi^B_{-,+}(c_1-c_2)|\right). \tag{6.26}$$

Before presenting the main results of the qubit-qubit correlations, it is important to emphasize that, the qubit dynamics can be reported with only one mechanical oscillator. In other words, one of the (scaled) qubit-mechanics coupling can be zero e.g, $k^B = 0$ [He2013]. However, our motivation to consider two oscillators is closely related with the open quantum case where both oscillators will be affected by mechanical energy losses, and therefore both subsystems will suffer detrimental effects due to the contact with their surroundings. Furthermore, it is of our interest to study the symmetry of the oscillators, as in a realistic setup the mechanical angular frequencies there will be always different $\tilde{\Omega}_m \neq 1$.

In Fig. 6.2 we compute the quantum discord for an initial qubit configuration where $c_1 = 1$, and $c_2 = -c_3$. We consider the dynamics for different qubit-oscillator coupling strength $k^A = 0.5$ and $k^B = 0.1$, both achievable under current technology; the coherent amplitudes were set as $\alpha^A = 2$ and $\alpha^B = 1$, and we consider a slightly different mechanical oscillators $\tilde{\Omega}_m = 0.9$. This particular initial condition for the qubit $c_1 = 1$, and $c_2 = -c_3$ give us a wide region where sudden transitions appears in the quantum discord dynamics. Additionally, the election both of the coherent amplitudes as well as the qubit-mechanics coupling do not gravitate in the quantum

sudden behavior (nor the angular frequencies for the oscillators). However, it has been shown that the particular Bell-diagonal type for the qubit evolution with initial parameters $\{c_i\}$ is strongly susceptible to exhibit quantum sudden changes [Lang2010].

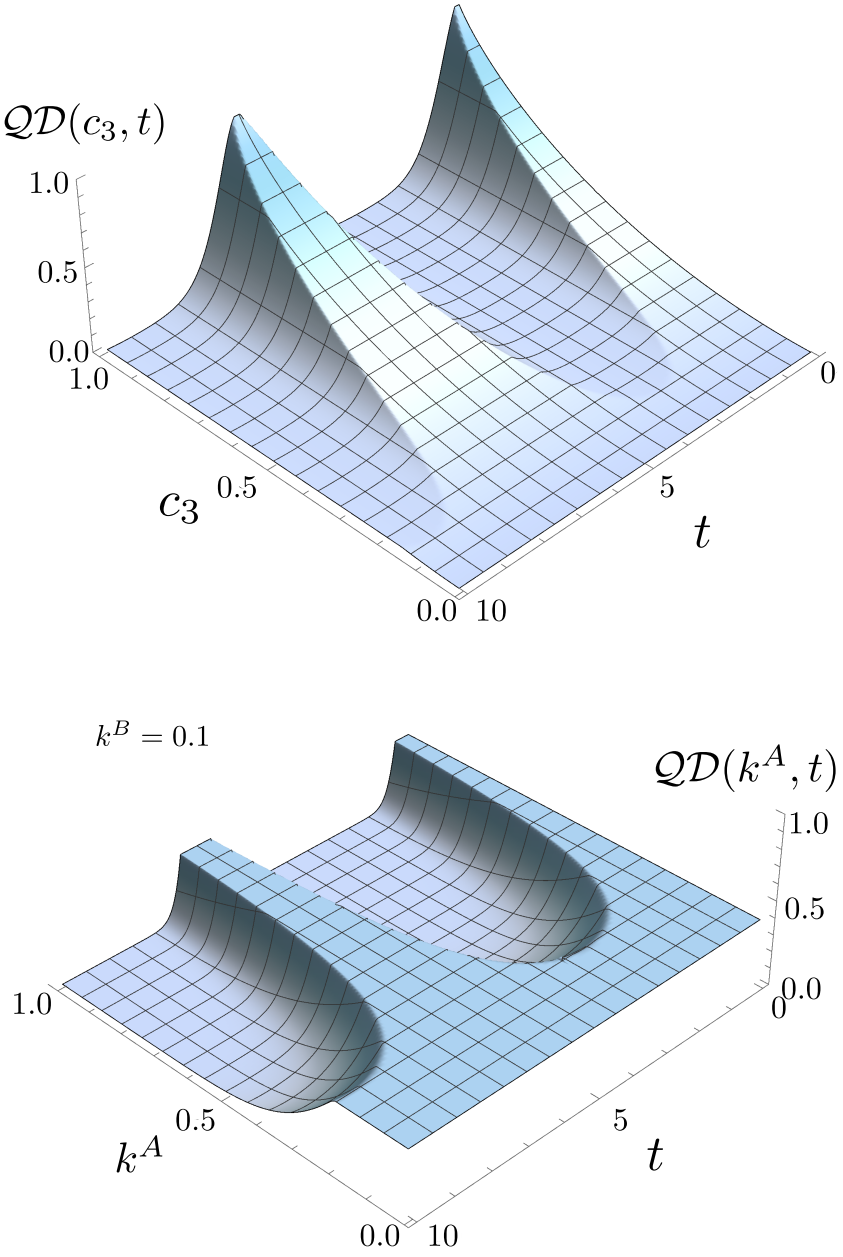

FIGURE 6.2: Top panel shows the quantum discord as function of c_3 and t with $k^A = 0.5$; Bottom panel, quantum discord as a function of k^A and t with $c_3 = 0.7$. Other parameters are: $\tilde{\Omega} = 0.9$, $k^B = 0.1$, $c1 = 1$, $c2 = -0.7$, and the coherent amplitudes $\alpha^A = 2$, $\alpha^B = 1$. In some temporal regions the freezing of QD is achieved, which is strongly depending on c_3 and k^A. In this non-dissipative scenario the periodicity of the quantum discord can be controlled by $\tilde{\Omega}$.

In the top panel of Fig. 6.2 we plot the quantum discord as a function of the parameter c_3 and time. Here, for a modest value of c_3 the quantum discord plateau is larger in contrast to higher values of c_3. Also, the transitions are more abrupt when $0.5 \leq c_3 \leq 1$. In the bottom panel of Fig. 6.2 we illustrate the dependence of the quantum discord as function of k^A and t —for a fixed $k^B = 0.1$. As seen in this figure, there is a region in which freezing of quantum correlations can be obtained [You2012, Aaronson2013]. This dynamics can be understood as following, for $k^A = 0$ and $k^B \neq 0$, we have the situation illustrated in Ref. [He2013], where the quantum discord remain constant. In fact, for a qubit-mechanics coupling threshold $k^A_{\text{thres}} \leq 1/4, k^B = 0.1$ the freezing of quantum discord is achieved —corresponding to its initial QD. For values higher than $k^A_{\text{thres}} > 1/4$ the quantum discord shows a time plateau (which decreases as k^A increases) followed by sudden transitions, i.e., $\partial \mathcal{QD}(k^A, t)/\partial t|_{k^A}$ does not exist.

The role of $\tilde{\Omega}_m$ is illustrated in Fig. 6.3. As seen, for mechanical oscillators with different angular frequencies, i.e., $\tilde{\Omega}_m \neq 1$ the quantum discord shows a decreasing dynamics. Interestingly, also a strong qubit-mechanics destroy the quantum correlations (for example for $k^A = 1$), weaker values are required not only to obtain a high value in the QD, but also to exhibits quantum sudden transitions (see Fig. 6.3-a). In the bottom panel of Fig. 6.3 we show the dynamics for larger times. It is important to pointed out that, for identical mechanical objects $\tilde{\Omega}_m = 1$ the period corresponds to 2π, whereas for $\tilde{\Omega}_m \neq 1$ the period become larger, in fact, for the case represented in Fig. 6.3 the relation is exactly $T = 2\pi/\tilde{\Omega}_m$, being T the period of the quantum discord generated in time.

6.3 Dissipative Dynamics

To give a more realistic scenario of our work we consider the open quantum case; where we consider the detrimental effects of the oscillators in contact with a thermal reservoir at zero temperature. The master equation under the Markov-Born approximation is:

$$\begin{aligned} \frac{d}{dt}\hat{\rho}(t) &= -i\left[\hat{H}_{\text{int}}, \hat{\rho}(t)\right] + \frac{\Gamma_m}{2}\Big[2\hat{a}_A\hat{\rho}(t)\hat{a}_A^\dagger - \hat{a}_A^\dagger\hat{a}_A\hat{\rho}(t) - \hat{\rho}(t)\hat{a}_A^\dagger\hat{a}_A \\ &+ 2\hat{a}_B\hat{\rho}(t)\hat{a}_B^\dagger - \hat{a}_B^\dagger\hat{a}_B\hat{\rho}(t) - \hat{\rho}(t)\hat{a}_B^\dagger\hat{a}_B\Big]. \end{aligned} \tag{6.27}$$

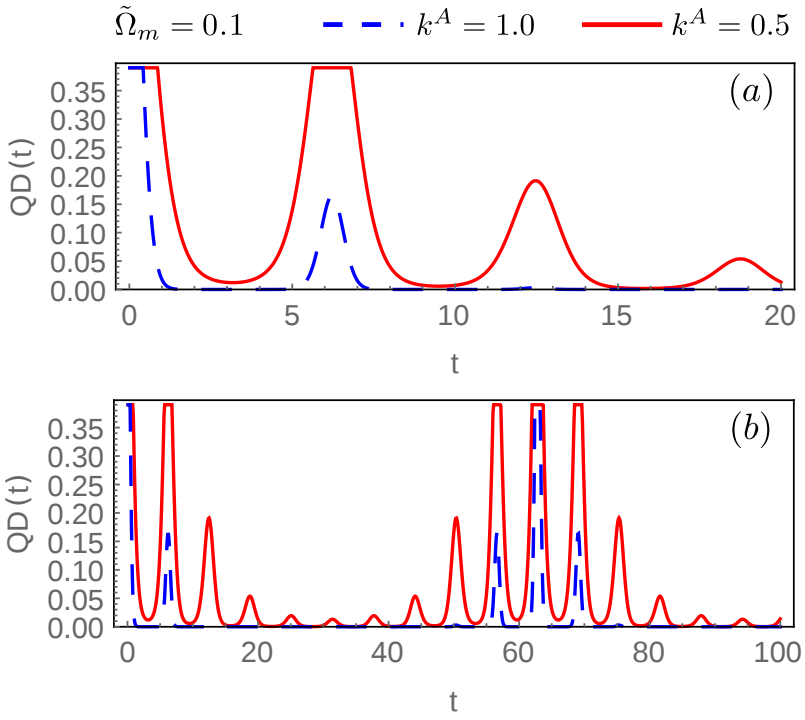

FIGURE 6.3: Quantum discord as a function of time for $\tilde{\Omega}_m = 0.1$ and two different qubit-oscillator coupling $k^A = 1$ and $k^A = 0.5$. As seen above, for non-identical mechanical oscillators and strong coupling qubit-oscillator value, the quantum discord does not exhibit quantum sudden transitions nor freezing. In Fig. 6.3-b) we show the same dynamics for larger times.

To give a full analytical solution of Eq. 6.3 we will follow the alternate-step procedure found in Ref. [Bose1997], and studied in detail in Chapter 3. Let us start from the following initial condition:

$$\hat{\rho}(0) = \hat{\rho}_q(0) \otimes \left|\alpha^A\right\rangle \left\langle\alpha^A\right| \otimes \left|\alpha^B\right\rangle \left\langle\alpha^B\right| . \tag{6.28}$$

For simplicity, we consider $\alpha^A = \alpha^B = 0$. In this case, the full density matrix is:

$$\begin{aligned}\hat{\rho}(t)^{AB} &= \frac{1}{4}\Big[(1+c_3)\,|e,e\rangle\langle e,e|\otimes\hat{\varrho}(\Gamma_m,t)_m^{+,+,+,+} \\ &+ (c_1-c_2)\,|e,e\rangle\langle g,g|\otimes\hat{\varrho}(\Gamma_m,t)_m^{+,+,-,-} \\ &+ (1-c_3)\,|e,g\rangle\langle e,g|\otimes\hat{\varrho}(\Gamma_m,t)_m^{+,-,+,-} \\ &+ (c_1+c_2)\,|e,g\rangle\langle g,e|\otimes\hat{\varrho}(\Gamma_m,t)_m^{+,-,-,+} \\ &+ (c_1+c_2)\,|g,e\rangle\langle e,g|\otimes\hat{\varrho}(\Gamma_m,t)_m^{-,+,+,-} \\ &+ (1-c_3)\,|g,e\rangle\langle g,e|\otimes\hat{\varrho}(\Gamma_m,t)_m^{-,+,-,+} \\ &+ (c_1-c_2)\,|g,g\rangle\langle e,e|\otimes\hat{\varrho}(\Gamma_m,t)_m^{-,-,+,+} \\ &+ (1+c_3)\,|g,g\rangle\langle g,g|\otimes\hat{\varrho}(\Gamma_m,t)_m^{-,-,-,-}\Big] \end{aligned} \tag{6.29}$$

where, following with the previous definitions, i.e., $\{a,b,c,d\}$ can take the symbols $\{+,-\}$:

$$\begin{aligned}\hat{\varrho}(\Gamma_m,t)_m^{a,b,c,d} &= \left|\Phi_a^A(\Gamma_m,t)\right\rangle\left\langle\Phi_c^A(\Gamma_m,t)\right| \\ &\otimes \left|\Phi_b^B(\Gamma_m,\tilde{t})\right\rangle\left\langle\Phi_d^B(\Gamma_m,\tilde{t})\right| \end{aligned} \tag{6.30}$$

and

$$\Phi_\pm^A(\Gamma_m,t) = \frac{\pm ik^A}{i+\frac{\Gamma_m}{2}}\left(1-e^{-(i+\frac{\Gamma_m}{2})t}\right) \tag{6.31}$$

$$\Phi_\pm^B(\Gamma_m,\tilde{t}) = \frac{\pm ik^B}{i+\frac{\Gamma_m}{2}}\left(1-e^{-(i+\frac{\Gamma_m}{2})\tilde{t}}\right). \tag{6.32}$$

As shown in Chapter 3, for the A subsystem we get

$$D_{\pm,\mp}^A(\Gamma_m,t) = \int_0^t |\Phi_\pm^A(\Gamma_m,t')|^2 + |\Phi_\mp^A(\Gamma_m,t')|^2 - 2\Phi_\pm^A(\Gamma_m,t')^*\Phi_\mp^A(\Gamma_m,t')dt'. \tag{6.33}$$

It is straightforward to show that $D_{+,-}^A(\Gamma_m,t) = D_{-,+}^A(\Gamma_m,t) \equiv D^A$, thus:

$$D^A = \frac{16(k^A)^2}{\left(\Gamma_m^2+4\right)^2}\left(\left(\Gamma_m^2+4\right)t + \left(\Gamma_m^2+4\right)\left(1-e^{-\Gamma_m t}\right)/\Gamma_m\right. \tag{6.34}$$

$$\left. + 4e^{-\frac{1}{2}(\Gamma_m t)}(\Gamma_m\cos(t)-2\sin(t)) - 4\Gamma_m\right). \tag{6.35}$$

The same dynamics follows for the oscillator in the subsystem B. Therefore, we only need to change $t \to \tilde{t}$, and $A \to B$ accordingly. In the following, we shall consider equal losses for both oscillators, i.e., $D = D^A + D^B$. Thus the open quantum dynamics reads as:

$$\begin{aligned}
\hat{\rho}(t)^{AB} &= \frac{1}{4}\Big[(1+c_3)\,|e,e\rangle\langle e,e| \otimes \hat{\varrho}(\Gamma_m,t)^{+,+,+,+}_m \\
&+ (c_1-c_2)\,|e,e\rangle\langle g,g| \otimes e^{-\frac{\Gamma_m}{2}D}\hat{\varrho}(\Gamma_m,t)^{+,+,-,-}_m \\
&+ (1-c_3)\,|e,g\rangle\langle e,g| \otimes \hat{\varrho}(\Gamma_m,t)^{+,-,+,-}_m \\
&+ (c_1+c_2)\,|e,g\rangle\langle g,e| \otimes e^{-\frac{\Gamma_m}{2}D}\hat{\varrho}(\Gamma_m,t)^{+,-,-,+}_m \\
&+ (c_1+c_2)\,|g,e\rangle\langle e,g| \otimes e^{-\frac{\Gamma_m}{2}D}\hat{\varrho}(\Gamma_m,t)^{-,+,+,-}_m \\
&+ (1-c_3)\,|g,e\rangle\langle g,e| \otimes \hat{\varrho}(\Gamma_m,t)^{-,+,-,+}_m \\
&+ (c_1-c_2)\,|g,g\rangle\langle e,e| \otimes e^{-\frac{\Gamma_m}{2}D}\hat{\varrho}(\Gamma_m,t)^{-,-,+,+}_m \\
&+ (1+c_3)\,|g,g\rangle\langle g,g| \otimes \hat{\varrho}(\Gamma_m,t)^{-,-,-,-}_m\Big]. \qquad (6.37)
\end{aligned}$$

As before, to have access to the qubit dynamics, we proceed to trace off the degrees of freedom of the oscillators

$$\begin{aligned}
\hat{\rho}(t)^{AB} &= \frac{1}{4}\Big[(1+c_3)\,|e,e\rangle\langle e,e| + (1-c_3)\,|e,g\rangle\langle e,g| \\
&+ (1-c_3)\,|g,e\rangle\langle g,e| + (1+c_3)\,|g,g\rangle\langle g,g| \\
&+ e^{-\frac{\Gamma_m}{2}D}\Big\{(c_1-c_2)\,|e,e\rangle\langle g,g|\,\phi^A_{-,+}(\Gamma_m,t)\phi^B_{-,+}(\Gamma_m,t) \\
&+ (c_1+c_2)\,|e,g\rangle\langle g,e|\,\phi^A_{-,+}(\Gamma_m,t)\phi^B_{+,-}(\Gamma_m,t) \\
&+ (c_1+c_2)\,|g,e\rangle\langle e,g|\,\phi^A_{+,-}(\Gamma_m,t)\phi^B_{-,+}(\Gamma_m,t) \\
&+ (c_1-c_2)\,|g,g\rangle\langle e,e|\,\phi^A_{+,-}(\Gamma_m,t)\phi^B_{+,-}(\Gamma_m,t)\Big\}\Big].
\end{aligned}$$

With the density matrix in Eq. 6.38, we can obtain all the ingredients to compute the quantum discord for the dissipative case. Firstly, we can calculate the mutual information and obtain its eigenvalues:

$$\lambda^{\Gamma_m}_{1,2} = \frac{1}{4}\Big(1 + c_3 \pm e^{-\frac{\Gamma_m}{2}D}|(c_1-c_2)\phi^A_{-,+}(\Gamma_m,t)\phi^B_{-,+}(\Gamma_m,t)|\Big) \qquad (6.38)$$

$$\lambda^{\Gamma_m}_{3,4} = \frac{1}{4}\Big(1 - c_3 \pm e^{-\frac{\Gamma_m}{2}D}|(c_1+c_2)\phi^A_{-,+}(\Gamma_m,t)\phi^B_{-,+}(\Gamma_m,t)|\Big). \qquad (6.39)$$

The classical correlation for the open case is:

$$\begin{aligned}
\hat{\rho}_q^{A(1)}(\Gamma_m,t) &= \frac{1}{2}\Big[(1+\cos(2\theta)c_3)\,|e\rangle\langle e| + \bar{f}(\mu,\theta)\,|e\rangle\langle g| \\
&+ \bar{h}(\mu,\theta)\,|g\rangle\langle e| + (1-\cos(2\theta)c_3)\,|g\rangle\langle g|\Big] \\
\hat{\rho}_q^{A(2)}(\Gamma_m,t) &= \frac{1}{2}\Big[(1-\cos(2\theta)c_3)\,|e\rangle\langle e| - \bar{f}(\mu,\theta)\,|e\rangle\langle g| \\
&- \bar{h}(\mu,\theta)\,|g\rangle\langle e| + (1+\cos(2\theta)c_3)\,|g\rangle\langle g|\Big].
\end{aligned} \tag{6.40}$$

where,

$$\begin{aligned}
\bar{f}(\mu,\theta) &= e^{-\frac{\Gamma_m}{2}D}\phi^A_{-,+}(\Gamma_m,t)e^{i\mu}\sin\theta\cos\theta\Big[(c_1-c_2) \\
&\times \phi^B_{-,+}(\Gamma_m,t) + (c_1+c_2)\phi^B_{+,-}(\Gamma_m,t)e^{-2i\mu}\Big], \\
\bar{h}(\mu,\theta) &= e^{-\frac{\Gamma_m}{2}D}\phi^A_{+,-}(\Gamma_m,t)e^{i\mu}\sin\theta\cos\theta\Big[(c_1+c_2) \\
&\times \phi^B_{-,+}(\Gamma_m,t) + (c_1-c_2)\phi^B_{+,-}(\Gamma_m,t)e^{-2i\mu}\Big]
\end{aligned} \tag{6.41}$$

with eigenvalues

$$\begin{aligned}
\varepsilon_{1,2}^{\Gamma_m(k)} &= \frac{1}{2}\left[1 \pm \frac{1}{2}\sqrt{2(c_3^2 + 2\bar{f}(\mu,\theta)\bar{h}(\mu,\theta) + c_3^2\cos 4\theta)}\right] \\
&= \frac{1}{2}\left[1 \pm \bar{\Lambda}(\mu,\theta)\right].
\end{aligned} \tag{6.42}$$

Finally, we have all the elements to compute the quantum discord in presence of detrimental effects from the mechanical oscillators. In Fig. 6.4 we have illustrated the dynamics of the quantum discord as a function of time. The effect of a modest damping rate $\Gamma_m = 0.01$ does not gravitate in the sudden changes nor in the time plateau generated in the quantum discord. Other (stronger) values for Γ_m, such as $\Gamma_m - 0.1$ and Γ_m show a semi-damped and a strong-damped behavior of the quantum discord, respectively.

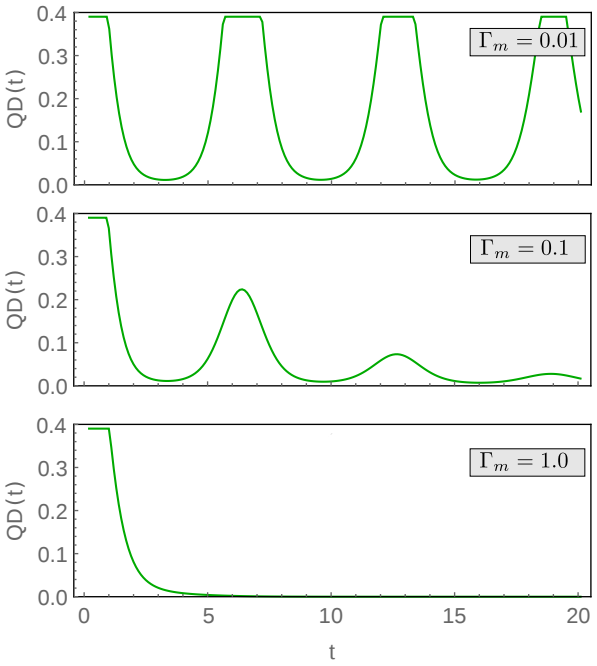

FIGURE 6.4: Quantum discord as a function of time for the quantum open case, where we have considered damping of the mechanical oscillators. Other values are : $c_1 = 1, c_2 = -0.7, c_3 = 0.7, k^A = 0.5, k^B = 0.1, \tilde{\Omega}_m = 0.9, \alpha^A = \alpha^B = 0$.

6.4 Concluding remarks

In this ongoing work we have demonstrated a few interesting effects of the quantum correlations in a quantum network of two systems with atomic-mechanical oscillator interaction. In general we studied the dynamics of classical and quantum correlations measured by entropic quantum discord for a two-qubit system initially prepared in Bell-diagonal states. As result we found that the quantum discord calculated by its original entropic measure evidence the process of freezing and sudden decoherence in time with some periodicity.

Furthermore, witnessing the sudden changes on the quantum discord remains as an open question for further investigation. In particular, in this feasible atomic-mechanical quantum system we show illustratively some interesting effects with possibilities to monitor the quantum correlations by tuning the physical parameters of the model - important tools for applications in quantum information science.

Chapter 7

Summary and Outlook

> "At the heart of quantum mechanics lies the superposition principle"
> —First Chapter of The Principles of Quantum Mechanics by P. A. M. Dirac (1984).

Perhaps the most fascinating feature of quantum theory is quantum entanglement. A quantum property which allow us to *entangle* or correlate two parties regardless the distant between them. Subsequently, this "spooky action at a distance" (in Einstein's words) was a crucial aspect to demonstrate the non-locality of quantum mechanics [Bell1964]. Far from being just a theoretical curiosity, quantum entanglement also can be used as a resource for quantum information purposes. In fact, there are some tasks that can only be realized within quantum processing, for instance, quantum teleportation and quantum cryptography. To accomplish those protocols it is required to manipulate highly entangled states. However quantum entanglement is a fragile resource susceptible to decohere in presence of thermal fluctuations or other sources of decoherence. To solve this problem, we can protect or enhance the entanglement against its environment, or we can increase it using concentration or distillation protocols. Both cases are heavily investigated in Chapters 2 and 3, respectively. Another key element of quantum information is the propagation of quantum entanglement over long distances, the so-called quantum networks. In general, two (or more) nodes are coupled through quantum and classical channels, where matter-like systems play the role as nodes due to their long coherence and storage times, meanwhile "flying qubits" or optical photons in optical fibres carry the information coherently between them. Essentially, quantum networking is our motivation for Chapters 4, 5, and 6. However, in the last two, we

also investigate two theoretical aspects of quantum mechanics, namely whether the quantum entanglement can be driven by thermal environments, and quantum sudden transitions in the quantum discord. In the following, we will briefly summarize some important points of the research presented here.

We present the stabilization of quantum entanglement in a non-linear qubit-oscillator system in Chapter 2. Particularly, we have investigated a spin qubit coupled to a quartic non-linear oscillator (NLO) through a conditional displacement Hamiltonian. This type of interaction has been heavily investigated under linear approximations, where basically the centre of the oscillator's potential is shifted conditioned on the eigenstate of the qubit. Some experimental implementations, together with a wide range of qubit-oscillator coupling was described in Chapter 2. Throughout that Chapter we have used two relevant parameters, namely, the qubit-NLO coupling k and the non-linearity δ. As a starting point, we solved the system dynamics analytically for the case $\delta = 0$. Here, the entanglement generation is due to the superposition principle of the hybrid system and it shows a periodic dynamics. On the other hand, when $\delta \neq 0$ and in the *weak coupling* regime ($k \ll 1$) we analytically show that a new Kerr-like term appears in the dynamics leading to *i)* quadrature squeezing of the oscillator state, *ii)* the suppression of the entanglement decay by the appearance of a stabilization region, and *iii)* an enhancement of the entanglement negativity compared to the linear case of $\delta = 0$.

The most interesting case corresponds to the *strong coupling regime* ($k \approx 0.5$), when we see that two- and four-phonon transitions play a relevant role both in the entanglement stabilization and in its enhancement. In particular, the entanglement negativity can reach its maximal value by virtue of the orthogonalization of the oscillator states relevant to the present dynamics. Furthermore, solving numerically the corresponding master equation, we have shown that these effects remain robust to the presence of decoherence in the oscillator system.

In addition, we have presented a section where the violation of the Bell function is achieved. We used a dichotomic measurement for the spin qubit, whereas an on/off measurement was considered for the oscillator's degrees of freedom. Perhaps, the most challenging part was the maximization of the Bell function, as we do not have the full analytical expression for the *strong* coupling regime —because the quartic undriven Hamiltonian does not have an analytical solution, it is hard to consider all the possible outcomes for the oscillator's field. However, under some approximations we can obtain a value above the classical limit in the Bell function.

Other numerics made in that Chapter were performed in different ways. For instance, MATLAB was useful to compute the dynamics for a truncated Fock space, and also using the Runge-Kutta algorithm for the quantum open systems case. Additionally, we used a quantum optics toolbox written in Python (QuTiP) [QuTiP], where we obtained the same results within a tolerance of approximately 10^{-4} using Backward Differentiation Formula "BDF" as the integration method.

As an outlook for this chapter, it may be interesting to recast the problem as a means to measure nonlinearities through a quantum probe – ideally a Ramsey type probe where only the spin is measured.

As mentioned above, quantum concentration/distillation is crucial for quantum networking purposes. Here, in Chapter 3 we have presented a first application of optomechanics in entanglement concentration. Our proposal uses an indirect measurement of the photon number of the electromagnetic field inside a cavity through the position measurement of a mechanical element coupled to it. For an optimal strength of the optomechanical coupling, the photon number is measured weakly or "unsharply" and this results in entanglement distillation conditioned to the position outcome. On the other hand, the position measurements of a mechanical oscillator can be highly precise, especially as we are not concerned about back-reaction as the measurement is at the end of our protocol (the oscillator can be reinitialized before performing distillation again). Other optimizations of our protocol may be attempted such as multiple modes in the cavity. Furthermore, we have considered only the detrimental effects of the light injection into the cavity via a beam splitter operations, as well as the damping of the mechanical object. However, to consider an even more realistic scenario we need to consider the photon leakage from the cavity.

The state obtained through our protocol is non-Gaussian, and thus it can serve as the first step of Gaussification [Browne2003b, Campbell2012] (see Section 3.3.2) — which can enhance its entanglement further and act on multiple copies — or, more generally, for quantum computation purposes [Menicucci2006]. Moreover, the procedure outlined here could be useful also in a quantum repeater scenario for long distance communication, considering that the extraction of the distilled state from the optical cavity is simplified in comparison to settings where the two distilled modes are trapped in two cavities (one node is always freely propagating in our case). However, the generalization to scalable repeaters is a separate topic for the future. The attractiveness of using optomechanics could be in the possibility of using integrated technology in the nodes of repeaters.

In Chapter 4, stimulated by quantum networks we present a feasible light-matter interfacing, as well as qubit-qubit quantum entanglement between two distant nodes. The physical model is composed of a parametric coupling of the qubit with a mechanical object, in conjunction with the radiation pressure coupling of the same object with light. In contrast to previous similar schemes based on exchange of energy excitations and linearized Hamiltonians in presence of an external drive (i.e., solving the Langevin's equations), we consider here a dispersive Hamiltonian (in the sense that both the qubit, as well as the cavity excitations remain constant throughout the dynamics), therefore it is not obvious that qubit-cavity entanglement will be generated dynamically. Furthermore, we exploit the trilinear radiation pressure interaction and the qubit-mechanical strength without further approximations. Our results shown to be quite promising under low qubit-mechanics and qubit-light coupling strength, for experimental values shown in Chapters 2 and 3 respectively. For instance, for optimal values $\alpha = 1, \bar{n} = 0.1, \lambda/\omega_m = 0.5, g/\omega_m = 0.1$ a high entanglement can be achieved for $\omega_m t = 2\pi$ ($\mathcal{N} \to 1$).

Furthermore, for some particular coupling values, we can also generate multicomponent Schrödinger-cat states for the cavity field when the qubit is measured. In practice, the advantage of a qubit projection is that it can be performed much more faithfully in comparison to a continuous position degree of freedom as shown previously, e.g., see Ref. [Bose1997].

Towards the remote qubit-qubit quantum entanglement between nodes. First, we shown how a partial qubit-fibre entanglement for an optimal cavity-fibre coupling can be achieved, where we have considered the short-fibre limit —only one mode of the fibre field is resonant with cavity mode. Additionally, we consider a second initial condition for the single cavity mode, $|\psi(0)\rangle \approx |0\rangle - |1\rangle$. Although this state is harder to prepare as a cavity mode experimentally, in contrast to a coherent state (i.e., Laser state), we use the initial Fock number state as we achieve a higher qubit-fibre entanglement. Secondly, we solved the master equation considering photon losses from the cavities, as well as energy losses from the mechanical object. The results shown that qubit-qubit entanglement can be generated between a generic and an atomic qubit. For modest losses $\Gamma_m = \kappa_c = 10^{-3}$, the qubit-fibre entanglement remain robust. Other scenarios can be extended, for example, within on-chip technologies we can eliminate the fibre and consider cavities directly coupled. Furthermore, an identical second tripartite node can be considered instead of a qubit-light Jaynes-Cummings Hamiltonian —situation not considered here mainly for its complexity and is left as an issue to address in the future.

Subsequently, we investigate in Chapter 5 a very interesting effect within the Born-Markov microscopic master equation (MME) framework. Essentially, our physical system corresponds to two distant two-level atoms trapped in fibre-coupled cavities. In general, thermal effects on the relevant system have been usually treated as a destructive source for quantum correlations —in fact, this is the case for all of our research reported in the previous Chapters. However, a counterintuitive dynamics was found a few years ago [Krauter2011, Muschik2011, Kastoryano2011, Memarzadeh2011] where thermal fluctuations might indeed induce quantum correlations.

To study the quantum correlations driven by thermal fluctuations, we initially consider that the qubit-fibre-cavities system starts from its ground state. As is known, if we consider only the closed quantum system with no initial excitations, then no quantum correlations will be generated in time. However, for an open quantum case the situation may vary. In particular, the Born-Markov MME can be understood as quantum jumps between eigenstates of the full system (Davies operators). Thus, as the Lindbladian contributes to create photon excitations, the dissipation term can be understood as an external drive.

This is an example that could give us a new insight into the effects of the system-environment exchange versus the quantum correlations. From the analysis of the obtained results, we conclude that the entanglement can be optimized by engineering the thermal bath of the fibre rather than the baths of each cavity, hence suggesting that the "quasi-local" manipulations produce a modest effect on the generation of entanglement. Furthermore, we found that our system evidences quantum correlations quantified by quantum discord prior to the appearance of the entanglement. Finally, the model discussed here could be experimentally implemented by using a quantum non-demolition experiment in order to test the fibre-cavity field state and evidences a sufficient high probability for a successful measurement.

Lastly, in Chapter 6 we present an ongoing investigation. Here, we have all the ingredients to assess a quantum network of two systems with atomic-mechanical oscillator interaction, where the interaction is of the type shown in Chapter 2. The main difference with previous works is that in this case the qubits are initially correlated in a Bell-diagonal form assisted by independent mechanical oscillators. The role of the quantum harmonic oscillators is to assist the qubit evolution, in the sense that they do not entangle with their respective qubits during the evolution. Therefore, considering the open quantum case for the damping of the mechanical objects, we can investigate the robustness of the qubits correlations.

In general we studied the dynamics of classical and quantum correlations measured by the entropic quantum discord for different physical conditions of the entire system in order to control the generation, propagation and preservation of the correlations. As a result we found that the quantum discord evidence the processes of freezing, quantum sudden transitions and revivals in time —with some periodicity depending on the symmetry of the oscillators.

To conclude, in this last chapter we presented a kind of atomic-mechanical quantum system which evidence illustratively some interesting effects with possibilities to monitor the quantum correlations by tuning the physical parameters of the model - important tools for applications in quantum information science.

Bibliography

[Aaronson2013] B. Aaronson, R. Lo Franco, and G. Adesso, Phys. Rev. A **88**, 012120 (2013).

[Abbott2009] B. P. Abbott *et. al.*, Rep. Prog. Phys. **72**, 076901 (2009).

[Abdi2015] M. Abdi, M. Pernpeintner, R. Gross, H. Huebl, and M. J. Hartmann, Phys. Rev. Lett. **114**, 173602 (2015).

[Agarwal2012] G. S. Agarwal, Quantum Optics, Cambridge University Press (2012).

[Akram2013] U. Akram, W. P. Bowen and G. J. Milburn, New Journal of Physics **15**, 093007 (2013).

[Ali2010] M. Ali, A. R. P. Rau, and G. Alber, Phys. Rev. A **81**, 042105 (2010).

[Anetsberger2009] G. Anetsberger, O. Arcizet, Q. P. Unterreithmeier, R. Riviere, A. Schliesser, E. M. Weig, J. P. Kotthaus, and T. J. Kippenberg, Nature Phys. **5**, 909 (2009).

[Armour2002] A. D. Armour, M. P. Blencowe, and K. C. Schwab, Phys. Rev. Lett. **88**, 148301 (2002).

[Ashhab2010] S. Ashhab and F. Nori, Phys. Rev. A **81**, 042311 (2010).

[Ashkin1978,Ashkin2006] A. Ashkin, Phys. Rev. Lett. **40**, 729 (1978); A. Ashkin, Optical trapping and manipulation of neutral particles using lasers (World Scientific) (2006).

[Asjad2014] M. Asjad, S. Zippilli, P. Tombesi and D. Vitali, arXiv:1411.7216 (2014).

[Aspelmeyer2010] M. Aspelmeyer, S. Gröblacher, K. Hammerer, and N. Kiesel, J. Opt. Soc. Am. B **27**, A189 (2010).

[Aspelmeyer2014] M. Aspelmeyer, T. J. Kippenberg, and F. Marquardt, Rev. Mod. Phys. **86**, 1391 (2014).

[Auyuanet2010] A. Auyuanet and L. Davidovich, Phys. Rev. A **82**, 032112 (2010).

[Bartley2013] T. J. Bartley, P. J. D. Crowley, A. Datta, J. Nunn, L. Zhang, and I. Walmsley, Phys. Rev. A **87**, 022313 (2013).

[Bell1964] J. Bell, Physics **1** (3): 195–200 (1964).

[Bennett1996] C.H. Bennett *et al.* Phys. Rev. A **53**, 2046 (1996); C.H. Bennett *et al.* Phys. Rev. Lett. **76**, 722 (1996).

[Blatt2008] R. Blatt and D.J. Wineland, Nature **453**, 1008 (2008).

[Blencowe2000] M. P. Blencowe and M. N. Wybourne, Appl. Phys. Lett. **77**, 3845 (2000).

[Bose1997] S. Bose, K. Jacobs, and P. L. Knight, Phys. Rev. A **56**, 4175 (1997).

[Bose1999a] S. Bose, K. Jacobs, and P. L. Knight, Phys. Rev. A **59**, 3204 (1999).

[Bose1999b] S. Bose, P. L. Knight, M. B. Plenio, and V. Vedral, Phys. Rev. Lett. **83**, 5158 (1999).

[Bose2006] S. Bose and G. S. Agarwal, New J. Phys. **8**, 34 (2006).

[Bouchiat1998] V. Bouchiat, D. Vion, P. Joyez, D. Esteve, and M. H. Devoret, Phys. Scr. **T76**, 165 (1998).

[Bourassa2009] J. Bourassa, J. M. Gambetta, A. A. Abdumalikov, Jr., O. Astafiev, Y. Nakamura, and A. Blais, Phys. Rev. A **80**, 032109 (2009).

[Bowden2007] B. Bowden, J. A. Harrington, and O. Mitrofanov, Opt. Lett. **32**, 2945 (2007).

[Braginsky1967] V. B. Braginsky and A. B. Manukin, Sov. Phys. JETP **25**, 653 (1967).

[Braginsky1970] V. B. Braginsky, A. B. Manukin, and M. Y. Tikhonov, Sov. Phys. JETP **31**, 829 (1970).

[Braginsky1995] V. B. Braginsky and F. Y. A. Khalili, Quantum Measurements (Cambridge University Press) (1995).

[Braunstein1998] S.L. Braunstein and H.J. Kimble, Phys. Rev. Lett. **80**, 869 (1998).

[Breuer-Book] H. P. Breuer and F. Petruccione, in *The Theory of Open Quantum Systems*, (Oxford University Press) (2007).

[Browne2005] Daniel E. Browne, arXiv:quant-ph/0507037v2 (2005).

[Browne2003a] D. E. Browne, J. Eisert, S. Scheel, and M. B. Plenio, Phys. Rev. A, **68**, 022312 (2003).

[Browne2003b] D. E. Browne, J. Eisert, S. Scheel and M. B. Plenio, Phys. Rev. A **67**, 062320 (2003).

[Campbell2012] E. T. Campbell and J. Eisert, Phys. Rev. Lett. **108**, 020501(2012).

[Castelleto2001] S. Castelleto, I.P. Degiovanni, and M.L. Rastello, J. Opt. B: Quantum Semiclass. Opt. **3** S60 (2001).

[Caves1980] C. M. Caves, Phys. Rev. Lett. **45**, 75 (1980).

[Chan2011] J. Chan, T. P. Mayer Alegre, A. H. Safavi-Naeini, J. T. Hill, A. Krause, S. Gröblacher, M. Aspelmeyer, and O. Painter, Nature (London) **478**, 89 (2011).

[Chang2010] D. E. Chang, C. A. Regal, S. B. Papp, D. J. Wilson, J. Ye, O. Painter, H. J. Kimble, and P. Zoller, Proc. Natl. Acad. Sci. U.S.A. **107** 1005 (2010).

[Chen2006] L. J. Chen *et al*, Opt. Lett. **31**, 308 (2006).

[Chen2014] M. Chen, N. C. Menicucci, and O. Pfister, Phys. Rev. Lett. **112**, 120505 (2014).

[Chiorescu2004] I. Chiorescu, P. Bertet, K. Semba, Y. Nakamura, C.J.P.M. Harmans, and J.E. Mooij, Nature **431**, 159 (2004).

[Cirac1997] J. I. Cirac, P. Zoller, H. J. Kimble, and H. Mabuchi, Phys. Rev. Lett. **78**, 3221 (1997).

[Clarke2008] J. Clarke and F. K. Wilhelm, Nature **453**, 1031 (2008)

[Cleland1998] A. N. Cleland and M. L. Roukes, Nature (London) **392**, 160 (1998).

[Cohadon1999] P.-F. Cohadon, A. Heidmann, and M. Pinard, Phys. Rev. Lett. **83**, 3174 (1999).

[Humphreys2014] P. C. Humphreys, W. S. Kolthammer, J. Nunn, M. Barbieri, A. Datta, and I. A. Walmsley, Phys. Rev. Lett. **113**, 130502 (2014).

[Datta2008] A. Datta, A. Shaji, and C. M. Caves, Phys. Rev. Lett. **100**, 050502 (2008).

[Datta2012] A. Datta, L. Zhang, J. Nunn, N. K. Langford, A. Feito, M. B. Plenio, I. A. Walmsley, Phys. Rev. Lett. **108**, 060502 (2012).

[DiVincenzo2012] D. P. DiVincenzo and J. A. Smolin, New J. Phys. **14**, 013051 (2012).

[Dong2008] R. Dong, M. Lassen, J. Heersink, C. Marquardt, R. Filip, G. Leuchs and U. L. Andersen, Nature Physics **4**, 919 (2008).

[Dorsel1983] A. Dorsel, J. D. McCullen, P. Meystre, E. Vignes, and H. Walther, Phys. Rev. Lett. **51**, 1550 (1983).

[Duan2000] L.-M. Duan, G. Giedke, J. I. Cirac and P. Zoller, Phys. Rev. Lett. **84** 4002 (2000).

[Duffing1918] G. Duffing, "Erzwungene schwingungen bei veranderlicher eigenfrequenz," F. Vieweg und Sohn, Braunschweig, 1918.

[Echternach2001] P. Echternach, C. P. Williams, S. C. Dultz, S. Braunstein, and J. P. Dowling, Quantum Inf. Comput. **1**, 143 (2001).

[Eichenfield2009] M. Eichenfield, R. Camacho, J. Chan, K. J. Vahala, and O. Painter, Nature (London) **459**, 550 (2009); M. Eichenfield, J. Chan, R. M. Camacho, K. J. Vahala, and O. Painter, Nature (London) **462**, 78 (2009).

[Eisert2002] J. Eisert, S. Scheel, and M. B. Plenio, Phys. Rev. Lett. **89**, 137903 (2002).

[Eisert2004] J. Eisert, D. E. Browne, S. Scheel, and M. B. Plenio, Annals of Physics, **311**, 431 (2004).

[EPR1935] A. Einstein, B. Podolsky, and N. Rosen, Phys. Rev. **47**, 777 (1935).

[Erbe2001] A. Erbe, C. Weiss, W. Zwerger, and R. H. Blick, Phys. Rev. Lett. **87**, 096106 (2001).

[Fanchini2010] F. F. Fanchini, T. Werlang, C. A. Brasil, L. G. E. Arruda, and A. O. Caldeira, Phys. Rev. A **81**, 052107 (2010).

[Favero2009] I. Favero, S. Stapfner, D. Hunger, P. Paulitschke, J. Reichel, H. Lorenz, E. M. Weig, and K. Karrai, Opt. Express **17**, 12813 (2009).

[Ferraro2005] A. Ferraro, S. Olivares and M. G. A. Paris, *Gaussian states in continuous variable quantum information* (Bibliopolis, Napoli, 2005); arXiv preprint quant-ph/0503237.

[Fiurasek2002] J. Fiurášek, Phys. Rev. Lett. **89**, 137904 (2002).

[Fiurasek2003] J. Fiurasek, L. Mista Jr, and R. Filip, Phys. Rev. A **67**, 022304 (2003).

[Franzen2006] A. Franzen, B. Hage, J. DiGuglielmo, J. Fiurasek and R. Schnabel, Phys. Rev. Lett. **97**, 150505 (2006).

[Gerke2015] S. Gerke, J. Sperling, W. Vogel, Y. Cai, J. Roslund, N. Treps, and C. Fabre, Phys. Rev. Lett. **114**, 050501 (2015).

[Giedke2002] G. Giedke and J. I. Cirac, Phys. Rev. A **66**, 032316 (2002).

[Glauber1963] R. J. Glauber, Phys. Rev. **130**, 2529 (1963); R. J. Glauber, Phys. Rev. **131**, 2766 (1963), R. J. Glauber, Phys. Rev. Lett. **10**, 84 (1963).

[Gozzini1985] A. Gozzini, F. Maccarone, F. Mango, I. Longo, and S. Barbarino, J. Opt. Soc. Am. B**2**, 1841 (1985).

[Grangier1998] P. Grangier, J. A. Levenson and J.-P. Poizat, Nature **396**, 537 (1998).

[Grimsmo2013] A. L. Grimsmo and S. Parkins, Phys. Rev. A **87**, 033814 (2013).

[Guerlin2007] C. Guerlin *et al*, Nature **448**, 889 (2007).

[Habraken2012] S. J. M. Habraken, K. Stannigel, M. D. Lukin, P. Zoller, and P. Rabl, New J. Phys. **14**, 115004 (2012).

[Hansch1975] T. W. Hänsch and A. L. Schawlow, Opt. Commun. **13**, 68 (1975).

[Hausinger2010] J. Hausinger and M. Grifoni, Phys. Rev. A **82**, 062320 (2010).

[He2012] B. He, Phys. Rev A **85**, 063820 (2012).

[He2013] Qi-liang He and Jing-bo Xu, J. Opt. Soc. Am. B **30**, 251-257 (2013).

[Henderson2001] L. Henderson and V. Vedral, J. Phys. A **34**, 6899 (2001).

[Hennessy2007] K. Hennessy, A. Badolato, M. Winger, D. Gerace, M. Atatüre, S. Gulde, S. Fält, E. L. Hu, and A. Imamoğlu, Nature (London) **445**, 896 (2007).

[Hensinger2005] W. K. Hensinger, D. W. Utami, H.-S. Goan, K. Schwab, C. Monroe, and G. J. Milburn, Phys. Rev. A **72**, 041405(R) (2005).

[Hilico1992] L. Hilico, J. M. Courty, C. Fabre, S. Giacobino, I. Abraham, and J. L. Oudar, Appl. Phys. B**55**, 202 (1992).

[Hohberger2004a] C. Höhberger and K. Karrai, in Proceedings of the 4th IEEE Conference on Nanotechnology (IEEE, New York) (2004).

[Hohberger2004b] C. Höhberger and K. Karrai, Nature **432**, 1002 (2004).

[Home2011] J. P. Home, D. Hanneke, J. D. Jost, D. Leibfried, and D.J. Wineland, New J. Phys. **13**, 073026 (2011).

[Horodecki2009] R. Horodecki, P. Horodecki, M. Horodecki, and K. Horodecki, Rev. Mod Phys. **81**, 565 (2009).

[Hunger2010] D. Hunger, S. Camerer, T. W. Hänsch, D. König, J. P. Kotthaus, J. Reichel, and P. Treutlein, Phys. Rev. Lett. **104**, 143002 (2010).

[Jacobs1994] K. Jacobs, P. Tombesi, M. J. Collett, and D. F. Walls, Phys. Rev. A **49**, 1961 (1994).

[Jiang2009] X. Jiang, Q. Lin, J. Rosenberg, K. Vahala, and O. Painter, Opt. Express **17**, 20911 (2009).

[Joshi2011] C. Joshi, M. Jonson, E. Andersson, and P. Öhberg, J. Phys. B: At. Mol. Opt. Phys. **44**, 245503 (2011).

[Kastoryano2011] M. J. Kastoryano, F. Reiter, and A. S. Sørensen, Phys. Rev. Lett. **106**, 090502 (2011).

[Kaviani2014] H. Kaviani, C. Healey, M. Wu, R. Ghobadi and P. E. Barclay, arXiv:1412.4431 (2014).

[Kim1998] M. S. Kim, G. Antesberger, C. T. Bodendorf and H.Walther, Phys. Rev. A **58**, R65 (1998).

[Kim2002] M. Kim, Journal of Modern Optics. **49**, 10, p. 1739-1746 (2002).

[Kimble2008] H. J. Kimble, Nature **453**, 1023 (2008).

[Knill1998] E. Knill and R. Laflamme, Phys. Rev. Lett. **81**, 5672 (1998).

[Kolkiran2006] A. Kolkiran and G. S. Agarwal, arXiv:0608621v2 (2006).

[Kolkowitz2012] S. Kolkowitz, A. C. Bleszynski Jayich, Q. P. Unterreithmeier, S. D. Bennett, P. Rabl, J. G. E. Harris, and M. D. Lukin, Science **335** (6076), 1603-1606 (2012).

[Krauter2011] H. Krauter, C. A. Muschik, K. Jensen, W. Wasilewski, J. M. Petersen, J. I. Cirac and E. S. Polzik, Phys. Rev. Lett. **107**, 080503 (2011).

[Kronwald2013] A. Kronwald, M. Ludwig, and F. Marquardt, Phys. Rev. A **87**, 013847 (2013).

[Kryszewski2008] S. Kryszewski and J. Czechowska-Kryszk, arXiv:0801.1757v1 (2008).

[Kurochkin2014] Y. Kurochkin, A. S. Prasad, and A. I. Lvovsky, Phys. Rev. Lett. **112**, 070402 (2014).

[LaHaye2004] M. D. LaHaye, O. Buu, B. Camarota, and K. C. Schwab, Science, **304**, 74 (2004).

[Lang2010] M. D. Lang and C. M. Caves, Phys. Rev. Lett. **105**, 150501 (2010).

[Law1995] C. K. Law Phys. Rev. A **51**, 2537 (1995).

[Leonhardt-Book] Ulf Leonhardt, in *Measuring the Quantum State of Light*, (Cambridge University Press) (2005).

[Lewenstein2013] M. Lewenstein, A. Sanpera, and V. Ahufinger, *Ultracold Atoms in Optical Lattices: Simulating quantum many-body systems*, Oxford U. Press (2013).

[Liao2012] J.-Q. Liao, H. K. Cheung, and C. K. Law, Phys. Rev. A **85** 025803 (2012).

[Liao2014] J.-Q. Liao and F. Nori, Scientific Reports **4**, 6302 (2014).

[Lu2011] X.-M. Lu, J. Ma, Z. Xi, and X. Wang, Phys. Rev. A **83**, 012327 (2011).

[Luo2008] S. Luo, Phys. Rev. A **77**, 042303 (2008).

[Ma2007] R. Ma, A. Schliesser, P. Del'Haye, A. Dabirian, G. Anetsberger, and T. Kippenberg, Opt. Lett. **32**, 2200 (2007).

[Machnes2012] S. Machnes, J. Cerrillo, M. Aspelmeyer, W. Wieczorek, M. B. Plenio, and A. Retzker, Phys. Rev. Lett. **108**,153601 (2012).

[Makhlin2001] Y. Makhlin, G. Schön, and A. Shnirman, Rev. Mod. Phys. **73**, 357 (2001).

[Mancini1994] S. Mancini and P. Tombesi, Phys. Rev. A **49**, 4055 (1994).

[Mancini1997] S. Mancini, V. I. Man'ko, and P. Tombesi, Phys. Rev. A **55**, 3042 (1997).

[Mancini2002] S. Mancini, V. Giovannetti, D. Vitali and P. Tombesi, Phys. Rev. Lett. **88**, 120401 (2002).

[Mancini2004] S. Mancini and S. Bose, Phys. Rev. A **70**, 022307 (2004).

[Maragkou2015] M. Maragkou, Nature Materials **14**, 468 (2015).

[Marshall2003] W. Marshall, C. Simon, R. Penrose and D. Bouwmeester, Phys. Rev. Lett. **91**, 159903 (2003).

[Memarzadeh2011] L. Memarzadeh and S. Mancini, Phys. Rev. A **83**, 042329 (2011).

[Menicucci2006] N.C. Menicucci, P. van Loock, M. Gu, C. Weedbrook, T.C. Ralph, M.A. Nielsen, Phys. Rev. Lett. **97**, 110501 (2006).

[Mertz1993] J. Mertz, O. Marti, and J. Mlynek, Appl. Phys. Lett. **62**, 2344 (1993).

[Mintert2001] F. Mintert and C. Wunderlich, Phys. Rev. Lett. **87**, 257904 (2001).

[Montenegro2011] V. Montenegro and M. Orszag, J. Phys. B: At. Mol. Opt. Phys. **44** 154019 (2011).

[Murch2008] K. W. Murch, K. L. Moore, S. Gupta, and D. M. Stamper-Kurn, Nature Phys. **4**, 561 (2008).

[Muschik2011] C. A. Muschik, E. S. Polzik, and J. I. Cirac, Phys. Rev. A **83**, 052312 (2011).

[Nizamani2011] A. Nizamani and W. K. Hensinger, Appl. Phys. B **106**, 327 (2011).

[Nunnenkamp2011] A. Nunnenkamp, K. Borkje, and S. M. Girvin, Phys. Rev. Lett. **107**, 063602 (2011).

[Olivares2003] S. Olivares, M.G.A. Paris, R. Bonifacio, Phys. Rev. A **67**, 032314 (2003).

[Ollivier2001] H. Ollivier and W. H. Zurek, Phys. Rev. Lett. **88**, 017901 (2001).

[Ong2011] F. R. Ong, M. Boissonneault, F. Mallet, A. Palacios-Laloy, A. Dewes, A. C. Doherty, A. Blais, P. Bertet, D. Vion, and D. Esteve, Phys. Rev. Lett. **106**, 167002 (2011).

[Opatrny2000] T. Opatrný, G. Kurizki, and D.-G. Welsch, Phys. Rev. A **61**, 032302 (2000).

[Ourjoumtsev2009] A. Ourjoumtsev, F. Ferreyrol, R. Tualle-Brouri, and P. Grangier, Nature Phys. **5**, 189 (2009).

[Park2012] J. Park, M. Saunders, Yong-il Shin, K. An, and H. Jeong, Phys. Rev. A **85**, 022120 (2012).

[Parkins2000] A. S. Parkins and H. J. Kimble, Phys. Rev. A **61**, 052104 (2000).

[Peano2006] V. Peano and M. Thorwart, New J. Phys. **8**, 21 (2006).

[Pellizzari1997] T. Pellizzari, Phys. Rev. Lett. **79**, 5242 (1997).

[Pirandola2006] S. Pirandola, D. Vitali, P. Tombesi and S. Lloyd, Phys. Rev. Lett. **97**, 150403 (2006).

[Pla2012] J. J. Pla, K. Y. Tan, J. P. Dehollain, W. H. Lim, J. J. L. Morton, D. N. Jamieson, A. S. Dzurak, and A. Morello, Nature **489**, 541–545 (2012).

[Plunien1986] G. Plunien, B. Müller, and W. Greiner, Phys. Rev. **134**, 87 (1986).

[Poot2011] M. Poot and Herre S.J. van der Zant, arXiv:1106.2060v2 (2011).

[Qing2011] C. Qing, C. Zhang, S. Yu, X. X. Yi, and C. H. Oh, Phys. Rev. A **84**, 042313 (2011).

[QuTiP] J. R. Johansson, P. D. Nation, and F. Nori: "QuTiP 2: A Python framework for the dynamics of open quantum systems.", Comp. Phys. Comm. **184**, 1234 (2013); J. R. Johansson, P. D. Nation, and F. Nori: "QuTiP: An open-source Python framework for the dynamics of open quantum systems.", Comp. Phys. Comm. **183**, 1760–1772 (2012).

[Rabl2009] P. Rabl, P. Cappellaro, M. V. Gurudev Dutt, L. Jiang, J. R. Maze, and M. D. Lukin, Phys. Rev. B **79**, 041302(R) (2009).

[Rabl2010] P. Rabl, S. J. Kolkowitz, F. H. L. Koppens, J. G. E. Harris, P. Zoller, and M. D. Lukin, Nature Physics **6**, 602–608 (2010).

[Raimond2006] J. M. Raimond, M. Brune, and S. Haroche, Rev. Mod. Phys. **73**, 565 (2001); H. Walther, B.T.H. Varcoe, B.G. Englert and T. Becker, Rep. Prog. Phys. **69**, 1325 (2006).

[Restrepo2014] J. Restrepo, C. Ciuti, and I. Favero, Phys. Rev. Lett. **112**, 013601 (2014).

[Rips2013] S. Rips and M. J. Hartmann, Phys. Rev. Lett. **110**, 120503 (2013).

[Safavi-Naeini2011] A. H. Safavi-Naeini, T. P. Mayer Alegre, J. Chan, M. Eichenfield, M. Winger, Q. Lin, J. T. Hill, D. E. Chang, and O. Painter, Nature **472**, 69 (2011).

[Sankey2009] J.C. Sankey et al., Nature Phys. 6, 707 (2009).

[Scala2007] M. Scala, B. Militello, A. Messina, J. Piilo and S. Maniscalco, Phys. Rev. A **75**, 013811 (2007).

[Scala2013] M. Scala, M. S. Kim, G. W. Morley, P. F. Barker, S. Bose, Phys. Rev. Lett. **111**, 180403 (2013).

[Schlosshauer2013] M. Schlosshauer, J. Kofler, and A. Zeilinger, Stud. Hist. Phil. Mod. Phys. **44**, 222-230 (2013).

[Schroedinger1935] E. Schrödinger, Naturwissenschaften **23**, 807; 823; 844 (1935); [Engl. transl. in Proc. Am. Philos. Soc. **124**, 323].

[Sekatski2014] P. Sekatski, M. Aspelmeyer, N. Sangouard, Phys. Rev. Lett. **112**, 080502 (2014).

[Serafini2006] A. Serafini, S. Mancini, and S. Bose, Phys. Rev. Lett. **96**, 010503 (2006).

[Solano2003] E. Solano, G. S. Agarwal, and H. Walther, Phys. Rev. Lett. **90**, 027903 (2003).

[Stannigel2010] K. Stannigel, P. Rabl, A. S. Sørensen, P. Zoller, and M. D. Lukin, Phys. Rev. Lett. **105**, 220501 (2010).

[Stannigel2011] K. Stannigel, P. Rabl, A. S. Sørensen, M. D. Lukin, and P. Zoller, Phys. Rev. A **84**, 042341 (2011).

[Stannigel2012a] K. Stannigel, P. Rabl, and P. Zoller, New J. Phys. **14**, 063014 (2012).

[Stannigel2012b] K. Stannigel, P. Komar, S. Habraken, S. D. Bennett, M. Lukin, P. Zoller, and P. Rabl, Phys. Rev. Lett. **109**, 013603 (2012).

[Steele2009] G. A. Steele, A. K. Hüttel, B. Witkamp, M. Poot, H. B. Meerwaldt, L. P. Kouwenhoven, and H. S. J. van der Zant, Science **325**, 1103 (2009).

[Stenholm1993] S. Stenholm, in Second International Workshop on Squeezed States and Uncertainty Relations, edited by D. Han, Y. S. Kim, and V. I. Man'ko (NASA Conference Publications, Greenbelt, MD, 1993).

[Sudarshan1963] E. C. G. Sudarshan, Phys. Rev. Lett. **10**, 277 (1963).

[Treutlein2007] P. Treutlein, D. Hunger, S. Camerer, T. W. Hänsch, J. Reichel, Phys. Rev. Lett. **99**, 140403 (2007).

[Treutlein2015] P. Treutlein, C. Genes, K. Hammerer, M. Poggio, P. Rabl, arXiv:1210.4151v2 (2015).

[Tufarelli2011] T. Tufarelli, M. S. Kim, and S. Bose, Phys Rev A **83**, 062120 (2011).

[Tufarelli2012] T. Tufarelli, A. Ferraro, M. S. Kim, and S. Bose, Phys. Rev. A **85**, 032334 (2012).

[Takahashi2010] H. Takahashi, J. S. Neergaard-Nielsen, M. Takeuchi, M. Takeoka, K. Hayasaka, A. Furusawa, and M. Sasaki, Nature Photonics **4**, 178 (2010).

[Teufel2011] J. D. Teufel, T. Donner, D. Li, J. H. Harlow, M. S. Allamn, K. Cicak, A. Sirois, J. D. Whittaker, K. W. Lehnert, and R. W. Simmonds, Nature **475**, 359 (2011).

[Tittonen1999] I. Tittonen, G. Breitenbach, T. Kalkbrenner, T. Müller, R. Conradt, S. Schiller, E. Steinsland, N. Blanc, and N. F. de Rooij, Phys. Rev. A **59**, 1038 (1999).

[Thompson2008] J. D. Thompson, B. M. Zwickl, A. M. Jayich, F. Marquardt, S. M. Girvin, and J. G. E. Harris, Nature (London) **452**, 72 (2008).

[vanEnk1999] S. J. van Enk, H. J. Kimble, J. I. Cirac, and P. Zoller, Phys. Rev. A **59**, 2659 (1999).

[Vanner2010] M. R. Vanner *et. al.*, Nat. Commun. **4**, 2295 (2010).

[Vanner2011] M.R. Vanner, I. Pikovski, G. D. Cole, M. S. Kim, C. Brukner, K. Hammerer, G. J. Milburn, and M. Aspelmeyer, Proc. Natl. Acad. Sci. U.S.A. **108**, 16182 (2011).

[Vanner2013] M. R. Vanner, J. Hofer, G. D. Cole, M. Aspelmeyer, Nature Communications **4**, 2295 (2013).

[Verhagen2012] E. Verhagen, S. Deléglise, S. Weis, A. Schliesser, and T. J. Kippenberg, Nature **482**, 63 (2012).

[Vidal2002] G. Vidal and R. F. Werner, Phys. Rev. A **65**, 032314 (2002).

[Vogel2003] M. Vogel, C. Mooser, K. Karrai, and R. J. Warburton, Appl. Phys. Lett. **83**, 1337 (2003).

[Wallraff2004] A. Wallraff, D. I. Schuster, A. Blais, L. Frunzio, R.-S. Huang, J. Majer, S. Kumar, S. M. Girvin, and R. J. Schoelkopf, Nature **431**, 162 (2004).

[Walls1985] D. F. Walls, M. J. Collett, and G. J. Milburn, Phys. Rev. D **32**, 3208 (1985).

[Wang2000] K. Wang, A.-C. Wong, and C. T.-C. Nguyen, J. Microelectromech. Syst. **9**, 347 (2000).

[Wenger2004] J. Wenger, R. Tualle-Brouri, and P. Grangier, Phys. Rev. Lett. **92**, 153601 (2004).

[Wineland1975] D. J. Wineland and H. Dehmelt, Bulletin of the American Physical Society **20**, 637 (1975).

[Wooters1998] W. K. Wootters, Phys. Rev. Lett. 80, 2245 (1998).

[Xu2013a] X.-W. Xu, Y.-J. Li, and Yu-xi Liu, Phys. Rev. A **87**, 025803 (2013).

[Xu2013b] X.-W. Xu and Y.-J. Li, J. Phys. B: At. Mol. Opt. Phys. **46**, 035502 (2013).

[Xuereb2012] A. Xuereb, C. Genes and A. Dantan, Phys. Rev. Lett. **109**, 223601 (2012).

[Yang2011] Z.B. Yang, H.Z. Wu, Y.Xia, and S.B. Zheng, Eur. Phys. J. D, **61**, 737 (2011) and the references [32-52] therein.

[Yin2013] Zhang-qi Yin, Tongcang Li, Xiang Zhang, L. M. Duan, Phys. Rev. A **88**, 033614 (2013).

[Yokohama2013] S. Yokoyama, R. Ukai, S. C. Armstrong, C. Sornphiphatphong, T. Kaji, S. Suzuki, Jun-ichi Yoshikawa, H. Yonezawa, N. C. Menicucci, and A. Furusawa, Nature Photonics **7**, 982 (2013).

[You2012] B. You and L.-X. Cen, Phys. Rev. A **86**, 012102 (2012).